Molecular characterisation of nodular sclerosing classical Hodgkin lymphoma derived fibroblasts and their beneficial interaction with Hodgkin Reed Sternberg cells

Dissertation

zur Erlangung des Doktorgrades

der Naturwissenschaften

vorgelegt beim Fachbereich 14

der Biochemie, Chemie und Pharmazie

der Johann Wolfgang Goethe – Universität

in Frankfurt am Main

von

Katrin Bankov

aus Magdeburg

Frankfurt am Main, 2020

vom Fachbereich 14 der Biochemie, Chemie und Pharmazie

Johann Wolfgang Goethe - Universität als Dissertation angenommen.

Dekan: Prof. Dr. Clemens Glaubitz

1. Gutachter: Prof. Dr. Rolf Marschalek

2. Gutachterin: Prof. Dr. Sylvia Hartmann

Datum der Disputation :   12.01.2021

Table of contents

List of abbreviations

A.U.	Arbitrary unit
APC	Allophycocyanin
APC-Cy7	Allophycocyanin cyanine dye
BA	Blocking antibody
BA-Iso	Blocking antibody isotype control
BC	B Cell
bFGF	Beta fibroblast growth factor
BL	Burkitt lymphoma
BL	Burkitt lymphoma
BV	Brentuximab-Vedotin
CAF	Cancer associated fibroblasts
CCL	CC chemokine ligand
CCR	CC chemokine receptor
CD	Cluster of differentiation
cDNA	copy desoxyribonucleic acid
cHL	classical Hodgkin lymphoma
cm	Conditioned media
CpG	" 5'—C—phosphate—G—3' " sequence of nucleotides
Ctrl	Control
CXCL	C-X-C motif chemokine ligand
DNA	Desoxyribonucleic acid
DAPI	4′,6-diamidino-2-phenylindole
DC	Dendritic Cell
DLBCL	Diffuse large B cell lymphoma
DLBCL	Diffuse Large B Cell Lymphoma
DPBS	Dulbecco's phosphate-buffered saline
DSMZ	German Collection of Microorganisms and Cell Cultures GmbH
EBV	Epstein-Barr virus
EBV	Epstein–Barr virus
ECM	Extracellular matrix
EDTA	Ethylenediaminetetraacetic acid
EGCG	Epigallocatechin gallate
ELISA	enzyme-linked immunosorbent assay
ERM	Ezrin, Radixin, Moesin proteins

eSASP	extracellular SASP
F	Flow cytometry
f	female
F-Iso	Flow cytometry Isotype control
FAM	Fluorescein amidites
FC	Fold Change
FCS	Fetal calf serum
FDC	follicular dendritic cell
FDR	False dicsovery rate
Fib	Fibroblasts
FITC	Fluorescein isothiocyanate
FL	Follicular lymphoma
FRC	Fibroblastic reticular cells
g	goat
GC	Germinal Centre
GEPS	Genomatix pathway system
GO	Gene ontology
H&E	Hematoxylin Eosin staining
HEV	high endothelial venules
HPLC	High-performance liquid chromatography
HRS	Hodgkin Reed Sternberg
ICF	Intracellular Flow cytometry
ICF-Iso	Intracellular Flow cytometry isotype control
IHC	Immunohistochemistry
IgG	Immunglobulin G
IL	Interleukin
ILR	Interleukin receptor
IMDM	Iscove's Modified Dulbecco's Medium
LA	Lymphadenitis
LN	Lymph node
Lut	Luteolin
m	male
MC	Mixed cellularity
MCL	Mantle Cell Lymphoma
MGB-NFQ	Minor groove binder - non-fluorescent quencher
mRNA	messenger Ribonucleic acid

ms	mouse
MZL	Marginal Zone Lymphoma
NK	Natural Killer Cell
NS	Nodular sclerosis
PC	Principal component
PCA	Principal component analysis
PCR	Polymerase chain reaction
PE	phycoerythrin
PE-Cy7	phycoerythrin cyanine dye
PFA	Paraformaldehyde
qPCR	quantitative polymerase chain reaction
rb	rabbit
RGD	tripeptide Arg-Gly-Asp
rHu	recombinant human
RPMI	Roswell Park Memorial Institute
rt	rat
RT	Reverse Transciptase
SASP	Senescence-associated secretory phenotype
SEM	Standard error of mean
SHM	Somatic hypermutation
STR	Short tandem repeat
TBS	Tris buffered saline
TC	T Cell
Treg	Regulatory T cell
UCT	Universitäres Centrum für Tumorerkrankungen
UKF	University Hospital Frankfurt
VIC	2′-chloro-7′phenyl-1,4-dichloro-6-carboxy-fluorescein
VIC-PL	VIC primer limited
WHO	World Health Organisation

List of figures

List of tables

Declaration and related publications

The submitted thesis contains collaborative work as stated below.

Except where stated otherwise by reference or acknowledgment, the work presented was generated by myself under the supervision of my advisors during my doctoral studies. All contributions from colleagues are explicitly referenced in the thesis. The material listed below was obtained in the context of collaborative research. The content of this thesis was published in Cancers including all collaboration partners as co-authors in 2019 (Bankov et al., 2019):

Bankov K, Döring C, Ustaszewski A, Giefing M, Herling M, Cencioni C, Spallotta F, Gaetano C, Küppers R, Hansmann ML, Hartmann S. Fibroblasts in Nodular Sclerosing Classical Hodgkin Lymphoma Are Defined by a Specific Phenotype and Protect Tumor Cells from Brentuximab-Vedotin Induced Injury. Cancers (Basel). 2019 Oct 30;11(11):1687. doi: 10.3390/cancers11111687. PMID: 31671543

The following parts of the thesis have been previously published in Cancers (PMID: 31671543):

Chapters, partially:

2.6 Cancer associated fibroblasts

5 Discussion

Figures:

Figure 7: Characterisation of FRCs obtained from lymph nodes according to minimum criteria by Dominici *et al.*

Isolation method including flow cytometry characterisation of fibroblasts was established by the former group of Prof. Carlo Gaetano and colleagues Chiara Cencioni, PhD, as well as Francesco Spallotta, PhD (Former group of Prof. Carlo Gaetano, University Hospital Frankfurt, Frankfurt am Main) (Meraviglia et al., 2014)*. Published data within the thesis was generated by the doctoral candidate under supervision of Prof. Dr. Sylvia Hartmann*

(Dr. Senckenberg Institute of Pathology, University Hospital Frankfurt, Frankfurt am Main) and Chiara Cencioni, PhD.

Figure 9: Fibroblasts derived from nodular sclerosing subtype of cHL (NS cHL) and lymphadenitis (LA) show considerable differences in their gene expression program.

Primary data analysis was established and held by the group of Dr. Claudia Döring (Dr. Senckenberg Institute of Pathology, University Hospital Frankfurt, Frankfurt am Main) as previously published. Sample preparation, data selection and identification of differentially regulated targets were done by the by the doctoral candidate under supervision of Prof. Dr. Sylvia Hartmann.

Figure 10: Transcript-based validation confirmed overexpression of selected prominent differentially regulated targets in NS cHL and partially MC cHL.

Published data within the thesis was generated by the doctoral candidate under supervision of Prof. Dr. Sylvia Hartmann (Dr. Senckenberg Institute of Pathology, University Hospital Frankfurt, Frankfurt am Main).

Figure 11: Independent validation using Immunohistochemistry confirmed overexpression of selected prominent differentially regulated targets in NS cHL and partially MC cHL.

Acknowledgement goes to technical assistance by Nina Becker (Dr. Senckenberg Institute of Pathology, University Hospital Frankfurt, Frankfurt am Main) for teaching and training of the methods of immunohistochemistry. Stainings were done by the doctoral candidate under her assistance.

Figure 12: Methylation profiles remain consistent in fibroblasts obtained from lymphadenitis and NS cHL.

Methylation workflow was outsourced to Atlas Biolabs in Berlin. Raw data was primarily analysed by Dr. Claudia Döring (Dr. Senckenberg Institute of Pathology, University Hospital Frankfurt, Frankfurt am Main) under supervision of Dr hab. n. med. Maciej Giefing and Dr. Adam Ustaszewski (Institute of human Genetics; Polish Academy of Sciences, Poznan) and Prof. Dr. Sylvia Hartmann (Dr. Senckenberg Institute of Pathology, University Hospital Frankfurt, Frankfurt am Main).

Figure 15: The impact of luteolin treatment on CAF viability and TIMP3 expression.

Published data within the thesis was generated by the doctoral candidate under supervision of Prof. Dr. Sylvia Hartmann (Dr. Senckenberg Institute of Pathology, University Hospital Frankfurt, Frankfurt am Main).

Figure 16: NS cHL CAF show enhanced proliferation in the presence of conditioned medium derived from cHL cell lines, even after application of luteolin.

Published data within the thesis was generated by the doctoral candidate under supervision of Prof. Dr. Sylvia Hartmann (Dr. Senckenberg Institute of Pathology, University Hospital Frankfurt, Frankfurt am Main).

Figure 19: HRS cells from cHL cell lines show strong adherence to NS cHL fibroblasts.

Published data within the thesis was generated by the doctoral candidate under supervision of Prof. Dr. Sylvia Hartmann (Dr. Senckenberg Institute of Pathology, University Hospital Frankfurt, Frankfurt am Main).

Figure 21: HRS cells adhering to NS cHL fibroblasts induce changes in the gene expression program of NS cHL fibroblasts.

Primary data analysis was established and held by the group of Dr. Claudia Döring as previously published (Brune et al., 2008)*. Sample preparation, data selection and identification of differentially regulated targets were done by the doctoral candidate under supervision of Prof. Dr. Sylvia Hartmann.*

Figure 23: HRS cells from cHL cell lines show strong adherence to NS cHL fibroblasts that can be partly blocked by anti-CD29 antibody.

Published data within the thesis was generated by the doctoral candidate under supervision of Prof. Dr. Sylvia Hartmann (Dr. Senckenberg Institute of Pathology, University Hospital Frankfurt, Frankfurt am Main).

Figure 24: HRS cells adhering to NS cHL fibroblasts are protected from Brentuximab-Vedotin treatment and induce changes in the gene expression program of NS cHL fibroblasts.

Brentuximab-Vedotin was kindly provided by PD Dr. Marco Herling (The Laboratory of Lymphocyte Signalling and Oncoproteome, Department I of Internal Medicine, Center for Integrated Oncology (CIO) Aachen-Bonn-Cologne-Duesseldorf, CECAD and CMMC, University of Cologne).

Author Contributions:

Design of the study, K.B. and S.H.; data acquisition and interpretation, K.B.; drafting the manuscript, K.B., C.D., A.U., C.C., C.G., F.S., M.H., M.G., R.K., and M.-L.H.; data analysis and interpretation, C.D. and A.U.; contributed essential material, C.C., C.G., F.S., M.H., M.G., R.K., and M.-L.H.; data interpretation, C.C., C.G., F.S., M.H., M.G., R.K., M.-L.H., and S.H.; writing of the manuscript, S.H.

Acknowledgments:

Acknowledgements go to Nina Becker (Dr. Senckenberg Institute of Pathology, University Hospital Frankfurt, Frankfurt am Main) and Kerstin Heise (Institute of Cell Biology, University Hospital Essen) for excellent technical support, PD Dr. Angela Brieger (Department of Internal Medicine 1, University Hospital Frankfurt, Frankfurt am Main) for the constant support and helpful discussions.

Conflicts of Interest:

The authors report no potential conflict of interest.

1 Abstract

Classical Hodgkin lymphoma (cHL) is one of the most common malignant lymphomas in Western Europe. The nodular sclerosing subtype of cHL (NS cHL) is characterised by a proliferation of fibroblasts in the tumour microenvironment, leading to fibrotic bands surrounding the lymphoma infiltrate. Several studies have described a crosstalk between the tumour cells of cHL, the Hodgkin- and Reed-Sternberg (HRS) cells, and cancer-associated fibroblasts (CAF). However, to date a deep molecular understanding of these fibroblasts is lacking. Aim of the present study therefore was a comprehensive characterisation of these fibroblasts. Moreover, only a few studies describe the interplay of HRS cells and CAF. The paracrine communication and direct interaction of these two cellular fractions have been investigated within this study. Finally, the influence of a few HRS cells within a lymph node orchestrate the mere alteration of its architecture and morphology. Gene expression and methylation profiles of fibroblasts isolated from primary lymph node suspensions revealed persistent differences between fibroblasts obtained from NS cHL and lymphadenitis. NS cHL derived fibroblasts exhibit a myofibroblastic - inflammatory phenotype characterised by MYOCD, CNN1 and IL-6 expression. TIMP3, an inhibitor of matrix metalloproteinases, was strongly upregulated in NS cHL fibroblasts, likely contributing to the accumulation of collagen in sclerotic bands of NS cHL. Treatment by luteolin could reverse this fibroblast phenotype and decrease TIMP3 secretion. NS cHL fibroblasts showed enhanced proliferation when they were exposed to soluble factors released from HRS cells. For HRS cells, soluble factors from fibroblasts were not sufficient to protect them from Brentuximab-Vedotin (BV) induced cell death. However, HRS cells adherent to fibroblasts were protected from BV-induced injury. The cHL specific interaction of both cell fractions reveals an initiation of inflammatory key regulators such as IL13 and IL4. Among important adhesion molecules known from literature the blocking of integrin beta 1 solely interrupted the adhesion of HRS cells to CAF. In summary, this study proves the stable reprograming of CAF phenotype and expression derived from NS cHL. It presents a suitable *in vitro* model for studying the interaction of HRS cells and CAF by paracrine factors and adherence. Most importantly the observations confirm the importance of fibroblasts for HRS cells´ inflammatory niche and cell survival associated with TIMP3 which probably acts as a major factor to the typical accumulation of fibrosis observed in NS cHL.

2   Introduction

2.1   The lymph node

Lymph nodes (LN) are organs of the secondary lymphatic system and can vary in size ranging from a few millimeters to > 1 cm. The human body consists of up to 450 lymph nodes (Ozdowski & Gupta, 2020; Willard-Mack, 2006) in adults (*can vary across literature) distributed throughout the body. LN facilitate immune response after appearance of organism-foreign agents to antigen presenting cells (APCs) and maturation of lymphocytes in order to expose them to an afferent extracellular fluid. They are soft tissues displaying the highest concentration of lymphocytes in the human body and are referred to as a side of lymphocyte activation and production.

2.1.1   Location and function

Lymph nodes (LN) are distributed in the interstitial space in discrete anatomical areas and can be single or grouped, fixed or mobile. They appear along the lymphatic system and build clusters in a few regions. Afferent lymph vessels bring in lymph from the blood system that is drained out after passing the LN through the efferent vessel (Tak W. Mak et al., 2008; von Andrian & Mempel, 2003). Cervical nodes drain the lymph in the head and neck region, axillary LN drain the lymph in the thoracic region and further clusters of LN occur auricular, inguinal, abdominal (supraclavicular), in the mediastinum, neck, pelvis, in association with blood vessels of the intestines and popliteal among others. LN are kidney-shaped encapsulated (Tak W. Mak et al., 2008) tissues containing high concentrations of lymphocytes, antigen-presenting cells (APC) and follicular dendritic cells as well as reticular cells building the lymph node skeleton (Hirosue & Dubrot, 2015; Willard-Mack, 2006). In brief, APCs present antigens to lymphocytes (Kaldjian et al., 2001). Reactive lymphocytes undergo clonal expansion to produce new lymphocytes and plasma cells which secrete antibodies into the lymph. The reticular network or discrete mass of fibrovascular tissue of mesenchymal origin organises (Bailey et al., 2018; Eikelenboom et al., 1978; Mebius, 2003; Roozendaal et al., 2008; Willard-Mack, 2006) the LN architecture and orchestrates the interaction of cells of the primary immune response (Anderson & Shaw, 1993; J E Gretz et al., 1996; J. Elizabeth Gretz et al., 1997).

2.1.2   Architecture and composition of the lymph node

Reticular connective fibers consist of a dense connective tissue of reticular cells producing collagenous fibers. These fibers compose the LN capsule as a unit of membranous structures or trabeculae extending from the inner surface towards the medullary centre of the node referred to as the subcapsular sinus. The medulla contains medullary cords, blood vessels and the sinuses. In general, the medulla contains less cells. Fibroblastic reticular cells (FRC) are a specialised form of myofibroblasts which create the lymph node skeleton with its conduit system (Anderson & Shaw, 1993; J E Gretz et al., 1996; J. Elizabeth Gretz et al., 1997, 2000; Roozendaal et al., 2008) and the hilus. The lymphatic endothelium lines the sac from where sinuses arise surrounding the lobules that differentiate of the mesenchymal tissue. The lobules are subdivisions of the LN and consist of the cortex, the paracortex and the medulla containing follicle B lymphocytes (B cells = BC) and T lymphocytes (T cells = TC), respectively (Brown & Turley, 2015; Ozdowski & Gupta, 2020; von Andrian & Mempel, 2003; Willard-Mack, 2006). The cortex displays the outer segment of a LN located underneath the capsule and subcapsular sinus and is further subdivided into the outer cortex where inactivated BC occur as follicles and the paracortex (von Andrian & Mempel, 2003). Figure 1 depicts a schematic and simplified overview of the architecture and cellular composition of the lymph node (adapted from (Miyasaka & Tanaka, 2004; Stebegg et al., 2018)).

Within the lobules APCs carried in the lymph drain, and lymphocytes and inflammatory mediators (secretory factors such as cytokines among others) are brought together (J. Elizabeth Gretz et al., 2000; von Andrian & Mempel, 2003). When activated, the BC follicles can develop into germinal centres. The paracortex is located deeper within a lymph node mainly consisting of TC (Haley et al., 2005). The FRC network within the paracortex is dense and it comprises up to 50% of the non-hematopoietic compartment in the lymph node (Fletcher et al., 2015; Fletcher, Malhotra, Acton, et al., 2011).
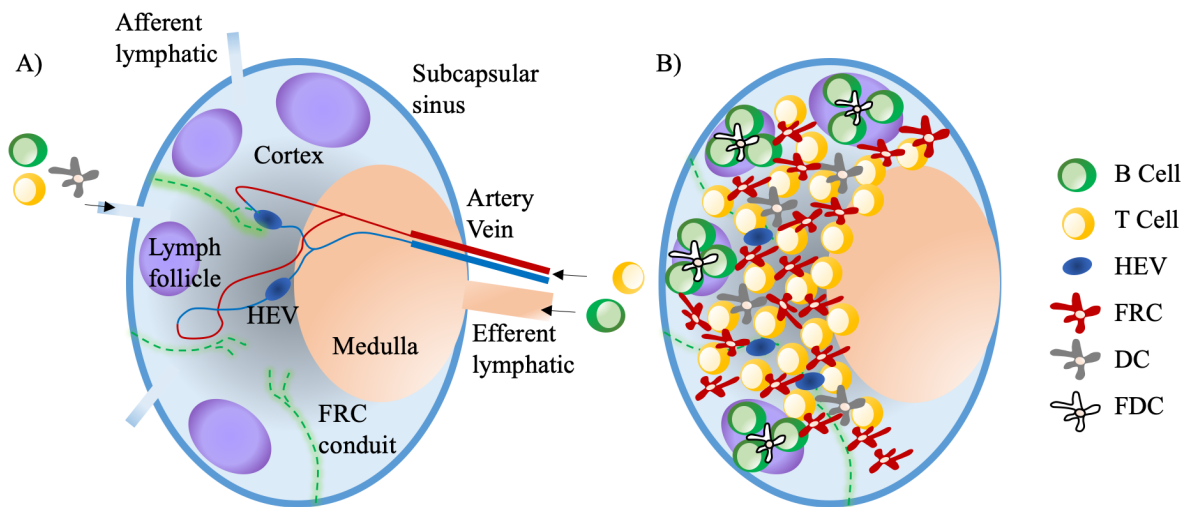
Figure 1: LN Architecture and cellular composition.

Reticular connective fibres consist of a dense connective tissue of reticular cells (FRC) producing collagenous fibres. (A) These fibres compose the LN capsule as a unit of membranous structures or trabeculae extending from the inner surface towards the medullary centre of the node referred to as the subcapsular sinus. The medulla contains medullary cords, blood vessels (artery in red, vein in blue), post capillary venous swellings (high endothelial venules (HEV)) and the sinuses. In general, the medulla contains less cells. (B) FRC are a specialised form of myofibroblasts which create the lymph node skeleton with its conduit system (green dotted line). The lobules are subdivisions of the LN and consist of the cortex, the paracortex and the medulla containing follicle B lymphocytes (B cells = BC) and T lymphocytes (T cells = TC), respectively. The cortex displays the outer segment of a LN located underneath the capsule and subcapsular sinus and is further subdivided into the outer cortex where inactivated BC occur as follicles and the paracortex. (schematic and simplified overview adapted from (Miyasaka & Tanaka, 2004; Stebegg et al., 2018).

2.1.3   The fibroblastic reticular network of the lymph node

Different subsets of FRCs are reported according to their location and function within the LN. FRCs of the (i) TC zone maintain the TC zone by the attraction of TC and construct the conduit network, (ii) BC zone FRCs maintain the BC zone and germinal centres and facilitate BC survival and proliferation (Cremasco et al., 2014; J E Gretz et al., 1996; Kaldjian et al., 2001; Malhotra et al., 2012, 2013), (iii) marginal FRCs located subcapsular can differentiate into follicular dendritic cells (FDC) and display IL-7 upon acute infection among others, (iv) this subset is represented by FRCs differentiated into FDCs which in return are migrating using the FRC network (Brendolan & Caamaño, 2012; Malhotra et

al., 2012) and (v) pericytic FRCs that are located around the high endothelial venules (HEV) for maintenance, permeability control and signalling to platelets (Chyou et al., 2008; Fletcher et al., 2015).

The most important role of FRCs located in the paracortex of LN is to directly activate lymphocyte trafficking during clonal expansion by producing and maintaining the tension through collagenous reticular fibers (Fletcher et al., 2015; Hayakawa et al., 1988; Miyasaka & Tanaka, 2004; Tykocinski et al., 1983; Vega et al., 2006). They express self-antigens representing tissue-specific features in order to induce CD8 TC tolerance induction for the prevention of autoimmunity (Cohen et al., 2010; Fletcher et al., 2010; Fletcher, Malhotra, & Turley, 2011; Leavy, 2010) response. Animal models have shown FRCs presenting tissue-restricted self-antigens and deleting autoreactive TC clones (J. W. Lee et al., 2007; Magnusson et al., 2008). They further control effector TC proliferation and affect regulatory TC (Treg) by the acquisition of MHC class II peptide-complexes from dendritic cells (DC) (Dubrot et al., 2014; Siegert et al., 2011; Siegert & Luther, 2012; Yang et al., 2014). The immunosuppressive role of FRCs preventing autoimmunity and damage to the LN infrastructure by preventive TC deletion during immune response is an established theory (Fletcher, Malhotra, & Turley, 2011; Siegert & Luther, 2012; Yang et al., 2014). Graw *et al.* have analysed the disruption of the FRC network- and seen that by losing filaments cell migration and trafficking in secondary lymphoid tissues is reduced (Graw & Regoes, 2012).

However, FRC contractility and proliferation is altered during pathogenesis of LN diseases (Astarita et al., 2015a; Martinez et al., 2019). A hallmark of the initiation of an immune response is the proliferation of FRCs and subsequent expansion of the LN to orchestrate clonal expansion of activated TC and BC by elongation as well as releasing the tension (stretching) prior to proliferation (Acton et al., 2014; Astarita et al., 2015b). Briefly, the transmembrane protein Podoplanin facilitates FRC contraction which signals through Ezrin, Radixin and Moesin (ERM proteins) to Ras homolog family member A (RhoA). Upon inflammation, activated DC express C-type lectin-like receptor (Clec2) which, by binding, impairs Podoplanin signalling resulting in FRC relaxation as shown in Figure 2 (adapted from (Vaahtomeri & Sixt, 2014)) (Acton et al., 2014; Astarita et al., 2015b; Martinez et al., 2019; Vaahtomeri & Sixt, 2014).

Figure 2: The process of proliferation of FRCs and subsequent expansion of the LN during immune response.

(A) The transmembrane protein Podoplanin (dark blue bar) facilitates FRC contraction which signals through Ezrin Radixin and Moesin (ERM proteins, light blue symbol) to RhoA (yellow symbol) and subsequent signaling towards myosin (pink symbol). (B) Upon inflammation, activated DC express C-type lectin-like receptor (Clec2, grey bar) which, by binding, impairs Podoplanin signaling resulting in FRC relaxation and elongation. (C) Once acute inflammation is ruled out FRCs accommodate recovery by IL7 expression which attracts IL7 receptor expressing TC. During extended immune response Treg secrete TGFβ isoform 1 which suppresses the activated immune response. TGFβ though, activates FRCs´collagen synthesis.

Once acute inflammation is ruled out, FRCs accommodate recovery by IL7 expression which attracts IL7 receptor expressing TC (Onder et al., 2012). In contrast, chronic inflammation can damage FRCs and impair systemic immune response (Martinez et al., 2019). During extended immune response Treg secrete TGFβ isoform 1 which suppresses the activated immune response. TGFβ though, activates FRCs´ collagen synthesis causing its accumulation (Scandella et al., 2008). Fibrosis makes the FRC network inaccessible to lymphocytes (Fletcher et al., 2015; Malhotra et al., 2013; Vaahtomeri & Sixt, 2014) resulting in a loss of survival signaling among different cell fractions (Figure 3; adapted from (Fletcher et al., 2015; Vaahtomeri & Sixt, 2014)).

Figure 3: Accumulation of fibrosis is facilitated through enduring inflammation.

(A) Once acute inflammation is ruled out FRCs accommodate recovery by IL7 expression which attracts IL7 receptor (IL7R) expressing TC. During extended immune response Treg secrete TGFβ isoform 1 which suppresses the activated immune response. TGFβ though, activates FRCs´ collagen synthesis. (B) Causing its accumulation fibrosis makes the FRC network inaccessible to lymphocytes resulting in a loss of survival signaling among different cell fractions.

2.2 Lymphadenopathies

Compartmental enlargement and transformation of a LN is well characterised by morphologic and immunologic appearance in different compartments. The etiology of Lymphadenopathies includes infectious disease, inflammatory disease, autoimmune disease, exposure to toxins and medication (Baum & Davis, 2014), metabolic storage disorder and neoplasms (Schwab, 2014). Some of the benign variations are opposed to malignant counterparts in Table 1 (Mills, 2012).

Table 1: Benign and malignant lymphadenopathies occurring within different compartments of the lymph node (Mills, 2012).

Compartment	Benign	Malignant
Follicle	Follicular hyperplasia	Follicular lymphoma
Paracortex	Paracortical hyperplasia Dermatopathic lymphadenopathy	T Cell non-Hodgkin lymphoma Mycosis fungoides
Medullary cords	Medullary hyperplasia Reactive plasmocytosis	Lymphoplasmacytic lymphoma Plasmacytoma
Sinuses	Sinus histiocytosis	Malignant histiocytosis

Benign transformation of the LN can occur localised and generalised and is mostly of self-limiting etiology. In the course of lymphadenopathy there is a multiplication of responding immune cells and an enlargement of the LN itself. Generally, it appears predominantly localised with the majority of lymphadenopathies being present in the head and neck region (Schwab, 2014). Follicular changes mostly occur in LN in the vicinity of an inflammation due to bacterial and viral infection, autoimmune conditions and idiopathic conditions such as reactive LN hyperplasia with strongly enlarged follicles. Benign lesions are defined by morphologic criteria such as well-defined mantle zones and follicle zonation, difference in size and shape of the follicles, increased mitotic figures, intact FDC network and cellular pleomorphism of the follicles. Upon benign transformation of the Paracortex various differential diagnoses can be considered that have different etiologies by the proliferation of predominantly small lymphocytes or equal expansion of blasts but intact paracortical architecture and cellular pleomorphism (Baum & Davis, 2014). Within the Medullary cords a preserved LN architecture and the presence of plasma cell precursors is a feature of a benign condition. Sinusoidal changes arise in LN draining tumours or inflammatory reactions resulting in sinus histiocytosis in which histiocytes surround lymphocytes without extinguishing them. Furthermore, the sinusoidal pattern is intact. The features of benign transformation can occur combined which is observed rarely in malignant conditions of the LN.

2.3   Malignant transformation of the LN

The WHO classification of tumours of the hematopoietic and lymphoid tissue (S.H. Swerdlow, E. Campo, N.L. Harris, E.S. Jaffe, S.A. Pileri, H. Stein, 2017) defines the following entities, (i) precursor lymphoid neoplasms, (ii) mature B cell lymphomas, (iii) mature T- and natural killer (NK) cell neoplasms and (iv) Hodgkin lymphomas. The entities are characterised their morphology, immunophenotype, genetic alterations reflecting a characteristic cell of origin and clinical features. As described by Scott and Gascoyne the cell of origin arises likewise the benign lymphadenopathies from different areas within the LN namely the follicles and germinal centers (GC) within the BC zone and cortex. Burkitt lymphoma (BL), Follicular lymphoma (FL) and Diffuse large B cell lymphoma (DLBCL) cells of origin most prominently acquire their transformation while entering the GC where somatic hypermutation (SHM) takes place which can be detected. Mantle cell lymphomas (MCL) mostly arise from naïve B cells but also after GC maturation from memory B cells. Marginal zone lymphoma (MZL) cells of origin arise from the marginal zone of follicles whereas primary mediastinal B cell lymphomas and classic Hodgkin lymphomas (cHL) arise of a germinal or post-germinal center origin supporting the theory of SHM (Thomas et al., 2004). Next to the identification of the cell of origin, the composition of the microenvironment of each entity is characteristic. BL is assigned as an entity effacing its environment by rapid expansion of neoplastic cells leading to a neoplastic cell content of up to 90%. The ratio of neoplastic cells to microenvironment decreases in DLBCL, MCL and FL following the strategy of neoplastic expansion accompanied by an re-education of the microenvironment for self-sustain. A third and rather different strategy is observed in cHL. The neoplastic cells of cHL namely Hodgkin-Reed-Sternberg (HRS) cells are rarely distributed within the infiltrated LN (Schmitz et al., 2009). The majority of the microenvironment in cHL sustains a pro-survival immunosuppressive niche for HRS cells which initially recruited and orchestrated their surrounding cells (Aldinucci et al., 2004, 2010).

2.4   Classical Hodgkin lymphoma

A total of 95% Hodgkin lymphomas are classic Hodgkin lymphomas which are one of the most frequent malignant lymphomas in the western world showing an incidence of around 3 cases per 100.000 per year (S.H. Swerdlow, E. Campo, N.L. Harris, E.S. Jaffe, S.A. Pileri, H. Stein, 2017; Swerdlow & Cook, 2020; Villanova et al., 2020). Unlike in most other types of B cell lymphoma, the tumour cells in cHL, the Hodgkin-Reed-Sternberg (HRS) cells only represent a minority in the infiltrate, frequently around 1% (Schmitz et al., 2009). In Western Europe, the nodular sclerosing (NS cHL) subtype is most frequently observed (around 80%). This subtype mainly affects adolescents, occurs frequently in the cervical and mediastinal localisation and is usually not EBV-associated unlike mixed cellularity subtype (MC) of cHL (Küppers et al., 2012). The proliferation of fibroblasts within NS cHL infiltrated LN is observed, leading to sclerosing bands, that confine nodular compartments (Swerdlow & Cook, 2020; *WHO Classification of Tumours of Haematopoietic and Lymphoid Tissues*, 2017). The typical architecture of the LN is not preserved as can be seen in representative stainings (H&E and Actin expression) in Figure 4 by the comparison of a reactive LN and a lymph node diagnosed with NS cHL.
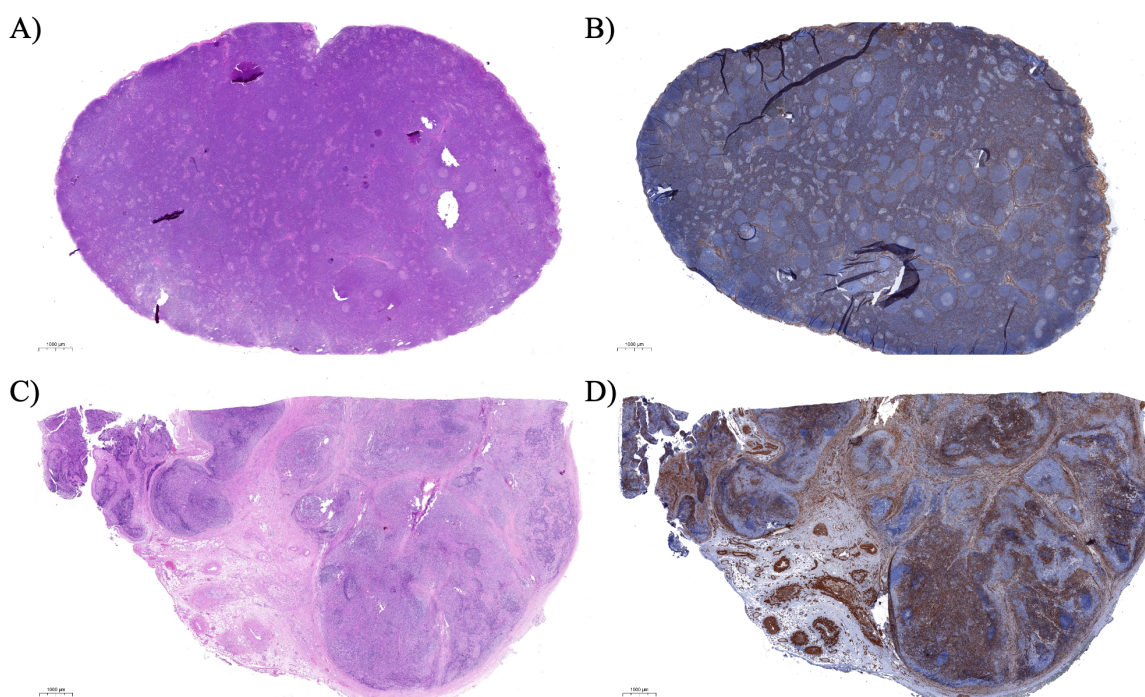
Figure 4: Unspecific reactive lymphoadenitis vs. nodular sclerosing classical Hodgkin lymphoma lymph nodes.

(A) H&E stained whole slide image (WSI) of a lymph node (LN) with unspecific reactive lymphoadenitis (LA) and its corresponding (B) fibroblastic reticular network visualised by alpha smooth muscle actin (αSMA) immunohistochemistry (IHC, detection system DAB, brown colour). Follicles are surrounded by FRCs that also set up the capsule. (C) Prominent sclerotic bands consisting of accumulated activated FRCs expand all over the LN. The light areas poorly allow round cell infiltrate and rearrange the LN architecture and structure. Follicles look irregular and loose. (D) The accumulation of the activated FRC network is visualised by αSMA IHC. (scale bar indicates 1000 µM)

cHL is eminently curable and achieve long-term remission rates even though two-third exhibit intrathoracic involvement. The clinicopathological staging of cHL depends on the involvement of infiltrated sites such as single or multiple LN and further lymphatic organs, the region allocated below to the diaphragm and involvement of further extranodal tissues (Diehl et al., 2004). Another subtype of cHL considered in this thesis is the mixed cellularity (MC) cHL often associated with EBV infection and also more often occurring in children as well as elderly.

2.5   Hodgkin-Reed-Sternberg cells

HRS cells carry clonal and somatically mutated rearrangements of their Immunglobulins (Ig) genes accounting loss of function mutations and nonsense mutations (Kuppers et al., 1994; Küppers et al., 2012; Küppers & Rajewsky, 1998; Marafioti et al., 2000; Tiacci et al., 2012) which would make them prone to negative selection in the GC and subsequent apoptosis. The neoplastic giant GC- derived HRS cells survive negative selection in the GC in dependence of deregulated NFκB signaling which in turn enhances the expression and secretion of Interleukin 6 (IL6) among others which is evidently associated with a worse prognosis (Aldinucci et al., 2004b; Villanova et al., 2020). HRS cells usually lack the characteristic BC phenotype by the loss of BC markers (CD19, CD20, CD79a) and can be detected by the expression of Tumour Necrosis Factor Receptor Superfamily, Member 8 (TNFRSF8) also called CD30 activation marker (Küppers et al., 2012; Schmitz et al., 2009; S.H. Swerdlow, E. Campo, N.L. Harris, E.S. Jaffe, S.A. Pileri, H. Stein, 2017). HRS cells further express markers related to other cell types such as T cell markers (CD3, NOTCH1, GATA3), cytotoxic cells (granzyme B, perforin), some still exhibit B cell markers (CD20, PAX5), dendritic cell markers (fascin, CCL17), NK cell markers (ID2), myeloid cell markers (CSFR1), and granulocyte markers (CD15) (Küppers et al., 2012). The HRS cells are composed of mononuclear Hodgkin cells and giant multinucleated Reed-Sternberg cells. Rengstl *et al.* have observed that Reed-Sternberg cells are generated by re-fusion of small mononuclear Hodgkin cells by either incomplete cytokinesis or nuclear division without cellular division (Küppers et al., 2012; Rengstl et al., 2013, 2014). Moreover, HRS cells exhibit constitutive active signaling of the JAK/STAT by autocrine Interleukin13 (IL13) expression (Ohshima et al., 2001; Oshima & Puri, 2001), NOTCH1 and aforementioned NFκB pathway which are usually only momentarily active in normal B cells. More pathways are altered in HRS cells such as PI3K/AKT and MAPK/ERK pathway all contributing to pro-survival signaling of HRS cells and partially involved in the accumulation of fibrosis through the FRC network as Figure 5 shows exemplarily.
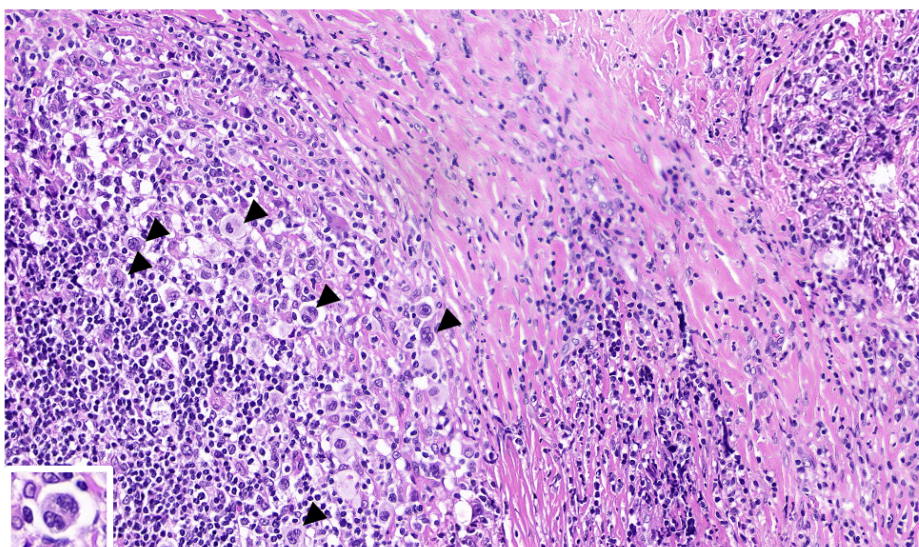
Figure 5: Hodgkin-Reed-Sternberg cells in a case of nodular sclerosing classical Hodgkin lymphoma.

Hodgkin-Reed-Sternberg cells (HRS, indicated by black arrows, enlarged in the bottom left corner) are mono- or multinucleated comparably giant cells within the infiltrated lymph node (LN) of nodular sclerosing classical Hodgkin lymphoma (NS cHL) case. Neoplastic cell fraction (here HRS cells) constitutes the smallest fraction among other round cell infiltrates and cells accumulating within the sclerotic bands (activated fibroblastic reticular cells (FRC), light-coloured bands). (H&E stain, 20x)

Table 2 gives a brief overview of the multifaceted signaling between HRS cells and its microenvironment resulting in recruitment and stimulation of further infiltrate in order to shape a beneficial niche while suppressing the immune response (Küppers et al., 2012; Scott & Gascoyne, 2014; Wein & Küppers, 2016).

Table 2: The multifaceted signalling between Hodgkin-Reed-Sternberg cells and their surrounding cells.

Hodgkin-Reed-Sternberg cells (HRS) show a complex interplay with their surrounding cells. The tables briefly sums up the involved molecules expressed by HRS cells and their corresponding counterpart within the microenvironment and its consequence between the involved cells. Some functions and molecules marked by asterisk (*) became prominent feature in diagnostics of classical Hodgkin lymphoma and are clinically important (Küppers et al., 2012; Scott & Gascoyne, 2014).

Signalling derived from	Microenvironment	HRS cells	Consequence	Clinically of importance
T helper cell (CD4+)	CD40L CD80	CD40 CD28	Attraction	

Signalling derived from	Microenvironment	HRS cells	Consequence	Clinically of importance
Regulatory T cell	CD54 IL4; IL13 CCR CCR	CD18/11a IL Receptors CCL5, CCL22 CCL5, CCL22, CCL20, TARC Galectin1	Adhesion & Rosetting* Attraction & Expansion	*Diagnosis
Eosinophil	CD30L ILR CCR5	CD30* IL5, IL9 CCL5 Eotaxin	Attraction	*Diagnosis and treatment by Brentuximab-Vedotin (BV)
Mast Cell	CD30L CCR5	CD30* CCL5	Attraction	*BV therapy
Neutrophil	NGF APRIL	TRKA BCMA	Stimulation	
Macrophages*		MIF CSF1*	Stimulation	*discussed as prognostic factor (Diehl, 2010; Staege et al., 2015; Steidl et al., 2010; Werner et al., 2020)
NK cells		TGFβ IL10 HLAG	Inhibition	
Cytotoxic T cell (CD8+)	PD1 CD95	PD1L* CD95L MIF, Galectin1 TGFβ IL10	Inhibition	*Checkpoint-Inhibitor therapy option (Mottok, 2020; Sasse et al., 2020)
FRC*(Aldinucci et al., 2004b)	TGFβ1R IL6, IL7R	TGFβ IL6, IL7 TNFα, βFGF (Aldinucci et al., 2004b)	Attraction & Stimulation	*Diagnosis of sclerotic bands

2.6   Cancer associated fibroblasts

Malignant cells recruit and re-educate their surrounding cells to establish a tumour-supportive milieu. Cancer associated fibroblasts (CAF) are considered as one compound of the tumour microenvironment belonging to the next generation hallmarks of cancer as stated by Hanahan and Weinberg in 2011 (Hanahan & Weinberg, 2011) which is the extension of their previous published work where they already recognised their presence within tumours as complex tissues (Hanahan & Weinberg, 2000). This explains that besides the acquisition of typically tumour-supportive features by the neoplastic cell itself emerging and enabling hallmarks refer to the deregulation of cellular energetics, immune destruction and tumour-promoting inflammation and genomic instability, respectively. The tumour microenvironment is often reprogrammed or orchestrated, respectively by its neoplastic cells in order to sustain a complex signaling network, which is of importance to tumour pathogenesis. The authors further state that two types of CAF mature with either similarity to fibroblasts as a supporting structural network or myofibroblasts that can be identified by their expression of αSMA contributing to inflammation. Dvorak *et al.* has compared tumours of non-healing wounds as one neoplastic hallmark very early limiting it to solid tumours (Flier et al., 1986) which was corrected by Schäfer et al. stating that carcinomas are in fact overhealing wounds (Schäfer & Werner, 2008). Öhlund *et al.* specified the suggested heterogeneity of CAF among cancers and their accommodation of many next generation hallmarks (Hanahan & Weinberg, 2011) within the cancer wound (Öhlund et al., 2014, 2017). They may drive angiogenesis, invasion and metastasis and rule the composition and strength of the extracellular matrix (ECM). Öhlund *et al.* further illustrated basic principles for clinical applications by targeting, (i) the stromal barrier, (ii) CAF-secreted factors, (iii) ECM interactions and (iv) the CAF itself (Öhlund et al., 2014).

This also affects the biology and function of FRCs within transformed LN. Once reprogrammed to (CAFs), they induce the remodeling of the ECM (Öhlund et al., 2014). It was reported that CAFs are able to protect lymphoma cells from apoptosis induced by chemotherapeutic treatments with Rituximab, Bortezumib and ABT-737 *in vitro* (Celegato et al., 2014; Mraz et al., 2011; Staiger et al., 2017). The protective effect seems to be achieved through the induction of drug tolerance and anti-apoptotic signaling (Singh et al., 2011; Staiger et al., 2017). Accordingly, the induction of ABC-transporters was shown *in vitro* for CAFs isolated from LNs affected by follicular lymphoma (FL) and diffuse large B

cell lymphoma (DLBCL) (Singh et al., 2011). In the microenvironment of NS HL cases CAFs and the collagen-rich ECM show crosstalk with the HRS cells (Aldinucci et al., 2010, 2012, 2016; Aldinucci & Colombatti, 2014; Cattaruzza et al., 2009). HRS cells secrete IL7, which stimulates CAFs to produce high levels of IL6, acting as a costimulatory factor for regulatory T cells (Tregs) and helping to create a tumour-supportive microenvironment (Cattaruzza et al., 2009). In addition, both molecules are overrepresented in the serum of cHL patients and correlate with an advanced stage of the disease (Aldinucci et al., 2011). Both primary HRS cells and cHL-derived cell lines were shown to express the matching receptors revealing an important paracrine crosstalk (S. M. Hsu et al., 1995; Tesch et al., 1992). HRS cells attract several types of bystander cells like eosinophils, mast cells and CD4+ cells by secretion of CCL5 (Fischer et al., 2003; Ma et al., 2008) (refer to Table 2). Furthermore, they secrete IL13 (Oshima & Puri, 2001) and Tumour Necrosis Factor alpha (TNFα), which induces the additional expression of Eotaxin and CCL5 by fibroblasts, thus attracting eosinophils. In NS HL, eosinophils were shown to display high levels of mRNA of TGFβ (Kadin et al., 1993; Karai et al., 2013). The production of profibrotic cytokines is higher in NS cHL compared to MC cHL (Karai et al., 2013; Oshima & Puri, 2001) explaining the pronounced fibrosis and sclerosis in the NS subtype.

2.7 Objectives

At present, literature suggests that CAFs are responsible for the typical fibrosis and sclerosis in the NS cHL subtype are important for the survival of the HRS cells in this subtype. However, the exact underlying molecular mechanisms are only partly understood. Aim of the present study was to better characterise these cHL-associated CAFs based on molecular features and elucidate the mechanisms involved in the crosstalk with HRS cells. Therefore, the following objectives are set up within this thesis. Objective 1, primary cases of unspecific reactive LN and cHL will be collected in order to isolate CAF by the described methods (refer to 3.2.1.3 and 3.2.1.4). Objective 2, upon confirmed diagnosis and feasibility of the cells (refer to 3.2.1.6) activated FRC´s transcriptome will be studied depending on pathological origin (LA, MC cHL and NS cHL) in order to identify prominent deregulated transcripts in NS cHL for further validation using independent methods (qPCR, refer to 3.2.2.5) and translational verification of selected key players in an independent cohort on protein level (IHC, refer to 3.2.2.8). Objective 3, methylation profiling (refer to 3.2.2.6) will be applied to selected specimens of CAF in order to connect epigenetic modifications and expression changes in order to identify mechanisms of transcript regulation and their stability. Objective 4 aims at studying the impact of CAF on HRS cells *in vitro* and vice versa by the application of secreted factors within the cells´ supernatant. It is considered that the cells will enhance each other's growth or proliferation in a paracrine manner mimicking distant signaling within infiltrated tissues. Besides this, it is of interest if literature mining can reveal a drug targeting key players in NS cHL CAF and affecting their expression. Objective 5 intents to study the direct interaction of CAF and HRS cells by designing a suited coculture model. The purpose of objective 4 and 5 is to understand the interplay and signaling between NS cHL CAF and HRS cells and the impact on drug susceptibility towards Brentuximab-Vedotin as reported in previous studies addressing lymphoma microenvironment (Celegato et al., 2014; Mraz et al., 2011; Staiger et al., 2017). To study the effects of paracrine and direct interplay of neoplastic and microenvironment cells, as well as the growth and proliferation of cells, numerous methods will be applied to cover expression changes on transcript and protein level. In case of a positive interaction of both fractions, the mechanisms of adherence and its inhibition by targeting binding molecules will be elucidated in order to identify the key binding factors. Apoptosis will be quantified to estimate the impact on cellular survival or death, respectively (refer to 3.2.1).

3 Material and methods

3.1 Materials

3.1.1 Antibodies

Antibodies used and their technical application in this study are depicted in Table 3.

Table 3: Antibodies

Ag, antigen; F, Flow Cytometry; F-Iso, Flow Cytometry Isotype control; ICF, Intracellular Flow Cytometry; ICF-Iso, ICF Isotype Control; IHC, Immunohistochemistry; BA, Blocking Antibody; BA-Iso, Blocking Antibody Isotype Control; IFA, Immunofluorescence assay; ms, mouse; rt, rat; rHu, recombinant human; g, goat; rb, rabbit.

Ag	Conjugate	Host	Isotype	Supplier	Catalogue ID	Clone	App-lication
CD29	PE	ms	IgG1, k	eBioscience, San Diego, CA, US	12-0299	TS2/16	F
CD45	APC-H7	ms	IgG1	BD, Franklin Lakes, NJ, US	560178	2D1	F
CD90	PE-Cy7	ms	IgG1, κ	BD, Franklin Lakes, NJ, US	561558	5 E10	F
CD146	VioBlue	ms	IgG1, κ	BD, Franklin Lakes, NJ, US	562136	P1H12	F
CD271	FITC	ms	IgG1	Miltenyi Biotec, Bergisch Gladbach, Germany	130-098-103	ME20.4-1.H4	F
CD362	APC	rt	IgG2B	R&D Systems, Minneapolis, MN, US	FAB 2965A	305515	F
CD73	FITC	ms	IgG1κ	Miltenyi Biotec, Bergisch Gladbach, Germany	130-095-183	AD2	F
IgG1	APC	ms	-	Miltenyi Biotec, Bergisch Gladbach, Germany	130-098-846	X-56	F-Iso
REA (S)	VioBlue	rHu	-	Miltenyi Biotec, Bergisch Gladbach, Germany	130-104-609	REA293	ICF-Iso

Ag	Conjugate	Host	Isotype	Supplier	Catalogue ID	Clone	App-lication
IgG2b	VioBlue	rt	-	Miltenyi Biotec, Bergisch Gladbach, Germany	130-102-661	ES26-5E12.4	F-Iso
REA (I)	VioBlue	rHu	-	Miltenyi Biotec, Bergisch Gladbach, Germany	130-108-346	REA293	ICF-Iso
TIMP3	APC	rHu	IgG1	Miltenyi Biotec, Bergisch Gladbach, Germany	130-106-480	REA417	ICF
TIMP3	-	ms	IgG1	LSB, Seattle, WA, US	LS-B2576	na	IHC
INHBA	-	rb	IgG	LSB, Seattle, WA, US	LS-B13396	na	IHC
Cal-ponin	-	ms	IgG1	DAKO, Jena, Germany	M355601-2	CALP	IHC
Actin	-	ms	IgG2a	DAKO, Jena, Germany	GA611	1A4	IHC
CD18	-	g	IgG	R&D Systems, Minneapolis, MN, US	AF1730	na	BA
CD29	-	ms	IgG	R&D Systems, Minneapolis, MN, US	MAB17781	P5D2	BA
CD47	-	ms	IgG	R&D Systems, Minneapolis, MN, US	MAB4670	472603	BA
CD54	-	ms	IgG	Bio-Rad, Hercules, CA, US	MCA532T	84H10	BA
CD49b	-	ms	IgG	Bio-Rad, Hercules, CA, US	MCA743T	AK7	BA
IgG	-	g	-	R&D Systems, Minneapolis, MN, US	AB-108-C	na	BA-Iso
IgG	-	ms	-	R&D Systems, Minneapolis, MN, US	MAB002	11711	BA-Iso
Actin	-	ms	IgG2a	Abcam, Cambridge, UK	ab202368	1A4	IFA
CD30	-	rb	IgG	LSB, Seattle, WA, US	LS-C162069-400	na	IFA

3.1.2 Buffers and solution compositions

Buffers and solution compositions used in this study are depicted in Table 4.

Table 4: Buffers and solution compositions

Article	Catalogue ID	Supplier
EnVision FLEX Wash Buffer (20x)	DM831	DAKO, Jena, Germany
EnVision FLEX Peroxidase-Blocking	SM801	DAKO, Jena, Germany
EnVision FLEX DAB+Chromogen	DM827	DAKO, Jena, Germany
ENVision FLEX/HRP	DM802	DAKO, Jena, Germany
EnVision FLEX Hematoxylin	SM806	DAKO, Jena, Germany
Envision FLEX TargetRetrieval Solution High pH	GV804	DAKO, Jena, Germany
VectaFluor Excel RTU Antibody Kit DyLight 488 Anti-Rabbit IgG	DK-1488	Vector, Burlingame, CA, US
VectaFluor Excel RTU Antibody Kit DyLight 594 Anti-Mouse IgG	DK-2594	Vector, Burlingame, CA, US
VectaShield Hard Set Mounting Medium	H-1400	Vector, Burlingame, CA, US
DAPI	D9542-10MG	SigmaAldrich, St. Louis, MO, US

3.1.3 Cell culture media and supplements

Cell culture media and supplements used in this study are depicted in Table 5.

Table 5: Cell culture media and supplements

Article	Catalogue ID	Supplier
EDTA (0,1 mM)	AM9912	Thermo Fisher Scientific, Waltham, MA, US
DPBS [Ca^{2+}/Mg^{2+})	14040133	Thermo Fisher Scientific, Waltham, MA, US
DPBS	14190250	Thermo Fisher Scientific, Waltham, MA, US

Article	Catalogue ID	Supplier
0,05% Trypsin-EDTA	25300-054	Thermo Fisher Scientific, Waltham, MA, US
FCS, qualified, heat inactivated	10500064	Thermo Fisher Scientific, Waltham, MA, US
IMDM	21980065	Thermo Fisher Scientific, Waltham, MA, US
RPMI 1640 Medium, Glutamax	61870044	Thermo Fisher Scientific, Waltham, MA, US
Penicillin-Streptomycin (5.000 U/ml)	15070063	Thermo Fisher Scientific, Waltham, MA, US
βFGF 10 ng/ml in PBS	AS-61070	Anaspec Inc, Fremont, CA, US
Luteolin	L9283-10MG	SigmaAldrich, St. Louis, MO, US
EGCG	EGCG4143-50MG	SigmaAldrich, St. Louis, MO, US
IL6; human	200-06-20UG	Peprotech, Hamburg, Germany
IL7; human	200-07-2UG	Peprotech, Hamburg, Germany

3.1.4   Commercial kits

Commercially available kits used in this study are depicted Table 6.

Table 6: Commercial Kits

Article	Catalogue ID	Supplier
Human TIMP3 ELISA Kit PicoKine	EK0523	BosterBio, Pleasanton, CA, US
PE Annexin V Apoptosis Detection Kit I (RUO)	559763	BD, Franklin Lakes, NJ, US
CellTrace Violet Cell Proliferation Kit	C34858	Molecular Probes Inc., Eugene, OR, US
Affymetrix Gene Arrays 1.0 ST	901086	Affymetrix, Santa Clara, CA, USA
Ovation Pico WTA System V2	3302-12	NUGEN, TECAN, Männedorf, Swiss
Infinium MethylationEPIC Kit	WG-317-1001	Illumina, service testing by Atlasbiolabs, Berlin, Germany

Article	Catalogue ID	Supplier
QIAGEN RNeasy Mini Kit	74104	QIAGEN, Hilden, Germany
QIAGEN UCP DNA MicroKit	56204	QIAGEN, Hilden, Germany
PCR Mycoplasma Test Kit I/C	PK-CA91-1024	PromoCell, Heidelberg, Germany
Senescence beta-Galactosidase Staining Kit	9860	Cell Signaling Technology, Danvers, MA, US

3.1.5   Laboratory equipment and instruments

Laboratory equipment and instruments used in this study are depicted in Table 7.

Table 7: Laboratory equipment and devices

Laboratory equipment and devices	Supplier
Brightfield microscope CKX41/DP21	OLYMPUS EUROPA SE & CO. KG, Hamburg, Germany
Confocal Microscope LSM 780	Zeiss, Oberkochen, Germany
Pannoramic Scan II	3D Histech, Budapest, Hungary
Infinite M200pro	Tecan, Männedorf, Swiss
Hybridization Oven 640	Affymetrix, Santa Clara, CA, US
Fluidics Station 450	Affymetrix, Santa Clara, CA, US
GeneChip Scanner 3000	Affymetrix, Santa Clara, CA, US
Fusion SL	Vilber Lourmat, Eberhardzell
MACS Quant 2011	Miltenyi Biotec, Bergisch-Glasbach, Germany
C-Chip Neubauer Improved	Nano EnTek, Seoul, Korea

3.1.6   Patients

Fresh native lymph node specimens are regularly obtained for routine diagnostics in the Dr. Senckenberg Institute of Pathology, University Hospital Frankfurt, Frankfurt am Main. In case of remaining tissue after establishment of the diagnosis, patients were included in

the study. In all cases, the diagnosis was done according to the current WHO classification (S.H. Swerdlow, E. Campo, N.L. Harris, E.S. Jaffe, S.A. Pileri, H. Stein, 2017; Swerdlow & Cook, 2020). The local ethics committee (Ethics committee of the Medical Faculty, UKF) approved the collection and work-up of patient and non-malignant donor samples (project number SHN-3-2018) and informed written consent was obtained from the patients in accordance with the Declaration of Helsinki. Patients´ characteristics are summarised in Table 8.

Table 8: Patients

Site, r = right, l = left; na. = not available

Pseudonym	Diagnosis	Tissue	Localisation	Site	Sex
KB14	MC cHL	LN	inguinal	r	male
KB22	MC cHL	LN	cervical	l	male
KB32	MC cHL	LN	cervical	r	female
KB37	MC cHL	LN	cervical	r	male
KB40	MC cHL	LN	na	na	na
KB12	NS cHL	LN	na	l	female
FST89	NS cHL	LN	na	na	male
KB20	NS cHL	LN	neck	r	female
KB16	NS cHL	LN	cervical	l	male
KB29	NS cHL	LN	cervical	l	female
KB30	NS cHL	LN	supraclavicular	l	male
KB33	NS cHL	LN	supraclavicular	l	male
KB39	NS cHL	LN	na	na	na
FST87	LA	LN	cervical	l	male
FST88	LA	LN	cervical	l	male
FST96	LA	LN	cervical	na	male
FST97	LA	LN	cervical	l	female

Pseudonym	Diagnosis	Tissue	Localisation	Site	Sex
FST119	LA	LN	cervical	l	male
FST124	LA	LN	neck	r	female
FST125	LA	LN	Intraabdominal	na	male
KB5	LA	LN	cervical	l	male
FST123	LA	LN	cervical	r	male
KB34	LA	LN	cervical	r	male
KB35	LA	LN	cervical	l	female
KB36	LA	LN	cervical	l	female
1	LA	LN	Level 2	r	male
2	LA	LN	cervical	r	male
3	LA	LN	neck	r	female
4	LA	LN	neck	na	female
5	LA	LN	na	na	male
6	LA	LN	neck	na	male
7	LA	LN	cervical	r	female
8	LA	LN	na	na	male
9	NS cHL	LN	neck	na	female
10	NS cHL	LN	cervical	na	female
11	NS cHL	LN	supraclavicular	r	female
12	NS cHL	LN	Level 5	l	male
13	NS cHL	LN	supraclavicular	na	female
14	NS cHL	LN	supraclavicular	na	male
15	NS cHL	LN	supraclavicular	na	male
16	NS cHL	LN	na	na	female
17	NS cHL	LN	cervical	na	male
18	NS cHL	LN	cervical	l	male

Pseudonym	Diagnosis	Tissue	Localisation	Site	Sex
19	NS cHL	LN	hip	r	male
20	NS cHL	LN	supraclavicular	na	male
21	NS cHL	LN	cervical	na	male
22	NS cHL	LN	na	na	female
23	NS cHL	LN	iliacal	l	female
24	NS cHL	LN	na	na	na
25	MC cHL	LN	iliacal	l	male
26	MC cHL	LN	na	na	male
27	MC cHL	LN	na	na	female
28	MC cHL	LN	na	na	male
29	MC cHL	LN	na	na	female
30	MC cHL	LN	supraclavicular	na	na
31	MC cHL	LN	cervical	na	male
32	MC cHL	LN	neck	r	male
33	MC cHL	LN	mediastinal	na	female
34	MC cHL	LN	na	na	male
35	MC cHL	LN	neck	l	male
Fib P15	Healthy donor	Foreskin	na	na	na
Fib P40	Healthy donor	foreskin	na	na	na
FST93	Tonsillitis	tonsil	na		female
FST94	Tonsillitis	tonsil	na	na	female
FST98	Tonsillitis	tonsil	na	na	male

3.1.7 Primary cells and cell lines

Cell lines and primary generated cells used in this study are depicted in Table 9.

Table 9: Cell lines
RRID, research resource identifier

Cell line	RRID	Media	Supplier
L-428	CVCL_1361	RPMI; 10% FCS	DSMZ, Braunschweig, Germany
L-1236	CVCL_2096	RPMI; 20% FCS	DSMZ, Braunschweig, Germany
KM-H2	CVCL_1330	RPMI; 20% FCS	DSMZ, Braunschweig, Germany
Raji	CVCL_0511	RPMI; 10% FCS	DSMZ, Braunschweig, Germany
CB5B8	na	RPMI; 20% FCS	Dr. R. Küppers, UKE, Essen, Germany
Human fibroblasts	na	Isolated from human LN; IMDM; 20% FCS; βFGF 10ng/ml	na

3.1.8 TaqMan commercial assay

TaqMan commercially available assays used in this study are depicted in Table 10.

Table 10: Taqman commercial assays

Target	Reporter	Quencher	Assay-ID	Supplier
GAPDH	VIC-PL	MGB-NFQ	Hs02786624_g1	Applied Biosystems, Foster City, CA, US
ACTA2	FAM	MGB-NFQ	Hs00426835_g1	Applied Biosystems, Foster City, CA, US
CNN1	FAM	MGB-NFQ	Hs00959434_m1	Applied Biosystems, Foster City, CA, US
IL6	FAM	MGB-NFQ	Hs00174131_m1	Applied Biosystems, Foster City, CA, US
TIMP3	VIC	MGB-NFQ	Hs00165949_m1	Applied Biosystems, Foster City, CA, US
MYOCD	FAM	MGB-NFQ	Hs00538076_m1	Applied Biosystems, Foster City, CA, US
INHBA	FAM	MGB-NFQ	Hs00170103_m1	Applied Biosystems, Foster City, CA, US

3.1.9 Tools and software for data analysis, visualisation and statistics

Tools and software used in this study are depicted in Table 11.

Table 11: Software

Software	Release	Supplier
GraphPad Prism 5	5.04	Graphpad Software Inc.; La Jolla, CA, USA
Caseviewer	2.3.0.99276	3D Histech, Budapest, Hungary
iControl	2.0	Tecan Group, Männedorf, Swiss
AGCC	4.1.2.1567	Affymetrix, Santa Clara, CA, US
Fusion Software	na	Peqlab, Erlangen, München, Germany
imageJ (Schneider et al., 2012)	1.52a	NIH, Bethesda, MD, USA
Genomatix Genome Analyzer (Berriz et al., 2003)	v3.90712	Genomatix, München, Germany
Cluego (Bindea et al., 2009)	2.5.6	INSERM UMRS1138 Laboratory of integrative cancer immunology, Paris, France
Cytoscape (Bindea et al., 2009)	3.7.2	ISB, Seattle, WA, USA
MACSQuantify	2.11	Miltenyi Biotech, Bergisch Gladbach, Germany
FlowJo	6.7	TreeStar Inc; Ashland, Oregon, US

3.2 Methods

3.2.1 Cell culture

3.2.1.1 Mycoplasma detection assay

Mycoplasma detection Assay is based on polymerase chain reaction with Mycoplasma specific detection oligonucleotides and was performed according to manufacturer´s instruction. Amplified Mycoplasma DNA fragments were visualised by gel electrophoresis and fusion detection system. Only Mycoplasma free cells and cell lines were used for functional experiments.

3.2.1.2 Senescence assay

Senescence β-Galactosidase Staining Kit (CST, Danvers, MA, USA) was used according to manufacturer´s instruction to prove primary cells´ suitability for further experiments.

3.2.1.3 Fibroblast isolation from human lymph nodes

The technique of mesenchymal cell fraction isolation from lymph nodes was based on the technique applied for cardiac fibroblasts by the group of Prof. C. Gaetano (Department of Cardiology, Division of Cardiovascular Epigenetics, Frankfurt) (Meraviglia et al., 2014; Rossini et al., 2011). According to these protocols the isolation, culture and flow cytometry analysis of primary adherent monolayer populations from lymphoid tissue was established. Briefly, suspensions can be produced by mechanical disruption and dissociation of the tissue through 100 µM pore size nylon cell strainer (BD, Franklin Lakes, New Jersey, US). Obtained suspensions can be taken into primary culture either directly or after storage in liquid nitrogen in DMSO-supplemented FCS until diagnosis is confirmed. The minimum criteria defining mesenchymal cells include the typical fusiform morphology with protrusions, plastic adherence and the expression of the surface markers CD29, CD73, CD90 (Table 12) (Dominici et al., 2006). To exclude cultivation of differentiated cells of other origin the lack of expression of CD45 (lymphocytes) and CD146 (Follicular dendritic cells) are taken into account.

Furthermore, the activation state of the cells in culture was determined by analysing the expression levels of aSMA and FAP via semi-quantitative PCR. The high expression of both factors confirmed that activated fibroblastic cells were obtained. If minimum defining criteria were passed by a population cells were analysed during passage 4-6 either directly or derivates such as supernatant, DNA and RNA were harvested and stably stored until further processing. Aliquots of cells were kept for future investigations in liquid nitrogen. Remaining cells were used for functional *in vitro* investigations till passage 9. Primary cells are a subject of limited growth and availability which highly ruled the set up and feasibility of *in vitro* experiments and their reproduction. Further quality assessments of primary adherent cells include mycoplasma testing and senescence testing.

Table 12: Minimum defining criteria of mesenchymal cells according to Dominici *et al.* (Dominici et al., 2006)

Feature	Minimum Criteria
Morphology	Spindle-shaped morphology with protrusions
Adherence	Plastic-adherence under culture conditions
Surface marker phenotype	CD29++, CD73++, CD90++, CD45-, CD146-

Pathological sectioning of lymph node specimen was done by assistant physicians at Dr. Senckenberg Institute of Pathology, University Hospital Frankfurt, Frankfurt am Main.

3.2.1.4 Cultivation of primary fibroblasts

All cells were cultivated with IMDM with 1% glutamate (Thermo Fisher Scientific, Waltham, Massachusetts, US) supplemented with 20% FCS (BioChrom, Berlin, Germany), 50 µg/ml streptomycin and penicillin (Thermo Fisher Scientific), 10 ng/ml βFGF (solvent PBS; Anaspec, Fremont, CA, US) and were maintained in a humified 95% air and 5% CO_2 atmosphere at 37°C. Cell counts were determined using Neubauer chamber.

3.2.1.5 Cultivation of commercial cell lines

The cHL cell lines L-428, L-1236 and KM-H2 were obtained from the German Collection of Microorganisms and cell cultures (DSMZ, Braunschweig, Germany) and cultured in RPMI with 10-20% fetal calf serum (FCS). Another cell line used as a non-Hodgkin lymphoma control within functional experiments was Raji, also obtained by DSMZ and cultured in RPMI with 10% FCS as well as CB5B8 cell line, kindly provided by Dr. R. Küppers (Essen) cultured in RPMI with 20% FCS. All cell culture medium recipes were supplemented with 1% Penicillin-Streptomycin. Cell culture´s identity was approved by STR Analysis (data not shown, data acquisition by Kerstin Heise (Institute of Cell Biology, University Hospital Essen)) and tested for mycoplasma contamination regularly. All cell lines were maintained in a humified 95% air and 5% CO_2 atmosphere at 37°C. Cell counts were determined using Neubauer chamber.

3.2.1.6 Flow cytometry-based characterisation of primary fibroblasts

The purity of fibroblast cultures was confirmed using the minimal defining criteria of mesenchymal cells (Dominici et al., 2006) by the typical fusiform morphology with protrusions, plastic adherence under culture conditions and the expression of the surface markers. Surface marker expression was determined by Flow cytometry and immunofluorescence staining using MACSQuant analyser (Miltenyi Biotech, Bergisch Gladbach, Germany) and fluorescence-conjugated antibodies CD29-PE (clone TS2/16, Thermo Fisher Scientific), CD73-APC (clone REA804, Miltenyi Biotech), CD90-PE-Cy7 (clone 5E10, BD); CD45-APC-Cy7 (clone 2D1, BD), CD146-VioBlue (clone P1H12, BD). Adherent cells were obtained by 0,05% Trypsin-EDTA treatment, washed using PBS solution and pelleted. Staining was performed by standard procedure and the population positive for the conjugated fluorophore was acquired in comparison to a non-stained control sample and respecting isotype control staining.

3.2.1.7 Proliferation assay after paracrine stimulation of primary adherent cHL-derived CAF

Single cultured primary adherent cHL-derived CAF were treated with either lymphoma cell line conditioned supernatant, 30 µM luteolin, IL6, IL7 (peprotech, Hamburg, Germany) or combined treatments. Proliferation rate was measured using CellTrace Violet Cell Proliferation Kit (Thermo Fisher Scientific) according to manufacturer´s instruction 48 h after treatment. Median Violet Fluorescence intensity of treated cells was compared to non-treated cells and non-conditioned supernatant treated cells.

3.2.1.8 Treatment of primary fibroblasts with luteolin

Luteolin was obtained from Sigma Aldrich (St. Louis, Missouri). A working concentration of 30 µM luteolin was applied to CAF to elucidate the changes in intrinsic gene expression, target molecule secretion, followed by the described functional experiments (Gray et al., 2014; Jang et al., 2008).

3.2.1.9 Cocultures of primary fibroblasts and cell lines

The classical Hodgkin lymphoma cell lines L-428, L-1236 and KM-H2 as well as Burkitt lymphoma cell line Raji and NS cHL derived activated fibroblasts cells were used. Adherent fraction (CAF) was seeded first to obtain a typical fusiform morphology before lymphoma cells were added. The ratio of adherent primary activated fibroblasts to lymphoma cell lines was 1:5 (e.g. 6-well dish: 4×10^4 cells/well CAF to 2×10^5 cells/well lymphoma cells). Interaction of lymphoma cells and fibroblasts was determined by adherence of both fractions with each other via 3.2.1.10 Adherence assay.

3.2.1.10 Adherence assay

Adherence-based interaction of lymphoma cells and fibroblasts was determined by Brightfield microscopy of the attached fractions. Classical Hodgkin lymphoma cells remaining in suspension were removed by repeated gentle washing with PBS [Mg^{2+}, CA^{2+}]. Taken images were inverted and interacting cHL cells identified and quantified with imageJ (Schneider et al., 2012).

The following commands and parameters were used for quantitative analysis of interacting cells after coculture. Output values were divided by image area to obtain cells/mm^2.

run("Invert");

//run("Brightness/Contrast...");

setMinAndMax(-72, 74);

run("Find Maxima...", "noise=35 output=Count");

Additionally, the interaction was visualised by immune fluorescence assay and immunohistochemistry of fixed interacting coculture fractions.

3.2.1.11 Interaction assay

Four independent cocultures consisting of CAF and L-428 were set up as described previously. After 48 h of incubation floating cells were washed off and adherent coculture

fraction was harvested and lysed to obtain mixed CAF-HRS cell RNA for further gene expression analysis. A mock control consisting of separately grown fractions of CAF and L-428 cells was incubated in parallel and merged directly before lysis. CD30 expression level was assessed as an internal quality control of cellular growth of HRS cells.

3.2.1.12 Apoptosis assay and Brentuximab-Vedotin assay

Brentuximab-Vedotin (BV) was applied in high dosage of 50 µg/ml as described before (Rengstl et al., 2017) and apoptosis rates were determined in both interacting adherent coculture fraction as well as the non-interacting floating fraction by APC-Annexin V Apoptosis Detection Kit (Thermo Fisher Scientific) at 48 h. Apoptosis rates of single cHL cell line culture supplemented with fibroblast conditioned media supernatant were also determined after equal BV treatment. BV was kindly provided by PD Dr. Marco Herling (Laboratory of Lymphocyte Signaling and Oncoproteome, Cologne, Germany).

3.2.2 Molecular biology

3.2.2.1 DNA isolation

DNA Isolation was performed using QIAamp UCP DNA Micro Kit (QIAGEN, Hilden, Germany) according to manufacturer´s instruction. DNA was eluted in HPLC-grade water and used for methylation profiling.

3.2.2.2 RNA isolation

RNA Isolation was performed using RNeasy Mini Kit (QIAGEN, Hilden, Germany) according to manufacturer´s instruction. RNA of 2×10^5 cells was eluted in HPLC-grade water and used for gene expression analysis.

3.2.2.3 cDNA synthesis and amplification

cDNA was generated using total RNA, which was reversely transcribed and amplified with the Ovation Pico WTA System V2 (NUGEN, TECAN, Männedorf, Swiss) and hybridised onto Affymetrix Gene Arrays 1.0 ST (Affymetrix, Santa Clara, CA, USA) for following gene

expression analysis according to manufacturer´s instruction and *in house* established workflows. Technical implementation was run by Tanja Schaffer-Horst (technical assistant at Dr. Senckenberg Institute of Pathology, University Hospital Frankfurt, Frankfurt am Main).

3.2.2.4 Gene expression analysis

Affymetrix Gene Arrays 1.0 ST (Affymetrix, Santa Clara, CA, USA) have probe sets for 28,869 human genes with 764,885 distinct probes (Pradervand et al., 2008). Data analysis was done by Dr. phil. nat. Claudia Döring (bioinformatics scientist at Dr. Senckenberg Institute of Pathology, University Hospital Frankfurt, Frankfurt am Main). In short, signal intensities of each probe set were scaled to a target value of 2000 based on internal control transcripts for quality assessment, as provided by Affymetrix.

Statistical analysis was performed using the computing environment R (Gentleman et al., 2004). Additional software packages (affy, geneplotter, multtest, vsn) were taken from the Bioconductor project (Gentleman et al., 2004). For microarray pre-processing, Huber *et al.* variance stabilisation method was applied for probe level normalisation (Huber et al., 2002). Considering the different probe affinities via the probe effect, an additional robust model on the logarithmic scale (base 2) was fitted across the arrays for each probe set (Irizarry et al., 2003). Log2 expression values ranging from 6.5 to a maximum value of 13 were taken into account assuming that findings below are assigned to noise or non-expressed. For secondary data analysis refer to section Data analysis, visualisation and statistics. This method was published in 2008 by Brune *et al.* where detailed description can be found in the supplement (Brune et al., 2008). Gene expression data is available through the GEO database (GSE86477 and GSE153517) (Bankov et al., 2019; Rengstl et al., 2017). Selected targets were validated using quantitative PCR and immunohistochemistry (IHC) Furthermore, TIMP3 secretion was analysed using Human TIMP3 PicoKine ELISA Kit according to manufacturer´s instruction (BosterBio, Pleasanton, CA, USA) for further validation.

3.2.2.5 Quantitative real-time PCR

For polymerase chain reaction (PCR), total RNA was extracted according to the manufacturer´s instruction using RNeasy Mini Kit (Qiagen, Hilden, Germany) as described previously. Each RNA sample was reversly transcribed using the High Capacity cDNA RT Kit (Thermo Fisher Scientific). FAM-MGB-conjugated oligonucleotides were used to assess relative expression of selected prominent deregulated targets identified by previous gene expression analysis.

Taq Man Gene Expression Mastermix and above listed assays (Thermo Fisher Scientific) were used according to manufacturer´s instruction.

3.2.2.6 Methylation profiling

Methylation profiling was performed using MethylationEPIC BeadChip Kit covering 850,000 CpG sites (Illumina, San Diego, CA, USA) according to the standard protocol. Raw data was normalised using minfi package (Fortin et al., 2017). Then data was filtered for promoter tags only. Tags were considered to be differentially methylated, when there was a difference in mean methylation > 30% between two groups and the p-value was $p < 0.05$. Results are shown in unsupervised hierarchical clustering using heatmaps. DNA was sent to commercial service Atlas Biolabs, Berlin, Germany. Data normalisation was done by Dr. hab. n. med. Maciej Giefing and PhD Adam Ustaszewski from polish academy of sciences, Poznan, Poland. Data visualisation was run by Dr. phil. nat. Claudia Döring.

3.2.2.7 TIMP3 secretion assay

CAF were seeded at ratios as described previously and treated with 30 μM Luteolin. Supernatants of treated and untreated CAFs were harvested and cleared from debris by centrifugation. The assay was performed according to manufacturer´s instruction to evaluate luteolin´s influence on TIMP3 secretion. Furthermore, it was used to validate gene expression profiles of CAF after luteolin treatment.

3.2.2.8 Immunofluorescence staining *in vitro*

After coculture adherent fraction consisting of HRS cells and CAF was fixed using 4% PFA and permeabilised using Triton-X-100 solution. Cells were blocked using BSA blocking solution and washed using TBS washing solution. Dualplex fluorescence labelled antibodies were used to target Actin-structures of fibroblasts and CD30 surface antigens of cHL cell line to visualise the interaction of HRS cells and CAF.

3.2.2.9 Immunohistochemistry

Selected prominent deregulated targets identified by previous gene expression analysis and successfully confirmed by real-time PCR were chosen to be further translationally confirmed on an independent cohort of primary cases selected from the archives of the Dr. Senckenberg Institute of Pathology, University Hospital Frankfurt, Frankfurt am Main (n = 11 MC cHL specimen, n = 16 NS cHL specimen and n = 8 reactive non-malignant lymph node specimen). Immunohistochemistry for CNN1, TIMP3 and Aktin was performed using the FLEX-Envision Kit (DAKO, Glostrup, Denmark) according to manufacturer´s instruction. Primary antibodies CNN1 (Clone CALP, DAKO, dilution 1:200), TIMP3 (LS- B2576, Lifespan, dilution 1:100), and Aktin (DAKO) were used for immunohistochemical epitope staining of target molecules Calponin 1, tissue inhibitor of metalloproteinase 3 and Aktin. CNN1 primary antibody was applied for 30 min after heat induced epitope retrieval in pH9. TIMP3 primary antibody was applied for 30 min after heat induced epitope retrieval in citrate buffer (pH6) for 10 min. Nuclear counterstain was done using hematoxylin solution. Slide staining was supported by Nina Becker (technical assistant at Dr. Senckenberg Institute of Pathology, University Hospital Frankfurt, Frankfurt am Main) and interpretation of staining was supported by Prof. Dr. med. Sylvia Hartmann (senior physician and senior researcher at Dr. Senckenberg Institute of Pathology, University Hospital Frankfurt, Frankfurt am Main).

3.2.3 Data analysis, visualisation and statistics

3.2.3.1 Unsupervised hierarchical clustering of gene expression data

Unsupervised hierarchical clustering was performed with a standard deviation ≥ 1 across all samples using the Manhattan distance and the average linkage method. R-script was run by Dr. phil. nat. Claudia Döring (bioinformatics scientist at Dr. Senckenberg Institute of Pathology, University Hospital Frankfurt, Frankfurt am Main). A heat map is a false colour display of a matrix of numerical values. Heat maps were generated with Spotfire software (Spotfire DecisionSite 9.1, 1996 – 2007) (Brune et al., 2008). Highly expressed transcripts were annotated to red-ish colours whereas less expressed transcripts were annotated to green-ish colours. Resulting dendrograms were assessed using Pvclust (Suzuki & Shimodaira, 2006).

3.2.3.2 Supervised analysis of gene expression data

Differentially expressed genes were identified by reducing the dimension of the microarray data due to the fact that not all genes on the microarray were expressed across all samples or showed a small variability across all samples, respectively. An intensity filter (probe set intensity > 100 in at least 25% across all samples) and a variance filter (interquartile range of log2 intensities ≥ 0,5) were applied. Afterwards two-sample t-test was used to identify differentially expressed transcripts assuming equal variances across groups. Selection of prominent deregulated candidates was done using fold change (FC) calculation for each transcript. False discovery rates (FDR) were calculated to account for multiple testing (Benjamini & Hochberg, 1995). Analysis was run by Dr. phil. nat. Claudia Döring (bioinformatics scientist at Dr. Senckenberg Institute of Pathology, University Hospital Frankfurt, Frankfurt am Main). The applied method was established and previously described by Brune *et al.* (Brune et al., 2008).

3.2.3.3 Principal component analysis

Principal component analysis (PCA) was applied using predefined groups across all samples according to the diagnosis of the tissue of origin. PCA results were displayed using principle component 1 (PC1) and principle component 2 (PC2) plotting the

expression signature of the given gene set and the samples of all groups, respectively. Analysis was run by Dr. phil. nat. Claudia Döring (bioinformatics scientist at Dr. Senckenberg Institute of Pathology, University Hospital Frankfurt, Frankfurt am Main). Method was established and previously described by Brune *et al.* (Brune et al., 2008).

3.2.3.4 Gene set characterisation analysis

Gene set characterisation analysis was performed using the Genomatix Pathway System (Genomatix, Munich, Germany) at default parameters, listing all canonical pathways and biological terms with a significant enrichment of the provided input genes (Homo Sapiens, NCBI build 37, ElDorado 12-2013) (Berriz et al., 2003). Additionally, Cytoscape system and ClueGo App were used for functional annotation of identified gene sets. All results were created with ClueGO v2.3.3 applying features listed in Table 13 (Bindea et al., 2009).

Table 13: Cytoscape ClueGO App settings

Category	Selection
Organism analysed	Homo Sapiens [9606]
Identifier types used	[SymbolID]
Evidence codes used	[All]
n [All unique genes in selected ontologies]	18188 (Biological process) 10881 (Reactome Pathways)
Merge redundant groups with	>50.0% overlap
n [GO All Terms Specific for Cluster #1]	38 (common regulated) 51 (Luteolin)
Ontology used	GO_BiologicalProcess-GOA_17.02.2020_00h00 (common) REACTOME_Pathways_17.02.2020 (Luteolin)
Statistical Test Used	Enrichment/Depletion (Two-sided hypergeometric test)
Correction Method Used	Bonferroni step down
Min GO Level; Max GO Level	2; 4
Number of Genes; Min Percentage	5; 2,0%

Category	Selection
GO Fusion; GO Group	False; true
Kappa Score Threshold	0,5
Over View Term	SmallestPValue
Group By Kappa Statistics	true
Sharing Group Percentage	50,0

3.2.3.5 Statistical confirmatory testing

All data were tested for the presence of a Gaussian distribution by a Kolmogorov-Smirnov-test. If a Gaussian distribution was present, a One-way-ANOVA test with Bonferroni correction for multiple comparisons or a two-tailed unpaired t-test was applied, otherwise as non-parametric tests, a Kruskal-Wallis-test with Dunn´s correction for multiple comparisons or a Mann-Whitney-test were performed.

4 Results

4.1 Molecular characterisation of fibroblast cultures

Following the idea that HRS cells reprogram their environment, the first part of experiments aims at uncovering the deregulated transcripts and addresses the mechanisms of transcriptional regulation by methylation profiling.

4.1.1 Fibroblast cultures obtained from different tissue of origin show a different gene expression signature

Fibroblasts were isolated from cell suspensions of tonsil biopsy (n = 3), lymphadenitis lymph node biopsy (n = 7) and foreskin specimen (n = 2). To confirm the methods efficacy gene expression profiles were compared in a case series pilot study showed in Figure 6. The heatmap shows weakly expressed transcripts in green colour and highly expressed transcripts in red colour. The legend indicated log-based values of expression. The cells obtained from lymph node suspensions after 4-6 passages showed the typical fusiform morphology of fibroblasts with protrusions and plastic adherence. Unsupervised hierarchical gene expression clustering resulted in three major groups in dependence of their tissue of origin considering one hundred transcripts with a standard deviation larger than one. Fibroblasts isolated from human foreskin specimens that were considered to be resting fibroblasts show the most similar signature whereas fibroblasts derived from chronic reactive lymph nodes show similarity but also reveal some heterogeneity within their group. Beyond this pilot study basic surface marker expression was examined in order to exclude primary outlier cultures as described within the next chapter.
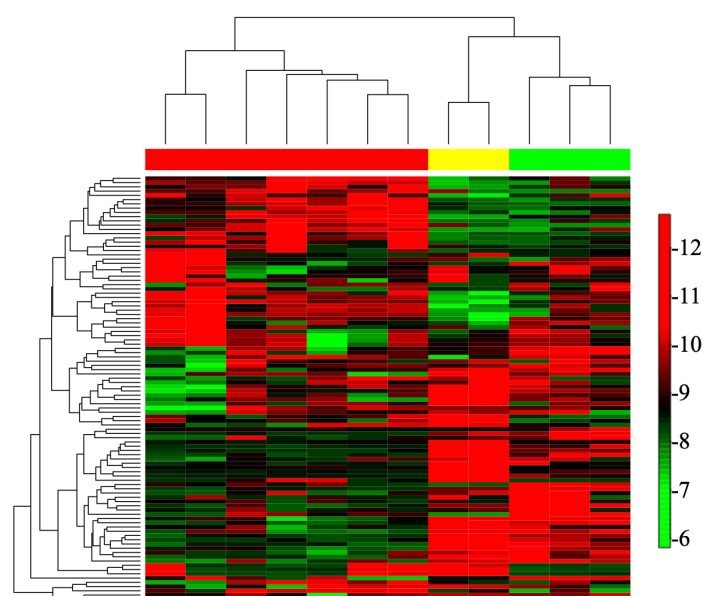
Figure 6: Fibroblasts derived from skin, tonsil and lymph node show considerable differences in their gene expression programme due to their tissue of origin.

Unsupervised hierarchical gene expression clustering of fibroblast samples derived from chronic reactive lymph node tissue (Fib LA, red-flagged, n = 7), from tonsil tissue (green-flagged, n = 3) and from skin (yellow-flagged, n = 2) considering 100 transcripts with a standard deviation >1. The heatmap shows less expressed transcripts in green colour and highly expressed transcripts in red colour. The legend indicated log-based values of expression.

4.1.2   Fibroblast cultures obtained from primary lymph node suspensions show a high purity

Fibroblasts (Fib) were isolated from cell suspensions of cHL and lymphadenitis (LA) lymph node biopsy specimens. To confirm that highly pure fibroblast cultures were obtained from primary suspensions, several steps of quality control were followed. The cells obtained from lymph node suspensions after 4-6 passages showed the typical fusiform morphology of fibroblasts with protrusions, plastic adherence (Figure 7A) alongside the expression of the surface markers CD29, CD73, CD90, and CD105 in > 94% of the cells shown in Figure 7C compared to isotype control staining (red histogram versus surface marker expression detection in blue histogram). This confirms the high purity of fibroblasts. Expression of CD45, CD146, and CD271 was lacking in the adherent cells, indicating that all cells of lymphoid origin were eliminated through the passaging procedures. Moreover, fibroblasts from all specimen express *ACTA* (Actin, Alpha 2, Smooth Muscle, Aorta) and *FAP*

transcripts (Fibroblast Activation Protein Alpha) proving their disease associated activation due to chronic reactive inflammation in LA and further malignancy associated transformation according to NS cHL and MC cHL diagnosis and following LN expansion (Figure 7B).
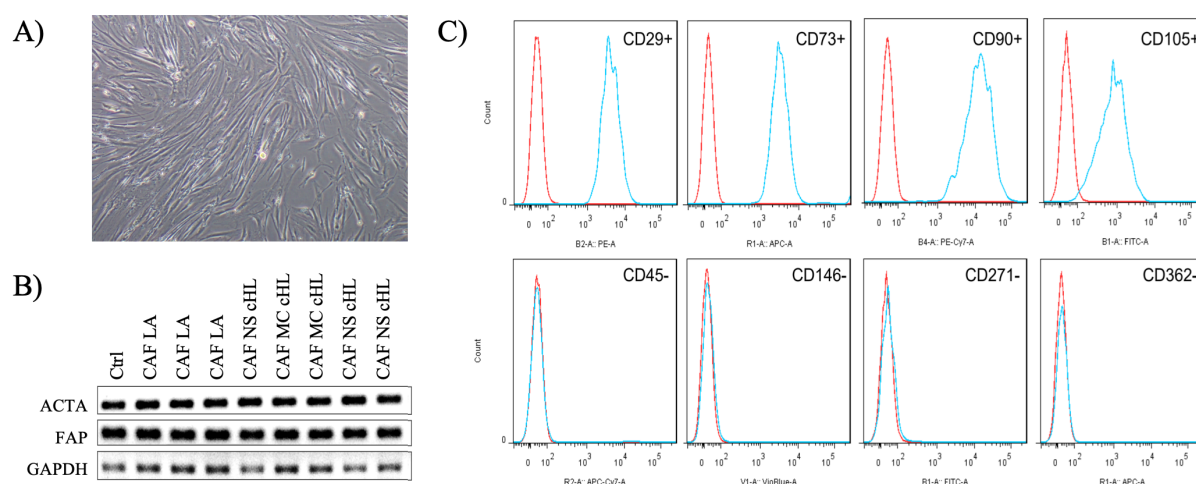
Figure 7: Characterisation of FRCs obtained from lymph nodes according to minimum criteria by Dominici *et al.* (Lupu & Menendez, 2006)

A) The typical morphology of cultured CAFs displaying a fusiform appearance. B) CAFs and activated fibroblasts typically express α-SMA and FAP. qPCR of α-SMA and FAP with GAPDH as housekeeping gene (ctrl = FRCs isolated from a non-malignant reactive LN; NS cHL = nodular sclerosing subtype of classical Hodgkin lymphoma; MC cHL = mixed cellularity subtype of cHL). C) The expression of the surface markers CD29, CD73, CD90, and CD105 as well as absence of CD45, CD146, CD271, and CD362 as determined by flow cytometry (red histogram marks isotype control staining).

4.1.3 Fibroblast cultures obtained from LN tissues of different lymphadenopathies share common regulated transcripts associated with cellular differentiation, activation, cell structure organisation and adhesion

Upfront gene expression analysis the purity and feasibility of isolated activated fibroblasts (referred to as CAF) were confirmed by flow cytometry for all CAF specimen. After successful RNA isolation and cDNA synthesis samples were processed for gene expression profiling. Initially, 7000 commonly expressed transcripts were identified. The majority of transcripts were related to metabolism or translation processes and have been excluded for further functional annotation as well as non-coding transcripts and those

located on chromosome X and Y. 233 commonly expressed transcripts remained of which 41 highly expressed transcripts have been considered for functional annotation of biological processes using Cytoscape ClueGo plugin. Of 41 uploaded IDs all genes were recognised by ClueGo and 100.00% were associated with functional annotations in all selected Ontologies from Cluster 1.
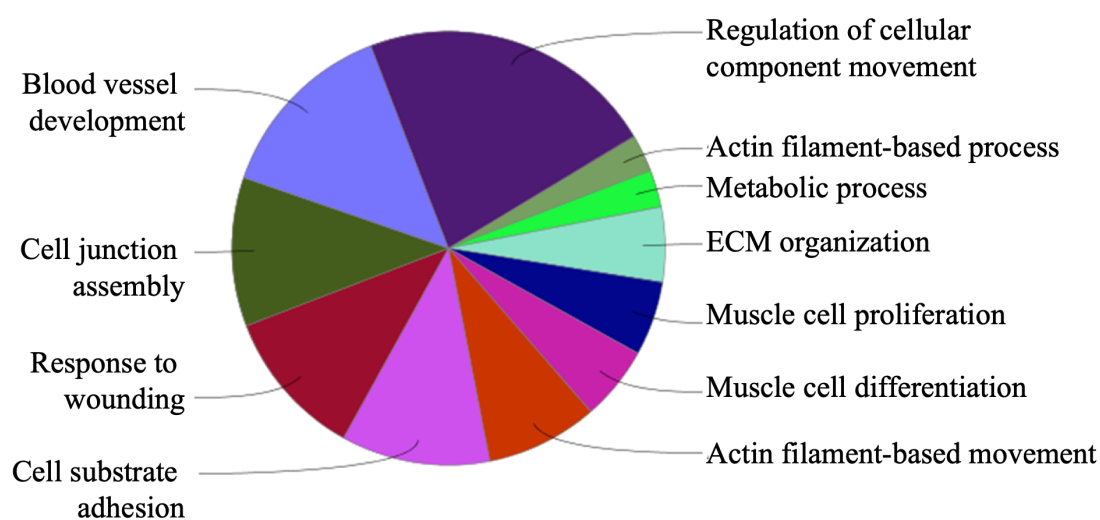
Figure 8: Genes commonly expressed between fibroblasts derived from cHL and lymphadenitis annotated to gene ontologies of biological processes library.
233 commonly expressed transcripts remained of which 41 highly expressed transcripts have been considered for functional annotation of biological processes using Cytoscape ClueGo plugin. Of 41 uploaded IDs all genes were recognised by ClueGo and 100.00% were associated with functional annotations in all selected Ontologies

38 genes (92.68%) from all Clusters were associated with representative terms and pathways. Table 14 and Figure 8 show gene ontologies that are commonly regulated for CAF of all subsets and origins. Briefly, isolated CAF commonly regulate transcripts that are associated with movement and blood vessel development, actin and ECM processes, cellular adhesion and cell junction assembly as well as response to wound healing and muscle cell phenotype. Transcripts such as *ENG* (CD105), *ITGB1* (CD29) and *ACTA2* (aSMA) (highlighted in red) have also been shown to be commonly expressed as minimum defining criteria of activated CAF referring to Figure 7.

Table 14: Overrepresented common pathways in CAF derived from different lymphadenopathies.
Annotated to gene ontologies of biological processes library; Transcripts such as ENG (CD105), ITGB1 (CD29) and ACTA2 (aSMA) (highlighted in red) have also been shown to be commonly expressed as minimum defining criteria of activated CAF

GO Term	GO Level	GO Group	% [Associated Genes]	n [Genes]	Associated Genes Found
Regulation of cellular component movement	[3, 4]	10	2.04	18	*[ACTN4, ANXA1, ATP2A2, CALR, CAV1, CFL1, CNN2, COL1A1, ENG, FN1, IGFBP3, IL6, IQGAP1, ITGAV, PFN1, RHOA, THBS1, TPM1]*
Response to wounding	[3]	07	2.60	18	*[ACTB, ACTG1, ANXA1, ANXA2, ANXA5, CAV1, CNN2, COL1A1, ENG, FN1, GJA1, IL6, LAMC1, MYL9, PLCG2, RHOA, THBS1, TPM1]*
Actin filament-based process	[3]	00	2.19	16	*[ACTB, ACTG1, ACTN4, ANXA1, ATP2A2, CALR, CAV1, CFL1, CNN2, GJA1, ITGB1, PFN1, RHOA, TPM1, TPM2, VIM]*
Extracellular matrix (ECM) organisation	[4]	02	3.47	12	*[ANXA2, CAPN2, CAPNS1, COL1A1, ENG, FN1, ITGAV, ITGB1, LAMC1, MMP2, THBS1, TIMP2]*
Cell junction assembly	[4]	08	5.07	11	*[ACTB, ACTG1, ACTN4, CAV1, CFL1, FN1, GJA1, IQGAP1, LAMC1, RHOA, THBS1]*
Blood vessel development	[3, 5, 6, 7, 8]	09	2.04	13	*[ACTA2, ANXA2, CAV1, COL1A1, ENG, FN1, IL6, ITGAV, ITGB1, JAK1, MMP2, RHOA, THBS1]*
Actin filament-based movement	[4]	05	5.07	7	*[ACTN4, ATP2A2, CAV1, GJA1, TPM1, TPM2, VIM]*

GO Term	GO Level	GO Group	% [Associated Genes]	n [Genes]	Associated Genes Found
Muscle cell proliferation	[3]	03	3.31	6	*[GJA1, IGFBP3, IL6, MMP2, THBS1, TPM1]*
Muscle cell differentiation	[4, 5]	04	2.06	8	*[ACTG1, ATP2A2, CALR, CAPN2, ENG, IGFBP3, ITGB1, TPM1]*
Multicellular organismal macromolecule metabolic process	[4]	01	3.97	5	*[COL1A1, ENG, IL6, ITGB1, MMP2]*
Cell-substrate adhesion	[3]	06	3.24	11	*[ACTN4, CALR, CFL1, COL1A1, FN1, IQGAP1, ITGAV, ITGB1, LAMC1, RHOA, THBS1]*

4.1.4 Fibroblast cultures obtained from LN tissues of different lymphadenopathies show a different gene expression signature

Figure 9 considers 185 transcripts with a standard deviation larger than one resulting in heterogeneous groups that uncover a more likely similarity of CAF derived from LA and MC cHL (yellow-flagged and blue-flagged group) than CAF derived from NS cHL (red-flagged group). The heatmap shows weakly expressed transcripts in green colour and highly expressed transcripts in red colour. The legend indicates log2 values of expression. NS cHL CAFs show heterogeneous expression profiles resulting in a wide spread distribution of expression similarity. Principal component analysis (PCA) considers the same transcripts and covers 64.3% variance confirming the inhomogeneous but altered expression of NS cHL CAF compared to a more likely grouping of CAFs derived from MC cHL and LA specimen (Figure 9B).
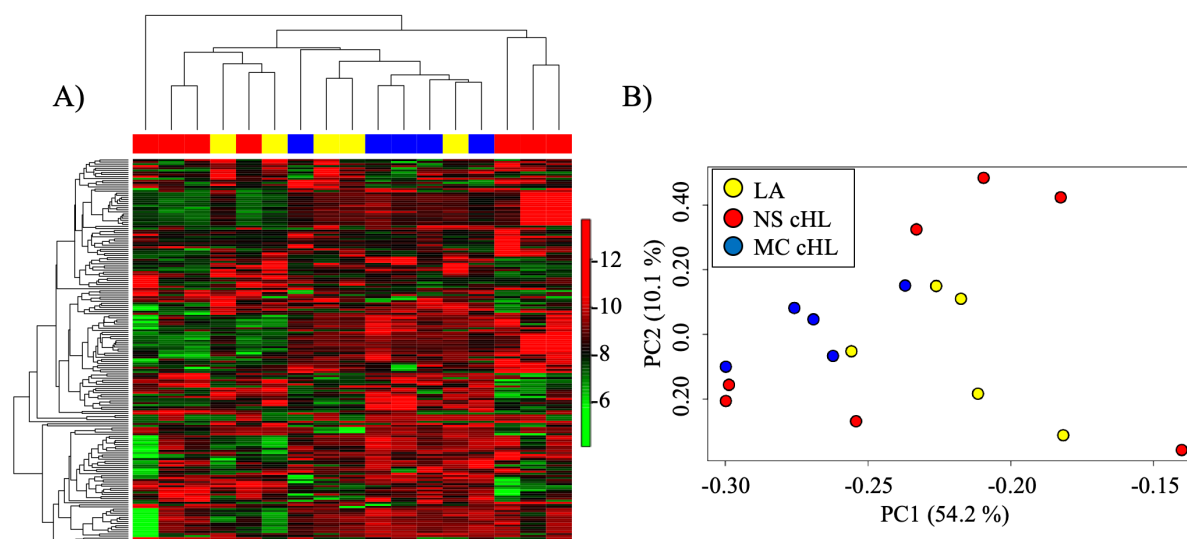
Figure 9: Fibroblasts derived from nodular sclerosing subtype of cHL (NS cHL) and lymphadenitis (LA) show considerable differences in their gene expression program.
(A) Unsupervised hierarchical gene expression clustering of fibroblast samples derived from lymphadenitis (Fib LA, yellow-flagged, n = 5), from mixed cellularity subtype of cHL (MC cHL, blue-flagged, n = 5) and from NS cHL (red-flagged, n = 7) considering 185 transcripts with a standard deviation >1. The heatmap shows less expressed transcripts in green colour and highly expressed transcripts in red colour. The legend indicated log-based values of expression. (B) Principal component analysis considering the same 185 transcripts with a standard deviation >1. Fibroblasts from LA (yellow), MC cHL (blue) and from NS cHL (red).

Supervised analysis of gene expression data identified differentially regulated transcripts between CAF LA and merged CAF derived from MC cHL and NS cHL. Table 15 shows transcripts significantly deregulated between the mentioned groups with a false discovery rate (FDR) less than 0.3 to exclude false positive transcripts. Eight transcripts are significantly deregulated in CAF cHL with a fold change (FC) larger than two. *PRKG2* (protein kinase, cGMP-dependent, type II), *VIT* (vitrin), *MT-TA* (mitochondrially encoded tRNA alanine), *GPNMB* (glycoprotein (transmembrane) nmb); *HTR2B* (5-hydroxytryptamine (serotonin) receptor 2B, G protein-coupled) and *DSC3* (desmocollin 3) are lower expressed transcripts in cHL CAFs whereas *TIMP3* (TIMP metallopeptidase inhibitor 3) and *MYOCD* (myocardin) are highly upregulated transcripts in cHL CAF.

45

Table 15: Genes differentially expressed between fibroblasts derived from cHL and lymphadenitis
($p < 0.05$; FC $\geq$ $|2|$; FDR $\leq$ 0.3).

FC CAF cHL vs. CAF LA	p-Value	FDR	Gene Symbol	Gene Description
4.2	0.0056	0.28	*TIMP3*	TIMP metallopeptidase inhibitor 3
3.9	0.0001	0.14	*MYOCD*	myocardin
-2.1	0.0027	0.25	*PRKG2*	protein kinase, cGMP-dependent, type II
-2.2	0.0002	0.14	*VIT*	vitrin
-2.4	0.0001	0.14	*MT-TA*	mitochondrially encoded tRNA alanine
-2.7	0.0004	0.14	*GPNMB*	glycoprotein (transmembrane) nmb
-2.9	0.0020	0.22	*HTR2B*	5-hydroxytryptamine (serotonin) receptor 2B, G protein-coupled
-4.0	0.0008	0.16	*DSC3*	desmocollin 3

Table 16 shows transcripts significantly deregulated between the mentioned groups with a FDR larger than 0.3 but less than 0.4. *TIMP3*, *KRT19* (keratin 19), *CNN1* (calponin 1, basic, smooth muscle) and *KRT34* (keratin 34) are significantly higher regulated in CAF cHL with a fold change (FC) larger than two in comparison to CAF LA. *DPP4* (dipeptidyl-peptidase 4), *ADAMTS5* (ADAM metallopeptidase with thrombospondin type 1 motif, 5), *TMTC1* (transmembrane and tetratricopeptide repeat containing 1), *CPA4* (carboxypeptidase A4), *SLC7A11* (solute carrier family 7 (anionic amino acid transporter light chain, xc- system), member 11), *OR2A42* (olfactory receptor, family 2, subfamily A, member 42), *CLDN1* (claudin 1), VCAM1 (vascular cell adhesion molecule 1), *SEPP1* (selenoprotein P, plasma, 1), *RSPO3* (R-spondin 3), *FBN2* (fibrillin 2), *SVEP1* (sushi, von Willebrand factor type A, EGF and pentraxin domain containing 1) as well as *CHI3L1* (chitinase 3-like 1 (cartilage glycoprotein-39) are found to be significantly less transcribed in CAF cHL than CAF LA.

Table 16: Genes differentially expressed between fibroblasts derived from cHL and lymphadenitis

(Filter criteria: p < 0.05; FC ≥ │2│; 0.3 ≤ FDR ≤ 0.4). Transcripts flagged by * are considered for further testing and validation

FC CAF cHL vs. CAF LA	p-Value	FDR	Gene Symbol	Gene Description
4.3	0.0099	0.33	*TIMP3**	TIMP metallopeptidase inhibitor 3
2.5	0.0170	0.35	*KRT19*	keratin 19
2.3	0.0280	0.39	*CNN1**	calponin 1, basic, smooth muscle
2.2	0.0121	0.34	*KRT34*	keratin 34
-2.0	0.0238	0.39	*DPP4*	dipeptidyl-peptidase 4
-2.0	0.0248	0.39	*ADAMTS 5*	ADAM metallopeptidase with thrombospondin type 1 motif, 5
-2.1	0.0074	0.32	*TMTC1*	transmembrane and tetratricopeptide repeat containing 1
-2.2	0.0071	0.32	*CPA4*	carboxypeptidase A4
-2.2	0.0156	0.35	*SLC7A11*	solute carrier family 7 (anionic amino acid transporter light chain, xc- system), member 11
-2.3	0.0148	0.34	*OR2A42*	olfactory receptor, family 2, subfamily A, member 42
-2.4	0.0165	0.35	*CLDN1*	claudin 1
-2.4	0.0080	0.32	*VCAM1*	vascular cell adhesion molecule 1
-2.5	0.0099	0.33	*SEPP1*	selenoprotein P, plasma, 1
-2.5	0.0173	0.35	*RSPO3*	R-spondin 3
-2.7	0.0188	0.36	*FBN2*	fibrillin 2
-2.7	0.0187	0.36	*SVEP1*	sushi, von Willebrand factor type A, EGF and pentraxin domain containing 1
-5.3	0.0231	0.38	*CHI3L1**	chitinase 3-like 1 (cartilage glycoprotein-39)

Supervised analysis between CAF NS cHL and CAF MC cHL as well as CAF NS cHL and CAF LA revealed a differential gene expression profile exceeding set FDR selection criteria (Table 17 and Table 18, respectively). Comparison between CAFs derived from NS cHL and MC cHL, respectively uncovered a prominent difference in *IL7R* (Interleukin 7 receptor) transcript level which however, displayed a high FDR (Table 17). A few individually chosen transcripts are shown in Table 18 considered for further functional annotation.

Table 17: Genes differentially expressed between fibroblasts derived from NS cHL and MC cHL
(Filter criteria: $p < 0.05$; FC $\geq$ $\lfloor 2 \rfloor$).

FC CAF NS cHL vs. MC cHL	p-Value	FDR	Gene Symbol	Gene Description
-2.7	0.018	0.979	*IL7R*	interleukin 7 receptor

Further differentially expressed transcripts in NS cHL fibroblasts compared to LA fibroblasts were also considered as prominent targets despite its high FDR shown in Table 18.

Table 18: Genes differentially expressed between fibroblasts derived from NS cHL and LA
(Filter criteria: $p < 0.05$; FC $\geq$ $\lfloor 1.8 \rfloor$).

FC CAF NS cHL vs. CAF LA	p-Value	FDR	Gene Symbol	Gene Description
6.2	0.0037	0.51	*TIMP3*	TIMP metallopeptidase inhibitor 3
6.0	0.0013	0.44	*TIMP3*	TIMP metallopeptidase inhibitor 3
3.5	0.0011	0.44	*MYOCD*	myocardin
2.7	0.0231	0.69	*NPPB*	natriuretic peptide B
2.4	0.0329	0.75	*KRT34*	keratin 34
2.3	0.0037	0.51	*CD200*	CD200 molecule
2.2	0.0089	0.60	*LIMCH1*	LIM and calponin homology domains 1

FC CAF NS cHL vs. CAF LA	p-Value	FDR	Gene Symbol	Gene Description
2.1	0.0298	0.73	*GEM*	GTP binding protein overexpressed in skeletal muscle
2.1	0.0052	0.56	*AMIGO2*	adhesion molecule with Ig-like domain 2
1.9	0.0195	0.68	*PTGS2*	prostaglandin-endoperoxide synthase 2 (prostaglandin G/H synthase and cyclooxygenase)
1.9	0.0358	0.75	*CDH2*	cadherin 2, type 1, N-cadherin (neuronal)
1.8	0.0372	0.75	*INHBA*	inhibin, beta A
-1.8	0.0320	0.74	*MIR21*	microRNA 21
-2.7	0.0171	0.65	*IL7R*	interleukin 7 receptor
-2.7	0.0022	0.45	*GPNMB*	glycoprotein (transmembrane) nmb
-2.8	0.0012	0.44	*VCAM1*	vascular cell adhesion molecule 1
-2.8	0.0135	0.63	*PSG7*	pregnancy specific beta-1-glycoprotein 7 (gene/pseudogene)
-2.9	0.0010	0.44	*CPA4*	carboxypeptidase A4
-2.9	0.0073	0.60	*MME*	membrane metallo-endopeptidase
-3.2	0.0105	0.60	HTR2B	5-hydroxytryptamine (serotonin) receptor 2B, G protein-coupled
-3.2	0.0194	0.68	*ENPP2*	ectonucleotide pyrophosphatase/phosphodiesterase 2
-3.3	0.0114	0.60	*PSG1*	pregnancy specific beta-1-glycoprotein 1
-3.4	0.0116	0.60	*SVEP1*	sushi, von Willebrand factor type A, EGF and pentraxin domain containing 1
-3.5	0.0129	0.61	*FBN2*	fibrillin 2
-4.7	0.0001	0.30	*DSC3*	desmocollin 3
-8.9	0.0026	0.45	*CHI3L1*	chitinase 3-like 1 (cartilage glycoprotein-39)

Transcripts assumed to be of relevance underwent technical validation using Taqman Gene expression assays qPCR. Previously generated cDNA of primary fibroblast derived total RNA was used to confirm significant transcript levels of selected targets. Figure 10 shows successful confirmation of four selected transcripts (*IL6, TIMP3, CNN1, MYOCD*). Since IL6 deregulation is a prominent key player in cHL associated with poor outcome and B-symptoms (Aldinucci et al., 2004; Cattaruzza et al., 2009; Vega et al., 2006), it was included despite the fact gene expression analysis could not detect high fold changes of transcript levels among the analysed groups. Further identified targets have been confirmed within this experiment (data not shown). Validation confirmed differential transcript levels among fibroblasts derived from LA in comparison to fibroblasts derived from cHL for *IL6*, *CNN1* and *MYOCD*. However, *TIMP3* transcript level is significantly elevated in fibroblasts derived solely from NS cHL.
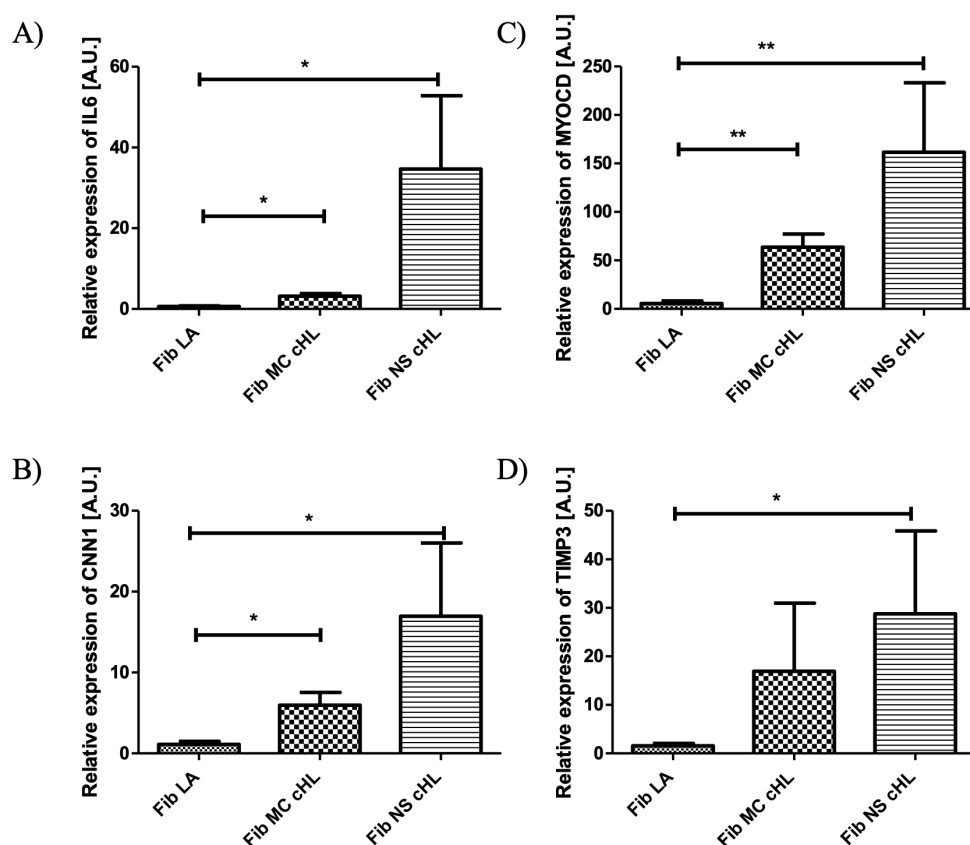
Figure 10: Transcript-based validation confirmed overexpression of selected prominent differentially regulated targets in NS cHL and partially MC cHL.

(A) Quantitative real time PCR showing significantly higher Interleukin 6 (*IL6*) transcript levels in NS cHL (n = 8) and in MC cHL (n = 5) compared with fibroblasts from lymphadenitis (n = 5) (Mann–Whitney U test, * p = 0.05). **(B)** Quantitative real time PCR showing significantly higher Myocardin (*MYOCD*) transcript levels in NS cHL (n = 8) and in MC cHL (n = 5) compared with fibroblasts from lymphadenitis (n = 5) (Mann–Whitney U test, ** p = 0.002). **(C)** Quantitative real time PCR showing significantly higher Calponin 1 (*CNN1*) transcript levels in NS cHL (n = 8) and in MC cHL (n = 5) compared with fibroblasts from lymphadenitis (n = 5) (Mann–Whitney U test, * p = 0.05). **(D)** Quantitative real time PCR showing significantly higher tissue inhibitor of metalloproteinase 3 (*TIMP3*) transcript levels in NS cHL (n = 8) compared with fibroblasts from lymphadenitis (n = 5) (Mann–Whitney U test, * p = 0.05).

Protein level expression was validated using an independent cohort of formalin-fixed paraffin embedded (FFPE) patient material (n (LA) = 8, n (NS cHL) = 14; n (M cHL) = 11). Figure 11 A_1, B_1, C_1 shows a H&E staining of a selected case per group highlighting prominent sclerotic bands in NS cHL (C_1). The second row represents immunohistochemical staining of αSMA expression revealing its presence among all cases and groups as basic lymph node structure. The third row confirms the upregulated

51

expression of CNN1 in cHL fibroblast sclerotic bands highly enriched in NS cHL cases. Basal expression of CNN1 can be found in blood vessels and lymph node capsule (A_3, B_3, C_3). TIMP3 immunohistochemical staining revealed expression patterns in a subset of paraimmunoblasts among all groups and cases (not highlighted) as well as a strong expression pattern in sclerotic bands and Hodgkin HRS cells as highlighted in C_4. In detail, 71.4% (5/7) LA cases express TIMP3 in pulpa blasts but not in their stroma network. 92.8% (13/14) NS cHL cases show a positive TIMP3 expression of HRS cells and 57% (8/14) TIMP3 expression in the lymph node while negative in capsule fibroblasts in 71% (10/14) of NS cHL cases. MC cHL cases do not express TIMP3 within their capsule or only weakly focally within the stroma network (1/14 cases). 82% (9/11 cases) HRS cells of MC cHL cases show a TIMP3 expression.
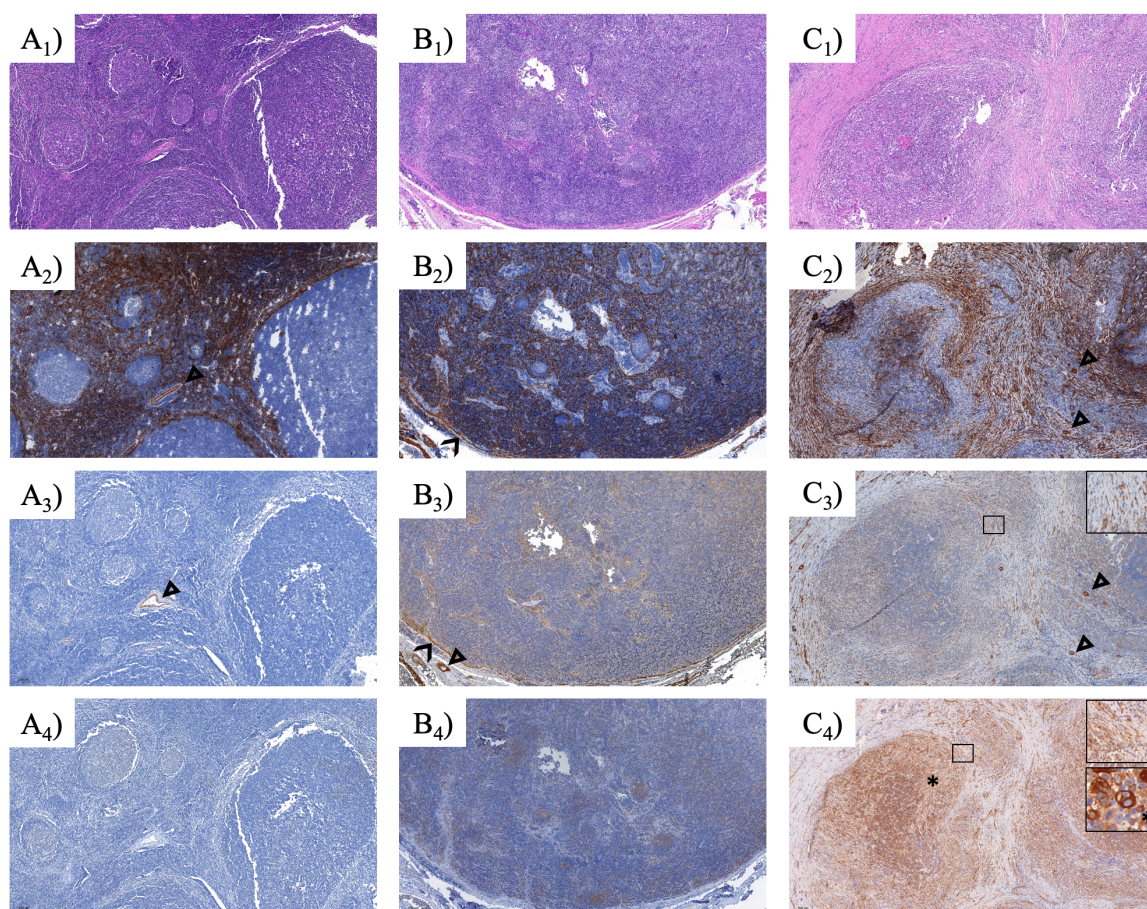
Figure 11: Independent validation using Immunohistochemistry confirmed overexpression of selected prominent differentially regulated targets in NS cHL and partially MC cHL.

(**A**) Representative H&E (A_1) and immunohistochemical (A_2, αSMA; A_3, CNN1; A_4, TIMP3) staining of a selected LA case (5×). Basic expression of αSMA and CNN1 in blood vessels is highlighted ($A_{2/3}$, arrowhead Δ). TIMP3 (A_4) is expressed in paraimmunoblasts (not shown). (**B**) Representative H&E (B_1) and immunohistochemical (B_2, αSMA; B_3, CNN1; B_4, TIMP3) staining of a selected MC cHL case (5×). Basic expression of αSMA and CNN1 in blood vessels ($B_{2/3}$, arrowhead Δ) and lymph node capsule ($B_{2/3}$, opened arrowhead Λ) is highlighted. (**C**) Representative H&E (C_1) and immunohistochemical (C_2, αSMA; C_3, CNN1; C_4, TIMP3) staining of a selected NS cHL case (5×). Basic expression of αSMA and CNN1 in blood vessels ($C_{2/3}$, arrowhead Δ) is highlighted. CNN1 and TIMP3 expression in NS cHL CAF is shown in attached insert in $C_{2/3}$. TIMP3 expression (20x). Moreover, immunohistochemical staining revealed Hodgkin- and Reed-Sternberg (HRS) cells´ enhanced expression of TIMP3 (C_4, *, attached insert, 40x).

4.1.5　　Fibroblasts derived from NS cHL maintain stable methylation profiles in culture when compared with lymphadenitis-derived fibroblasts

Since differences in gene expression between different CAF subsets were observed, CAFs from six cases of NS cHL and four cases of LA obtained after 5 passages were studied for their methylation profiles using Methylation EPIC BeadChip Kit that interrogates 850,000 CpG sites in the human genome, to reveal if the differences in gene expression are linked to distinct DNA methylation profiles.
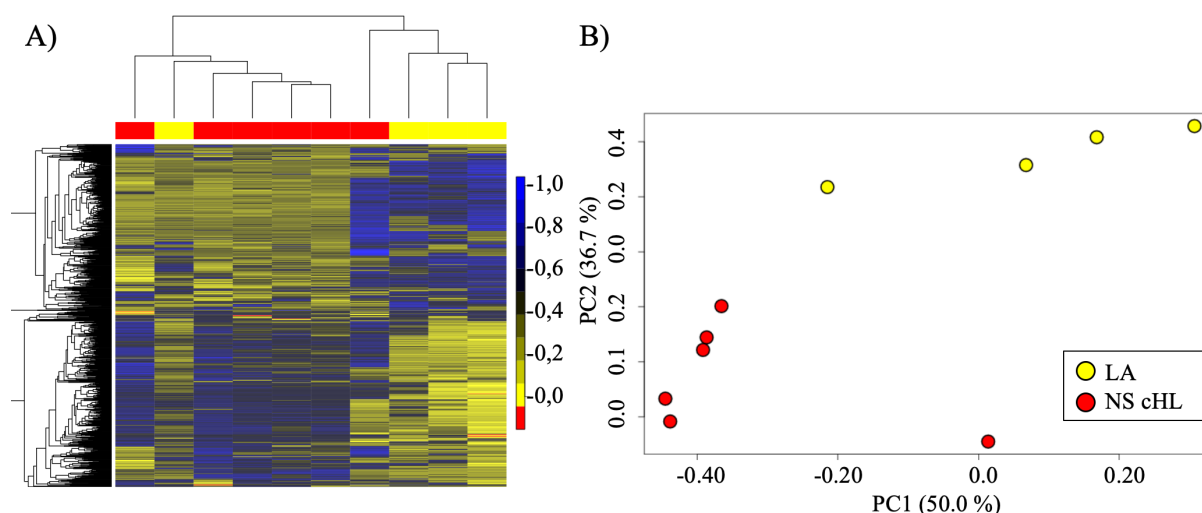
Figure 12: Methylation profiles remain consistent in fibroblasts obtained from lymphadenitis and NS cHL.

(**A**) Unsupervised hierarchical clustering of fibroblasts from lymphadenitis (Fib LA, n = 4, yellow-flagged) and from NS cHL (n = 6, red-flagged) considering all tags (848) with a differential methylation and standard deviation >0.25. (**B**) Principal component (PC) analysis of methylation patterns in fibroblasts from lymphadenitis (Fib LA, n = 4, yellow) and NS cHL (n = 6, red) considering all tags with a differential methylation and standard deviation >0.25.

In an unsupervised hierarchical clustering, CAF from NS cHL and LA separated well from each other with the exception of one outlier each (Figure 12A). In a principal component analysis both CAF groups were considerably different (Figure 12B). In the supervised comparison, there were 5815 tags that were significantly differentially methylated (p<0.05 (p-values adjusted using the FDR approach)) with mean differences of more than 30% (not shown). A total of 170 tags among these were located in promoter regions. Correlation

of gene expression data and methylation results, however, revealed that only for one gene, which was differentially methylated in NS cHL CAF and LA (*SLC38A1;* tag:cg17090968) a respective significant regulation of gene expression (1.8-fold higher expression in NS cHL fibroblasts, p = 0.012 and 45% lower methylation) was observed. Thus, differential expression of genes between these different CAF types at their mRNA level is not regulated by methylation of their gene promoters considering the given data.

4.2   Targeting NS cHL CAFs

If CAFs have a beneficial impact on cHL pathogenesis and progress it is of interest how these cells can be targeted and reversed and how HRS cells orchestrate their accumulation in the lymph node. The following results describe options of targeting CAFs.

4.2.1   Luteolin reverses the expression of prominently upregulated targets in NS cHL CAF

To address the idea of a reversion of NS cHL derived CAF gene expression profile literature research presented the flavonoid Luteolin with anti-inflammatory (Lupu & Menendez, 2006) activities among others. Briefly, CAFs derived from NS cHL LN were treated with 30 µM luteolin for 48 h. Cells were harvested and total RNA isolated for further transcriptome analysis as mentioned before. 124 transcripts with a standard deviation larger than one resulting in two major clusters representing homogenous luteolin-treated biological replicates (black-flagged column) and untreated replicates (green-flagged column) are shown in an unsupervised hierarchical clustering heatmap in Figure 13A. Again, hierarchical clustering again reveals increased heterogeneity in untreated CAFs as aforementioned in Figure 9. The heatmap shows transcripts expressed in lower levels in green colour and highly expressed transcripts in red colour. The legend indicated log2 values of expression. Additionally, luteolin-treated cells show an altered morphology when compared to untreated cells resulting in less-proliferating cells established an altered stress-induced shape (Figure 13B and C). Working concentration of luteolin was exhibited in preliminary experiments (data not shown).
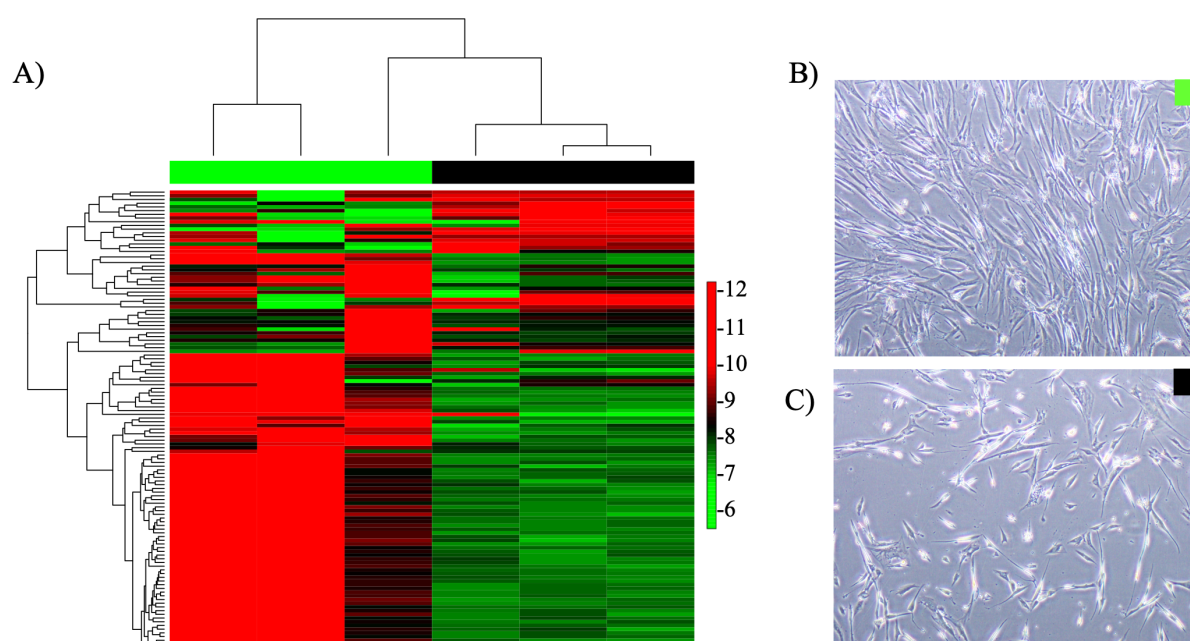
Figure 13: Treatment with luteolin of NS cHL CAF results in considerable reversal of their gene expression program.

(A) Unsupervised hierarchical clustering of gene expression profiles derived from untreated NS cHL CAF (green) and luteolin treated NS cHL CAF (black). Three biologically independent samples per group considering 124 transcripts with a standard deviation >1. The heatmap shows less expressed transcripts in green colour and highly expressed transcripts in red colour. The legend indicated log-based values of expression. (B) Corresponding morphology of untreated subconfluent NS cHL CAF. (C) Corresponding morphology of luteolin treated subconfluent NS cHL CAF.

Supervised analysis of gene expression data identified differentially regulated targets between the two groups. After applying selection criteria ($p \leq 0.05$; $FC \geq \left| 3 \right|$; $FDR \leq 0.1$) 65 genes from all clusters were associated to representative terms and pathways. Figure 14 and Table 19 show REACTOME pathways that are overrepresented as a consequence of luteolin treatment using Cytoscape ClueGo plugin (Bindea et al., 2009). Of 65 uploaded IDs all genes were recognised by ClueGo and 51 (78.5%) were associated with functional annotations in all selected ontologies from cluster 1. Annotated pathways are dominated by pathways contributing to cell cycle regulation and its progression and further linking the impact of luteolin to senescence-associated secretory phenotype (SASP) (Coppé et al., 2008).
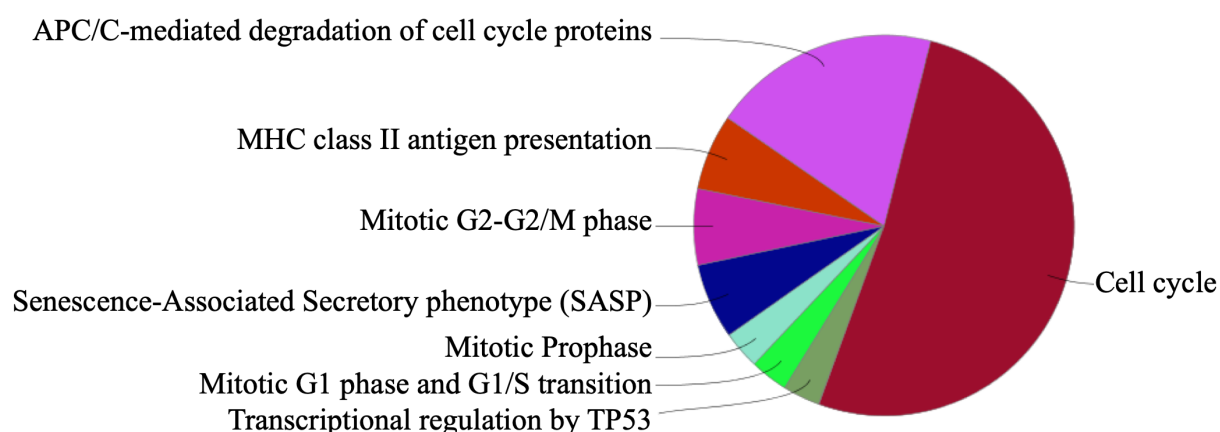
Figure 14: Overrepresented pathways following luteolin treatment of NS cHL CAFs.

Supervised analysis of expression data revealed 65 deregulated transcripts of which 51 highly have been considered for functional annotation of biological processes using Cytoscape ClueGo plugin. All genes were recognised by ClueGo and 78.5% were associated with functional annotations in all selected REACTOME pathways.

Table 19 shows pathway annotated transcripts and presence within the pathways in %. *IL6* is considered as a central key regulator in CAF activation according to previous findings (Figure 8, Figure 9) and therefore highlighted in red.

Table 19: Overrepresented pathways in NS cHL CAFs following luteolin treatment.
(Annotated to gene ontologies of REACTOME_Pathways library; Filter criteria: p $\leq$ 0.05; FC $\geq$ $\left|3\right|$; FDR $\leq$ 0.1)

GO Term	GO Level	GO Group	% [Associated Genes]	n [Genes]	Associated Genes Found
APC/C-mediated degradation of cell cycle proteins	[-1]	6	8.14	7	*[AURKA, CCNA2, CCNB1, CDC20, PLK1, PTTG1, UBE2C]*
Cell Cycle	[-1]	7	3.57	23	*[AURKA, BIRC5, BUB1, CCNA2, CCNB1, CCNB2, CDC20, CDC45, CENPE, CENPF, CENPW, H2BC14, H3C2, HJURP, KIF23, KNL1, NCAPG, PLK1, PTTG1, RRM2, TOP2A, TPX2, UBE2C]*

GO Term	GO Level	GO Group	% [Associated Genes]	n [Genes]	Associated Genes Found
MHC class II antigen presentation	[-1]	5	4.07	5	*[CENPE, CTSK, KIF11, KIF23, KIF4A]*
Mitotic G1 phase and G1/S transition	[-1]	1	3.36	5	*[CCNA2, CCNB1, CDC45, RRM2, TOP2A]*
Mitotic G2-G2/M phases	[-1]	4	3.54	7	*[AURKA, CCNA2, CCNB1, CCNB2, CENPF, PLK1, TPX2]*
Mitotic Prophase	[-1]	2	3.52	5	*[CCNB1, CCNB2, H2BC14, H3C2, PLK1]*
Senescence-Associated Secretory Phenotype (SASP)	[-1]	3	4.50	5	*[CCNA2, H2BC14, H3C2, IL6, UBE2C]*
Transcriptional Regulation by TP53	[-1]	0	2.47	9	*[AURKA, BIRC5, BTG2, CCNA2, CCNB1, SESN1, TNFRSF10D, TP53INP1, TPX2]*

Table 20 shows manually selected transcripts significantly deregulated between the mentioned groups with a FDR less than 0.1. Six transcripts that have been identified by cHL CAF signature transcript panel are significantly deregulated with a fold change (FC) larger than two: *MYOCD, CNN1, CD200*. In contrast, *IL6* and *TIMP3* transcripts have been downregulated by luteolin treatment by more than 4-fold. Additionally, *MKI67 (*marker of proliferation Ki-67) is 5-fold downregulated in luteolin-treated CAFs acting as a biomarker contributing to decreased proliferation. *LTBP1* (latent transforming growth factor beta binding protein 1), a key regulator of CAF activation via transforming growth factor beta (TGFβ), is also 3.8-fold decreased after luteolin treatment.

Table 20: Reversed signature transcripts between luteolin treated NS cHL fibroblasts and untreated NS cHL fibroblasts
(Filter criteria: $p \leq 0.05$; FC $\geq \lvert 2 \rvert$; FDR ≤ 0.1)

FC CAF-Lut vs. CAF	p-value	FDR	Gene Symbol	Gene Description
-2.0	0.023	0.06	*MYOCD*	myocardin
-2.1	0.016	0.05	*CNN1*	calponin 1, basic, smooth muscle
-2.1	0.028	0.06	*CD200*	CD200 molecule
-3.8	0.019	0.05	*LTBP1*	latent transforming growth factor beta binding protein 1
-4.0	0.018	0.05	*IL6*	interleukin 6
-4.8	0.001	0.02	*TIMP3*	TIMP metallopeptidase inhibitor 3
-5.1	0.018	0.05	*MKI67*	marker of proliferation Ki-67
-5.5	0.003	0.02	*TIMP3*	TIMP metallopeptidase inhibitor 3

To further identify and validate the impact of luteolin on cHL CAFs cell viability was determined using BD Apoptosis kit. Briefly, cells were seeded at equivalent cell density. After plastic adherence luteolin was applied and viability was determined after 48 h (Figure 15A). Cells floating in suspension and adherent cells were considered for analysis. Flow cytometry gating strategy (not shown) shows viable cells at double-negative gate (7-AAD-AnnV-). The majority of treated cells is viable in comparison to the non-treated group (Figure 15A). From the same sample set up cells were harvested and lysed for RNA isolation and qPCR validation of *TIMP3* expression via qPCR and TIMP3 secretion was quantified using respective supernatants after luteolin treatment and absorbance-based TIMP3 ELISA assay. TIMP3 expression and secretion relative to untreated CAF is plotted in Figure 15B and C confirming the substantial decrease revealed by supervised analysis (Table 20) on multiple functional levels: transcription, translation and functional release of TIMP3. Mean + SEM of four independent experiments in triplicates are shown in Figure 15.
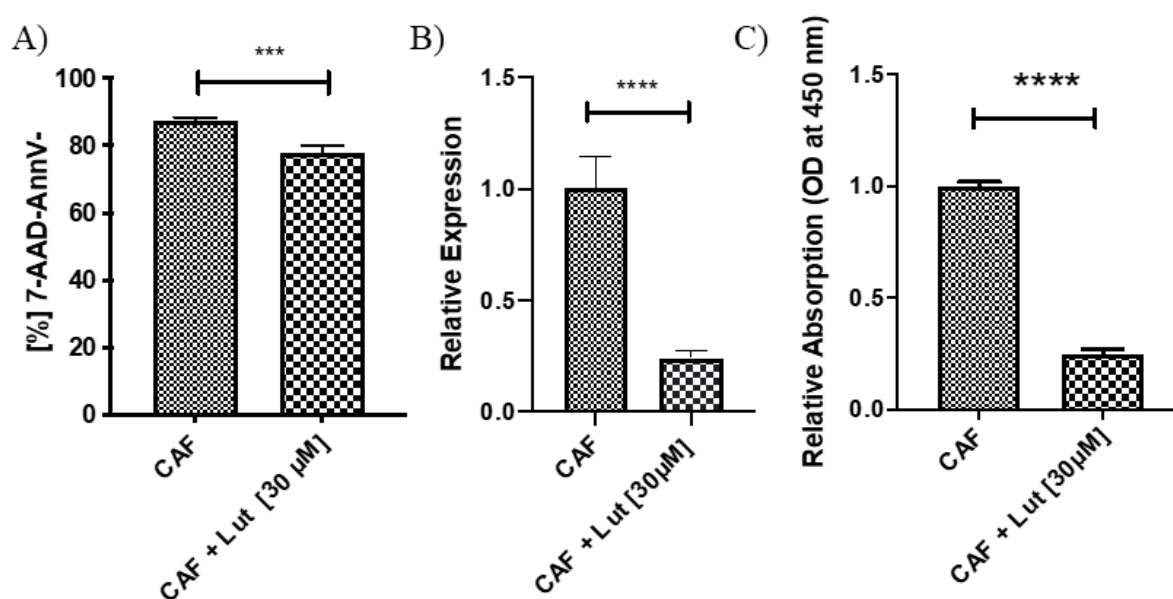
Figure 15: The impact of luteolin treatment on CAF viability and TIMP3 expression.

(A) Viable cells in untreated and luteolin treated fibroblasts 48 h after luteolin treatment. *** p<0.001 unpaired t-test. Four experiments with three replicates. (B) Quantitative real time PCR showing significantly higher TIMP3 transcript levels in untreated NS cHL CAF compared with luteolin treated NS cHL CAF **** p<0.001 unpaired t-test. Four experiments with three replicates. (C) Absorption at 450 nm is significantly decreased in the supernatants derived from luteolin treated fibroblasts after 48 h reflecting a significantly downregulated TIMP3 secretion in the ELISA. Mean + SEM of four independent experiments in triplicates. *** p<0.001, paired t-test.

4.2.2 HRS cell lines specifically promote CAF proliferation by paracrine signaling and overrule luteolin´s effect.

Given the theory of malignant cells reprogramming their environment it is of further interest if HRS cell lines as a model for cHL *in vitro* impact growth and behavior of NS cHL CAFs. Briefly, CAF cells were labeled prior to treatment using Cell Trace Violet Blue flow cytometry assay (Thermo Fisher Scientific) and seeded at equivalent cell density. After plastic adherence conditioned media of several cell lines (mock: blank HRS cell line medium; specific HRS cell lines: L-428 and L-1236; Burkitt lymphoma cell line: Raji), cytokine IL7 and/or luteolin were applied and proliferation was determined after 48 h using flow cytometry. Cells floating in suspension and adherent were considered for analysis. Arbitrary units (A.U.) of median fluorescence intensity (proliferation median) were plotted for statistical testing. Fluorescence values were inverted and normalised to the control

60

(CAF). Mean + SEM of three independent experiments in triplicates are shown in Figure 16. Conditioned media derived from HRS cell lines specifically promote CAF´s proliferation. Luteolin´s negative effect on proliferation is overruled by aforementioned HRS cell line conditioned media but not by IL7 addition. Burkitt lymphoma cell line conditioned medium of Raji cell line shows a weak, not significant increase of CAF proliferation.
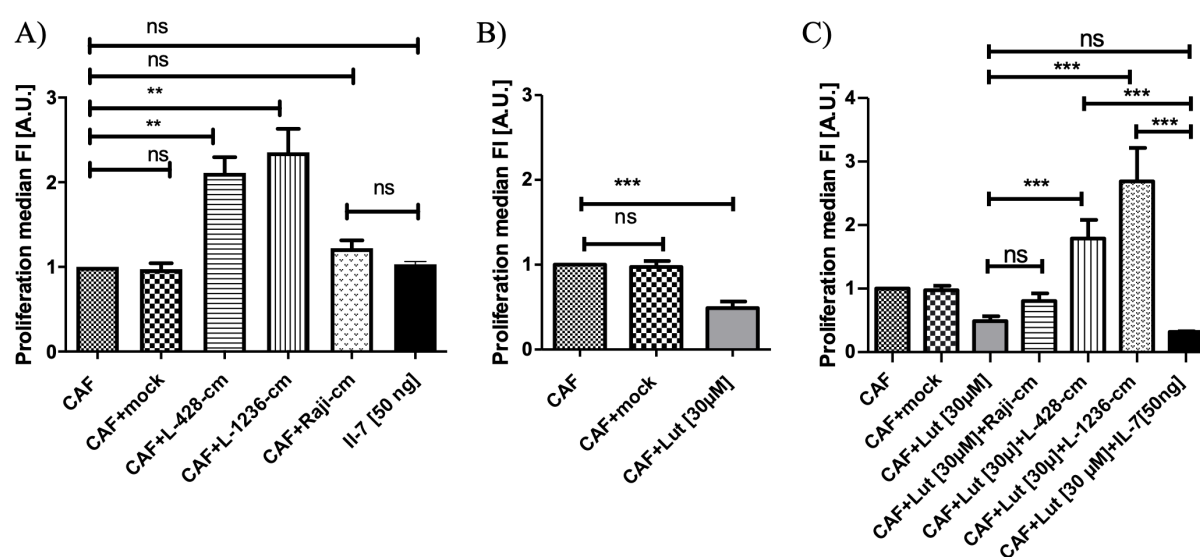
Figure 16: NS cHL CAF show enhanced proliferation in the presence of conditioned medium derived from cHL cell lines, even after application of luteolin.

(A) NS cHL CAF show a significantly higher proliferation after the application of conditioned media from the cHL cell lines L-428 and L-1236 when compared with IMDM (CAF) or RPMI medium (mock) only, conditioned medium obtained from the Burkitt lymphoma cell line Raji or IL7. Proliferation was measured by Cell Trace Violet Blue flow cytometry assay. Fluorescence values were inverted and normalised to the control (CAF). Mean + SEM of three independent experiments in triplicates, ** $p<0.01$, *** $p<0.001$, ns = no significance, One-Way-ANOVA with Bonferroni correction for multiple comparisons. (B) NS cHL CAF show a significantly decreased proliferation after the application of luteolin. Proliferation was measured by Cell Trace Violet Blue flow cytometry assay. Fluorescence values were inverted and normalised to the control (CAF). Mean + SEM of three independent experiments in triplicates, *** $p<0.001$, ns = no significance, One-Way-ANOVA with Bonferroni correction for multiple comparisons. (C) luteolin treatment dependent decreased proliferation of NS cHL CAF can be reversed by addition of conditioned media from the cHL cell lines L-428 and L-1236, but not by addition of IL-7. Proliferation was measured by Cell Trace Violet Blue flow cytometry assay. Fluorescence values were inverted and normalised to the control (CAF). Mean + SEM of three independent experiments in triplicates, *** $p<0.001$, ns = no significance, One-Way-ANOVA with Bonferroni correction for multiple comparisons.

4.2.3   CAF do not impact HRS cell line proliferation by paracrine signaling.

The next experimental set up aims at investigating if NS cHL CAF impact HRS cell line proliferation. HRS cell lines L-428 and L-1236 were labeled prior to treatment using Cell Trace Violet Blue flow cytometry assay and seeded at equivalent cell density. After over-night incubation conditioned media of CAF cells (mock: blank CAF medium) was applied and proliferation was determined after 48 h using flow cytometry. All cells were considered for analysis. Arbitrary units (A.U.) of median fluorescence intensity (proliferation median) were plotted for statistical testing. Fluorescence values were inverted and normalised to the control. Mean + SEM of three independent experiments in triplicates are shown in Figure 17. Conditioned media derived from CAF do not promote HRS cell line proliferation.
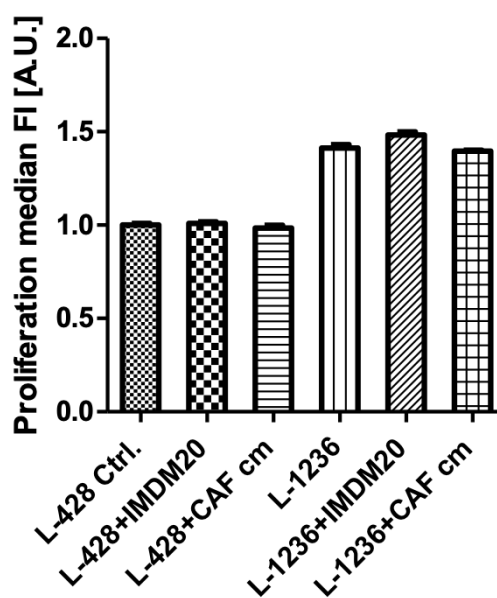
Figure 17: HRS cell lines do not show enhanced proliferation in the presence of conditioned medium derived from NS cHL CAF.

The addition of CAF-derived conditioned media did not show any impact on proliferation of cHL cell lines. Proliferation was measured by Cell Trace Violet Blue. Fluorescence values were inverted and normalised to the control (L-428 Ctrl., L-1236 Ctrl.). Mean + SEM of three independent experiments in triplicates. No significance testing applied.

4.3 The HRS – CAF coculture model

The coculture model set up was designed to study the effects of any interaction between CAFs and HRS cell lines. An early-stage pilot experiment was meant to implement the optimum coculture settings for further investigations.

4.3.1 HRS cells rapidly and specifically adhere to NS cHL CAFs

In order to titrate optimum cell numbers CAF were seeded in equivalent cell density. After plastic adherence L-428 HRS cells were added at different cell density and observed post 24 hr. L-428 HRS cells being naturally in suspension adhered to CAF cells. Repeated gentle washing with PBS [Mg^{2+}, CA^{2+}] and shaking did not impair the adherence. To visualise the interaction the set up was repeated using coverslips and stained for actin (CAF) and CD30 (HRS cell biomarker) (Figure 18).
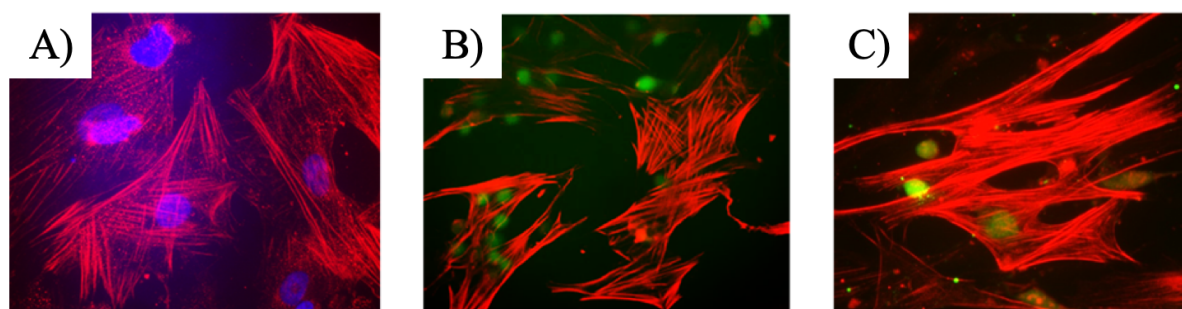
Figure 18: HRS cells stably establish a rapid adherent-based direct interaction with the NS cHL CAF.

A) Representative image of cancer-associated fibroblasts (CAF) stained for actin (red) and nucleic counterstain DAPI (blue) (4x magnification). B) Representative image of cancer-associated fibroblasts (CAF) stained for actin (red), L-428 HRS cells stained for CD30 (green) and nucleic counterstain DAPI (blue) (4x magnification). C) Representative enlarged image of cancer-associated fibroblasts (CAF) stained for actin (red), L-428 HRS cells stained for CD30 (green) and nucleic counterstain DAPI (blue) (4x magnification).

Further characterisation of the interaction potential required additional coculture models consisting of non-malignant lymphoblastoid cell line CB5B8 (kindly provided by Dr. R. Küppers; Table 9), commercial Burkitt lymphoma cell line Raji and HRS cell lines L-428, L-1236 and KM-H2. The ratio of adherent CAF to lymphoma cell lines was 1:5. Adherence-based interaction of lymphoma cells and fibroblasts was determined by Brightfield

microscopy of the attached fractions. Cells remaining in suspension were removed by repeated gentle washing with PBS [Mg^{2+}, CA^{2+}]. ImageJ "Finding Maxima" (Schneider et al., 2012) identified and counted HRS cells adhered to CAF. Mean + SEM counts per area of adhered cells of four independent experiments is plotted in Figure 19. L-1234 and KM-H2 HRS cell line show increased numbers of adhering cells when compared to L-428. However, non-HRS cell lines CB5B8 and Raji adhere to less extent to NS cHL CAF than HRS cell lines. L-428 does not exhibit any ability to adhere to plastics. In contrast, a small portion of L-1236 and KM-H2 cells is able to adhere to plastics. Taking this into account, further experiments will address the coculture model consisting of NS cHL CAF and L-428 cells.
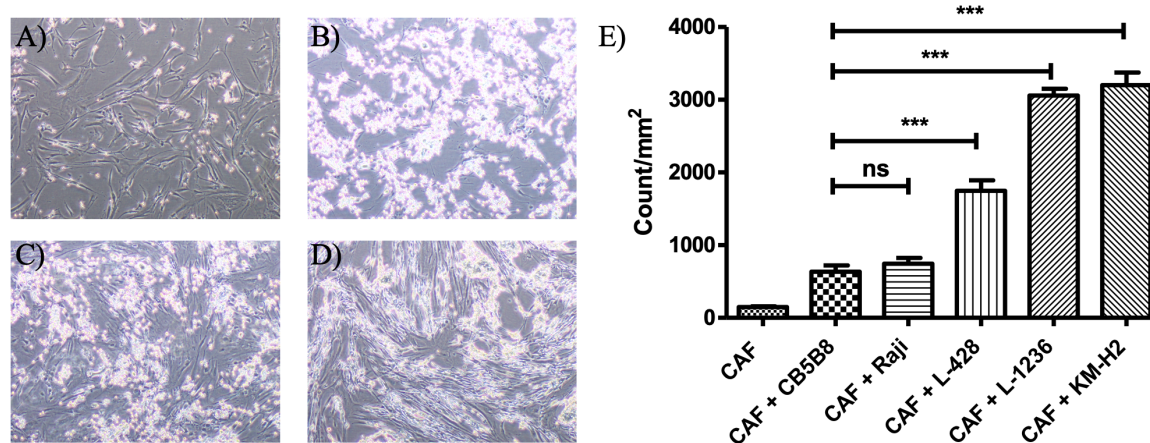
Figure 19: HRS cells from cHL cell lines show strong adherence to NS cHL fibroblasts.

A) Representative image of cancer-associated fibroblasts (CAF) cocultured with a lymphoblastoid cell line (CB5B8) after removal of the floating cells in suspension by washing of the fibroblasts (4x magnification). B) Representative image of cancer-associated fibroblasts (CAF) cocultured with cHL cell line L-428 after removal of the floating cells in suspension by washing of the fibroblasts (4x magnification). C) Representative image of cancer-associated fibroblasts (CAF) cocultured with the cHL cell line L-1236 after removal of the floating cells in suspension by washing of the fibroblasts (4x magnification). D) Representative image of cancer-associated fibroblasts (CAF) cocultured with the cHL cell line KM-H2 after removal of the floating cells in suspension by washing of the fibroblasts (4x magnification). E) Quantification of cells adhering to cancer-associated fibroblasts (CAF) after coculture for 12 h and removal of the floating cells in suspension by washing of the fibroblasts. Means + SEM of four independent experiments in biological and technical duplicates using two locations per well, *** $p < 0.001$, One-Way-ANOVA with Bonferroni correction for multiple comparisons.

Luteolin effectively decreases the ability of HRS cells (L-428) to adhere to CAFs. Figure 20A and B show representative images of interaction without luteolin treatment and interaction after the addition of luteolin, respectively. Mean + SEM counts per area of adhered L-428 cells of four independent experiments is plotted in Figure 20C and confirms visual observation by aforementioned quantification as significantly altered. The extent of blocked interaction is increased if luteolin is first applied to CAF (Figure 20C bar: "CAF + Luteolin [30 µM]+ L-428"). Once interaction took place luteolin addition did not address all adhered cocultures (Figure 20C bar: "CAF + L-428 + Luteolin [30 µM]").
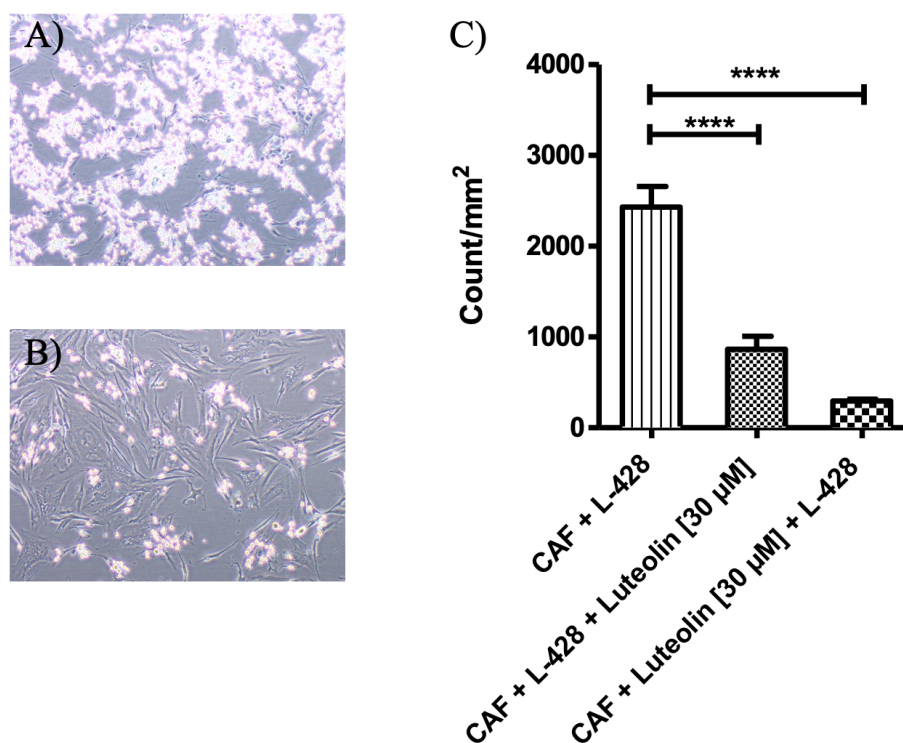
Figure 20: Luteolin impairs the strong adherence-based interaction between cHL derived CAFs and HRS cell line L-428.

A) Representative image of cancer-associated fibroblasts (CAF) cocultured with a cHL cell line L-428 after removal of the floating cells in suspension by washing of the fibroblasts (4x magnification). B) Representative image of CAF cocultured with cHL cell line L-428 and treated with luteolin after removal of the floating cells in suspension by washing of the floating cells (4x magnification). C) Quantification of cells adhering to CAF after coculture for 12 h and removal of the floating cells in suspension by washing of the fibroblasts. Means + SEM of four independent experiments in duplicates using two locations per well, **** $p<0.0001$, One-Way-ANOVA with Bonferroni correction for multiple comparisons.

4.3.2 HRS cells - CAF interaction triggers migration and chemotaxis

Assuming that aforementioned specific adherence of HRS cells to CAF (section 3.3.1) plays a crucial role in NS cHL pathogenesis and orchestration of the microenvironment real cocultures expression was compared to a mock coculture. CAF were seeded in equivalent cell density. After plastic adherence L-428 HRS cells were added to the real coculture. For the mock coculture L-428 cells and CAF were cultured separately and pooled upon harvest. The ratio of adherent CAF to lymphoma cell lines was 1:5. Cells that remained in suspension or were improperly attached were removed by repeated gentle washing with PBS [Mg^{2+}, CA^{2+}] after 48 h. Interacting cocultured cells were harvested and total RNA isolated for further transcriptome analysis as mentioned before. Mock coculture fractions were pooled prior to cell lysis. 32 transcripts with a standard deviation larger than one resulted in two major clusters representing homogenous interacting cocultured cells. Biological replicates (blue-flagged column) and mock cocultured cells biological replicates (red-flagged column) are shown in an unsupervised hierarchical clustering heatmap in Figure 21. The heatmap shows weakly expressed transcripts in green colour and highly expressed transcripts in red colour, in three independent experiments. The legend indicates log2 values of expression.
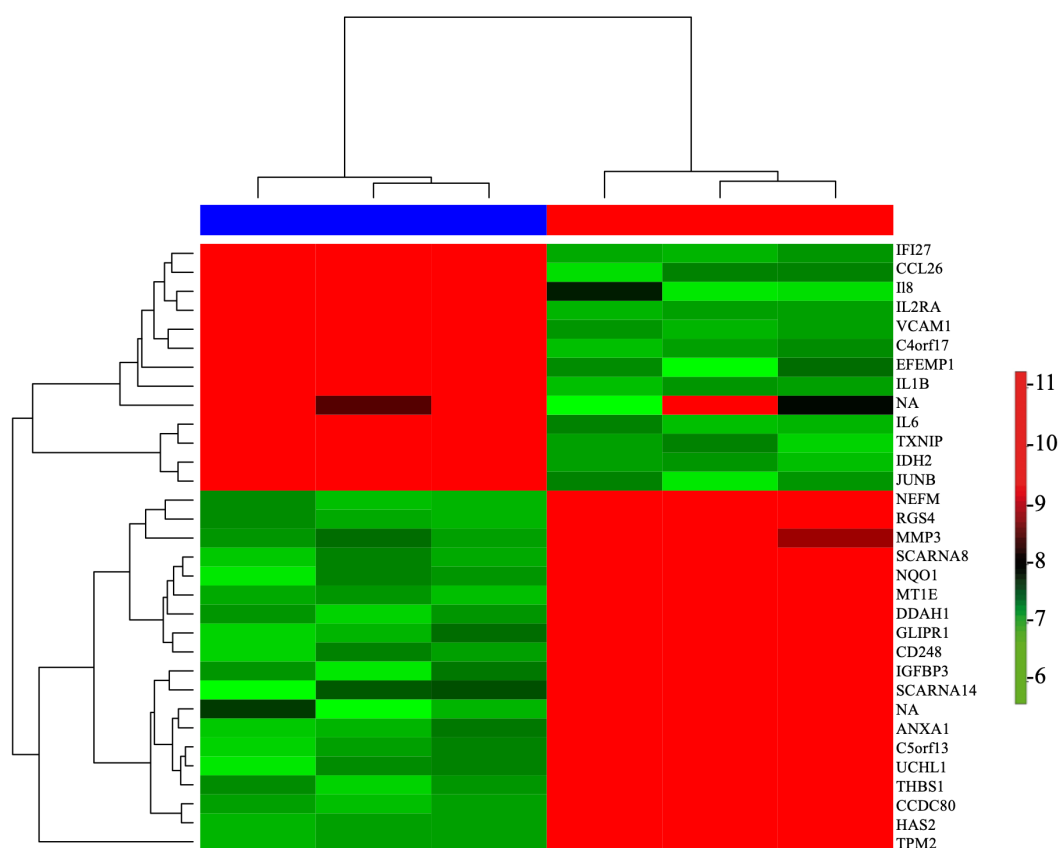
Figure 21: HRS cells adhering to NS cHL fibroblasts induce changes in the gene expression program of NS cHL fibroblasts.

Unsupervised hierarchical clustering of gene expression profiles derived from NS cHL fibroblasts (CAF) and HRS cells of the cHL cell line L-428 after 48 hr coculture (blue) and mixture of NS cHL CAF and HRS cells of the cHL cell line L-428 in the same ratio immediately prior to cell lysis (mock = red). The cluster considers all genes with a standard deviation ≥ 1 which was observed in 32 genes of three biologically independent samples per group. The heatmap shows less expressed transcripts in green colour and highly expressed transcripts in red colour. The legend indicates log-based values of expression.

Supervised analysis of gene expression data identified differentially regulated targets between the two groups. 38 genes shown in Table 21 fulfilled the applied selection criteria (p ≤ 0.05; FC ≥ |3|; FDR ≤ 0.1). Fold changes (FC) range from -8.1 to 9.1. Among all targets several **immune modulating** transcripts such as CAF key regulator *IL6* (interleukin 6), *CXCL8* (chemokine (C-X-C motif) ligand 8), *CCL26* (chemokine (C-C motif) ligand 26), *IFI27* (interferon, alpha-inducible protein 27), *IL1B* (interleukin 1B) and *HCST* (hematopoietic cell signal transducer) are upregulated upon interaction. **Extracellular matrix assembly** is deregulated via *MMP3* (matrix metallopeptidase 3 (stromelysin 1, progelatinase)), *THBS1* (thrombospondin 1) and *EFEMP1* (EGF containing fibulin-like

extracellular matrix protein 1). **Adhesion** is altered via expression of e.g. *VCAM1* (vascular cell adhesion molecule 1), *DCBLD2* (discoidin, CUB and LCCL domain containing 2) and *THBS1*. Furthermore, **MAPK cascade (mitogen-activated protein kinase)** activation is positively influenced by *RGS4* (regulator of G-protein signaling 4), *THBS1* and *IL1B*.

Table 21: Deregulated transcripts following adherence-based interaction of CAF and HRS cells coculture (co) *in vitro* in comparison to mock cocultured CAF and HRS cells.
(Filter criteria: $p \leq 0.05$; FC $\geq |3|$; FDR ≤ 0.1)

FC co vs. mock	p-value	FDR	Gene Symbol	Gene Description
-8.1	0.00006	0.0005	*HAS2*	hyaluronan synthase 2
-7.0	0.00002	0.0004	*CCDC80*	coiled-coil domain containing 80
-5.7	0.00003	0.0005	*MT1E*	metallothionein 1E
-5.1	0.00002	0.0004	*NEFM*	neurofilament, medium polypeptide
-5.0	0.00085	0.0017	*RGS4*	regulator of G-protein signaling 4
-4.8	0.00004	0.0005	*DDAH1*	dimethylarginine dimethylaminohydrolase 1
-4.7	0.00005	0.0005	*NQO1*	NAD(P)H dehydrogenase, quinone 1
-4.6	0.00015	0.0007	*SCARNA8*	small Cajal body-specific RNA 8
-4.5	0.00010	0.0006	*ANXA1*	annexin A1
-4.3	0.00012	0.0006	*CD248*	CD248 molecule, endosialin
-4.1	0.00012	0.0006	*TPM2*	tropomyosin 2 (beta)
-4.0	0.00168	0.0026	*SCARNA14*	small Cajal body-specific RNA 14
-3.8	0.00002	0.0004	*THBS1*	thrombospondin 1
-3.7	0.00046	0.0012	*UCHL1*	ubiquitin carboxyl-terminal esterase L1 (ubiquitin thiolesterase)
-3.7	0.00015	0.0007	*NREP*	neuronal regeneration related protein
-3.5	0.00009	0.0005	*IGFBP3*	insulin-like growth factor binding protein 3
-3.3	0.00028	0.0009	*GLIPR1*	GLI pathogenesis-related 1

FC co vs. mock	p-value	FDR	Gene Symbol	Gene Description
-3.2	0.00041	0.0011	*MT1L*	metallothionein 1L (gene/pseudogene)
-3.2	0.00025	0.0008	*DKK1*	dickkopf WNT signaling pathway inhibitor 1
-3.2	0.00004	0.0005	*SCARNA11*	small Cajal body-specific RNA 11
-3.1	0.01389	0.0147	*MMP3*	matrix metallopeptidase 3 (stromelysin 1, progelatinase)
-3.0	0.00195	0.0029	*DCBLD2*	discoidin, CUB and LCCL domain containing 2
-3.0	0.00068	0.0014	*PDGFC*	platelet derived growth factor C
3.2	0.00046	0.0011	*HCST*	hematopoietic cell signal transducer
3.2	0.00015	0.0007	*TVP23A*	trans-golgi network vesicle protein 23 homolog A (S. cerevisiae)
3.3	0.00008	0.0005	*SERPING1*	serpin peptidase inhibitor, clade G (C1 inhibitor), member 1
3.3	0.00028	0.0009	*EFEMP1*	EGF containing fibulin-like extracellular matrix protein 1
3.5	0.00012	0.0006	*VCAM1*	vascular cell adhesion molecule 1
3.5	0.00129	0.0022	*CXCL8*	chemokine (C-X-C motif) ligand 8
3.6	0.00000	0.0003	*IDH2*	isocitrate dehydrogenase 2 (NADP+), mitochondrial
3.6	0.00003	0.0004	*IL6*	interleukin 6
3.8	0.00007	0.0005	*IFI27*	interferon, alpha-inducible protein 27
4.0	0.00012	0.0006	*JUNB*	jun B proto-oncogene
4.4	0.00009	0.0006	*IL2RA*	interleukin 2 receptor, alpha
4.5	0.00002	0.0004	*TXNIP*	thioredoxin interacting protein
5.2	0.00006	0.0005	*FDCSP*	follicular dendritic cell secreted protein
5.4	0.00087	0.0017	*CCL26*	chemokine (C-C motif) ligand 26
9.1	0.00000	0.0002	*IL1B*	interleukin 1, beta

Table 22 shows REACTOME pathways and biological processes that are overrepresented in consequence of coculture interaction using Cytoscape ClueGo plugin. Of 38 uploaded IDs all genes were recognised by ClueGo and eight (21.1%) were associated with overrepresented functional annotations in all selected ontologies from cluster 1. Annotated pathways are dominated by pathways contributed to leukocyte chemotaxis, myeloid leukocyte migration and interleukin-4 and interleukin-13 signaling.

Table 22: Overrepresented pathways after direct interaction of NS cHL CAF and HRS cells *in vitro*.
(Annotated to gene ontologies of REACTOME_Pathways and Biological processes library; Filter criteria: p ≤ 0,05; FC ≥ |3|; FDR ≤ 0,1)

GO Term	GO Level	GO Group	% [Associated Genes]	n [Genes]	Associated Genes Found
Interleukin-4 and Interleukin-13 signaling (REACTOME_ Pathways)	[-1]	0	6.48	7	[*ANXA1, CXCL8, IL1B, IL6, JUNB, MMP3, VCAM1*]
Leukocyte chemotaxis (BiologicalProcess)	[3, 5, 6]	1	2.60	5	[*ANXA1, CCL26, CXCL8, IL1B, IL6*]
Myeloid leukocyte migration (BiologicalProcess)	[3, 5, 6]	1	3.03	5	[*ANXA1, CCL26, CXCL8, IL1B, IL6*]

As demonstrated in Figure 22 upon interaction upregulated key regulators *IL1B* and *IL6* regulate the subsequent expression of further transcripts involved in leukocyte chemotaxis, and myeloid leukocyte migration as well as the signaling axis of IL4 and *IL13*. *IL1B* activates the expression of *VCAM*, *CXCL8*, *IL6* and suppresses *MMP3* expression. *IL6* in turn activates *JUNB* expression by a predicted transcription factor binding site. *IL6* further shows some experimentally validated association to the regulation of *CCL26* and *ANXA1*. Relations among transcripts have been assessed by Genomatix pathway system integrated data mining.
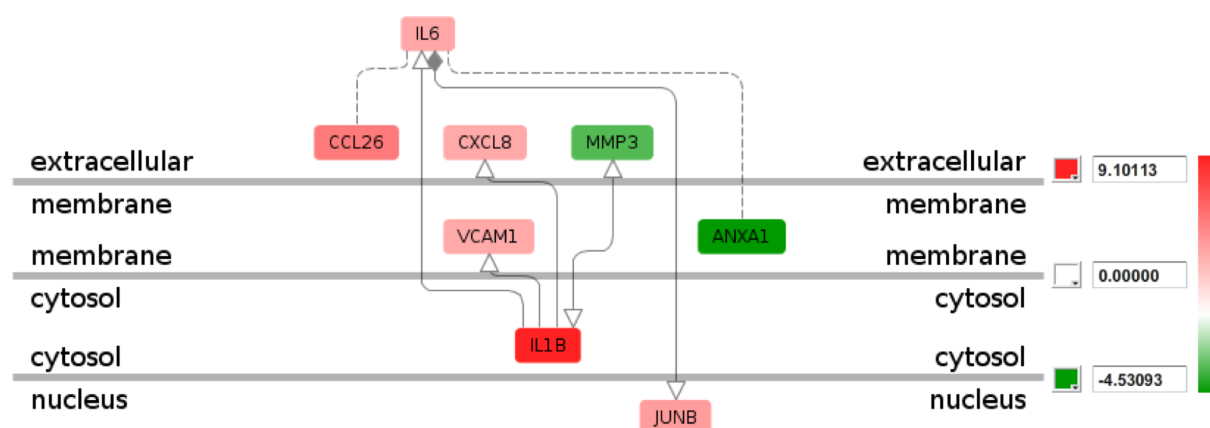
Figure 22: HRS-CAF interaction is characterised by the deregulation of 8 transcripts and its key regulators IL6 and IL1B.

Leukocyte chemotaxis, myeloid leukocyte migration and interleukin 4 and 13 signaling pathways are affected upon CAF-HRS coculture interaction by shown transcripts. The scheme shows less expressed transcripts in green colour and highly expressed transcripts in red colour. The legend indicates fold change values of expression. The scheme further depicts subcellular localisation of transcripts as indicated and their interplay. Dashed line, Association by experimental validation; solid line, Association by expert-curation; arrowhead, activation; white arrowhead, there is no promoter binding noted; rhombus, predicted or validated transcription factor binding site; grey rhombus, if gene A has a known matrix and gene B has a corresponding binding site in one of its promoters. Map and interplay have been generated by Genomatix pathway system. Fold changes are displayed by red colour for upregulation and green colour for downregulation.

4.3.3   CD29 rules the interaction of NS cHL CAF and HRS cell line

Since interaction of NS cHL CAF and HRS cell line L-428 initiates the expression of crucial pathways in cHL microenvironment it is of great interest to study the molecules involved in binding. Molecules known from literature (Fromm et al., 2006; Fromm & Wood, 2012) and from own experimental data to be involved in cell-cell contact were blocked before coculture set up by incubation with blocking antibodies (BA). Afterwards, the HRS cells properly adhered to NS cHL CAF were quantified as described before and displayed in Figure 23. The impact of blocking CD18, CD29, CD49b, CD47 and CD54 alone or combined was previously assessed in a single experiment with up to six technical replicates to identify high impact blocking mechanisms. Isotype controls have been applied as well to evaluate specificity of BA. Isotype control experiments did not show any impact on interaction (data not shown). Furthermore, pre-incubation of either CAF or L-428 cells or both was tested. No statistical testing was applied. A clear effect of CD29

71

blocking was observed which led to extended testing of CD29 blocking including HRS cell lines L-428, L-1236 and KM-H2 (Figure B). CD29 significantly blocked adherence of all HRS cell lines to NS cHL CAF. Means + SEM of three or six independent experiments in triplicates are shown assuming that by the completion of this experiment CD29 is one potential molecule facilitating CAF-HRS cell interaction from both, malignant and microenvironment site.
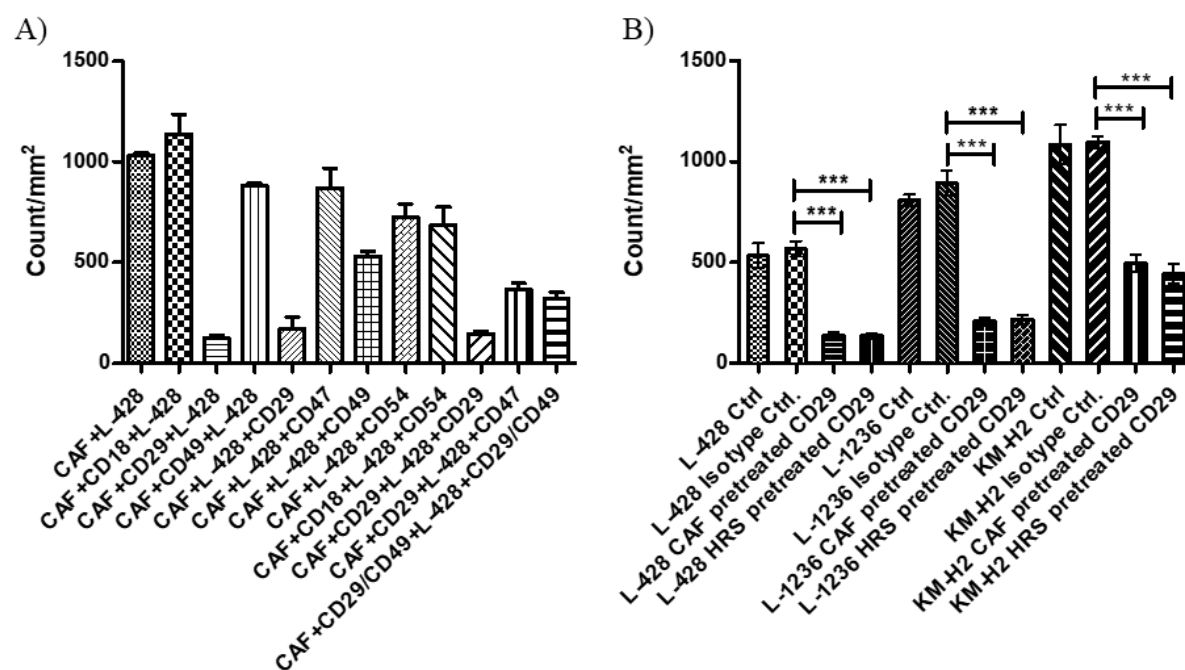
Figure 23: HRS cells from cHL cell lines show strong adherence to NS cHL fibroblasts that can be partly blocked by anti-CD29 antibody.

F. Pre-incubation of cancer-associated fibroblasts (CAF) or HRS cells with CD29 blocking antibodies before coculture significantly decreases adherence of HRS cells to fibroblasts. Either HRS cells or fibroblasts were pre-incubated with the CD29 blocking antibody. Means + SEM of three or six independent experiments in triplicates, *** p<0.001, One-Way-ANOVA with Bonferroni correction for multiple comparisons.

4.3.4 HRS cells require direct fibroblast contact to gain protection against Brentuximab-Vedotin

To clarify whether HRS cells need a direct interaction with fibroblasts or whether soluble factors delivered from fibroblasts would be sufficient to provide this effect, the following experiments were set up. In this setting, 50 µg/ml cell culture volume Brentuximab-Vedotin (BV), a CD30-specific antibody drug conjugate, was applied as previously published (Rengstl et al., 2017). Cells were stained for Annexin V and 7-amino-actinomycin D (7-AAD) and the proportion of positive cells was determined by flow cytometry after 48 h. First, HRS cell lines L-428 and L-1236 were incubated with supernatants from fibroblasts and treated with BV. However, no enhanced survival due to the addition of CAF conditioned media was observed (data not shown). Next, L-428 cells were cocultured with NS cHL CAF in a ratio of 5:1 for 12 h prior to BV treatment. For comparison, the same procedure was performed with the CD30-negative Burkitt lymphoma cell line Raji. The number of Annexin V- and 7-AAD-double positive (deceased) L-428 cells was significantly increased after BV both in the floating L-428 fraction and in adherent cells, indicating the efficiency of BV to kill HRS cells (Figure 24B). However, HRS cells that did not attach to CAF deceased in a vastly higher extent.

With respect to the viable cells, only a small, albeit significant reduction in viable cells was observed in the HRS cells adhering to fibroblasts (Figure 24A) indicating that a relevant number of HRS cells can overcome BV-induced reduction of viability when adherent to fibroblasts. No effect was observed after BV application to CD30-negative Raji cells.
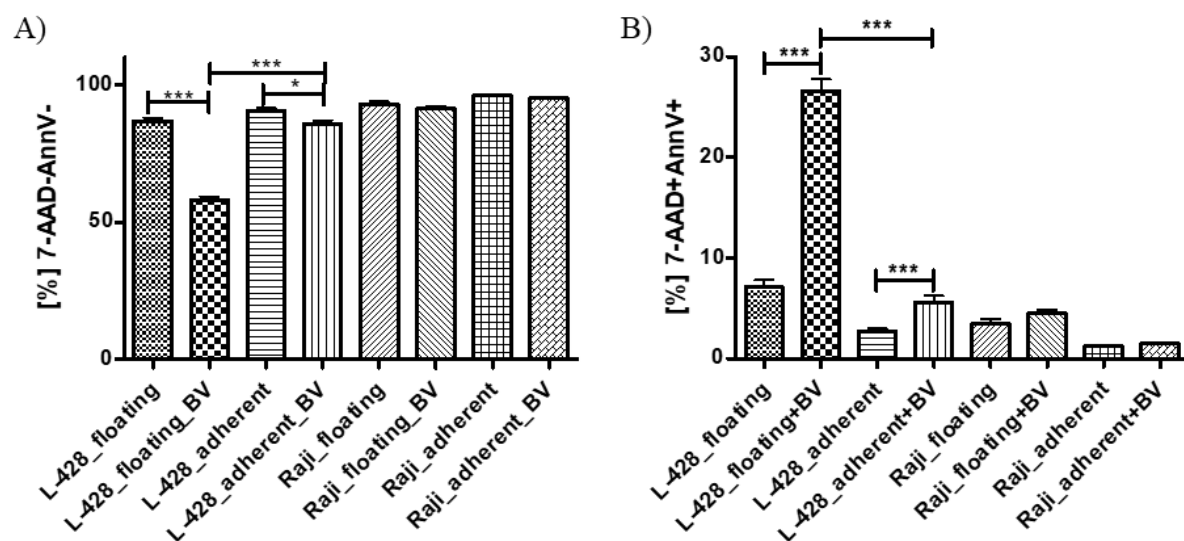
Figure 24: HRS cells adhering to NS cHL fibroblasts are protected from Brentuximab-Vedotin treatment and induce changes in the gene expression program of NS cHL fibroblasts.

(A) Number of 7-AAD and Annexin V double negative cells, representing the viable population, are substantially decreased in floating L-428 cells after BV treatment. This effect is less dramatic in L-428 cells adherent to NS cHL fibroblasts. Mean + SEM of three independent experiments in triplicates, *** p<0.001, Mann-Whitney U test. (B) Number of 7-AAD and Annexin V double positive deceased cells are significantly increased in L-428 cells after Brentuximab-Vedotin (BV) treatment. This effect is particularly observed in the cells free floating in suspension and to a lesser degree in L-428 cells adherent to NS cHL fibroblasts. Mean + SEM of three independent experiments in triplicates, *** p<0.001, Mann-Whitney U test.

5 Discussion

The complex composition of tissues leads to the circumstance that a single cellular fraction itself cannot fully display the pathogenesis of a given disease. Even though there are pathologies abolishing the microenvironment in order to fully expand, there are conditions which depend on an interplay with their surrounding cells. Burkitt lymphoma features neoplastic cells that proliferate strongly and constitute the main cellular infiltrate within a lymph node. Hodgkin Reed Sternberg cells in contrast make up a minor rare cell fraction within infiltrated tissues diagnosed Hodgkin disease. Classical Hodgkin lymphoma can be divided into four subtypes of which every subtype features a characteristic complex composition of microenvironmental accumulation of cells or their specific depletion. The unique characteristic observation within nodular sclerosing classical Hodgkin lymphoma (NS cHL) are the sclerotic bands built by recruited activated fibroblastic reticular cells (FRC). The aim of this study was to clarifiy the distinct role of the FRC (referred to as CAF) network within NS cHL. It is the first study analysing NS cHL fibroblasts obtained from primary lymphoma tissue on a molecular basis.

5.1 Fibroblasts differ according to their tissue of origin and maintain their transcript profile during cultivation

Within this study fibroblastic cells of lymph nodes of LA, MC cHL and NS cHL were extracted in order to characterise and understand their impact. An advanced isolation method as described by Fletcher *et al.* would allow for a more distinct profiling of subgroups of isolated cells right after tissue collection (Fletcher, Malhotra, Acton, et al., 2011) although limiting the amount of options for subsequent experimental set ups at the same time. Dominici *et al*. reported a method for isolation of fibroblasts which was refined by isolation methods published by Gaetano *et al.* (Dominici et al., 2006; Rossini et al., 2011). The applied method was fully sufficient to obtain the desired cells due to plastic adherence, morphology and subsequent flow cytometry quality assurance. Furthermore, it is a gentle and time saving method without the application of complex enzymatic digestion and following enrichment as applied by Fletcher *et al.* (Fletcher, Malhotra, Acton, et al., 2011). However, this advanced selection would allow to distinguish between stromal subsets originating from different areas of a lymph node like the subcapsule, medulla and

cortex. It would also allow to directly analyse the enriched cell fractions of choice in order to identify the whole signaling range. This depicts one limitation of cultivating the fibroblasts for up to five passages. During cultivation the cells lose their microenvironment and therefore might lose some of their characteristics. Nonetheless, the study proves evidence that a certain signature exists permanently which assorts the cells towards their tissue of origin (Figure 6). This finding was confirmed by several studies (Fletcher, Malhotra, Acton, et al., 2011; Rossini et al., 2011b). When collecting cells derived from primary tissues, the diagnosis needs to be confirmed before including the specimen in downstream analysis. Another requirement is the storage of excessive tissue as a suspension for later use as long as the cellular phenotype is not altered by this process. This led to the trial conserving bulk tissues suspensions in liquid nitrogen. Isolation of fibroblasts, their cultivation and expansion was still fully functional and the global transcriptome was conserved according to unsupervised analyses of transcripts (data not shown). These preliminary experiments enabled a flexible sample management of irretrievable unique primary tissues in order to reproduce trials without exceeding a critical passage in which cells become senescent. Nonetheless, permanent quality assurance and observation of the cells during the experimental phase was needed (mycoplasma testing, senescence assay, target confirmation).

5.2 Fibroblasts of different lymphadenopathies have a certain gene expression signature in common

Pointing out the basic function of FRC within the LN, common features among the three studied groups were expected. It was not possible to observe any difference by the cells´ ability to attach, their morphology, doubling time or surface marker expression during initial expansion (data not shown). All cells exhibited a stable and homogenous expression of CD29, CD90 and CD73 by complete lack of lymphocyte and follicular dendritic cell markers as CD45, CD362 and CD271. The group of LA fibroblasts was included due to the lack of healthy tissue donors accommodating the advantage to not study basic features of activated FRC but features that truly belong to NS cHL CAF. The group of MC cHL CAF was included to specifically characterise the NS cHL CAF that build the sclerotic bands. Besides the initial surface marker expression (Figure 7) αSMA and FAP were confirmed as common features. The prognostic significance is discussed among some

solid cancers. However, according to a revision by Cortez *et al.* (Cortez et al., 2014), it is not sufficient to identify all subsets of CAF. They rather suggest a differentiation of CAF into four groups by expression of either Fibroblast Activation Protein Alpha (FAP), Fibroblast-Specific Protein-1 (FSP1, also S100 Calcium Binding Protein A4 (S100A4)), and Platelet Derived Growth Factor Receptor (PDGFRα/β) with their corresponding impact on ECM modulation and immunomodulatory functions (CAF^{FAP}), metastatic colonisation, macrophage infiltration (CAF^{FSP1}), growth and angiogenesis as well as macrophage recruitment (CAF$^{PDGFR\alpha}$) and metastatic spread accommodated by high interstitial fluid pressure (CAF$^{PDGFR\beta}$) (Cortez et al., 2014; Koczorowska et al., 2016). Isolated fibroblasts commonly regulate transcripts that are associated with movement and blood vessel development, actin and ECM processes, cellular adhesion and cell junction assembly as well as response to wounding and muscle cell phenotype which are reported features of CAF in inflammatory conditions and malignant solid cancers as well as lymphomas (Becker & LeBleu, 2018; Costa et al., 2018; Dominici et al., 2018; Fletcher et al., 2010, 2015; Jeon et al., 2010; J. il Lee & Campbell, 2014; Malhotra et al., 2012, 2013; Paulsson & Micke, 2014; Staiger et al., 2017). Wernig *et al.* identified c-Jun N-Terminal Kinase 1 as a unifying mechanism in αSMA-expressing fibroblasts. C-Jun is proto-oncogene forming a transcription complex (AP-1 Transcription Factor Subunit) inducing its own and further expression driving cell cycle progression. C-Jun is further regulated by Extracellular Signal-Regulated Kinase (ERK) and RhoA signaling which is also widely described as a common feature of fibrotic diseases and myofibroblast and activates further key players that are correlated with angiogenesis, invasion and metastasis (CD47, VEGF, PDGF) (Gray et al., 2014; Wernig et al., 2017). These unifying mechanisms can depict clinical targets in order to reduce fibrosis. But there is also evidence that a basic screening of unifying fibrosis biomarkers is insufficient for explaining the fibroblasts impact. By targeting a single key player different subpopulations of fibroblasts may react differently which was summarised by Wagner referring to the studies of Pallangyo and Koliaraki pointing out the different impact of each CAF subpopulation by collagen expression (Allen & Louise Jones, 2011; Koliaraki et al., 2015; Pallangyo et al., 2015; Wagner, 2016). Taken together the given data, the studied CAFs show a phenotype which can be assorted to activation (αSMA, FAP), Collagen-I type expression (*COL1A1*), inflammation and immunomodulatory function (elevated IL6 among all). Another reported factor named lysyl

oxidase (LOX) could not be identified as deregulated among all groups or distinct groups (Tang et al., 2017).

5.3   cHL Fibroblasts differ from lymphadenitis-derived fibroblasts

Results confirmed a high purity in all samples, being a necessary requisite for all subsequent analyses. Although all fibroblasts were kept in culture up to five passages in order to expand and obtain highly pure cultures, they still displayed differences in gene expression even when bystander cells were absent. In line with this observation of a conserved gene expression programme, a highly stable methylation pattern was observed between NS cHL CAF and LA fibroblasts. Surprisingly, there was only a very weak correlation between methylation patterns and gene expression, indicating that most genes upregulated in NS cHL fibroblasts are regulated by either other mechanisms after activation by HRS cells or by proteins located upstream being in charge of writing or reading methylation. In our gene expression analysis and verification of previously published data, its confirmation shows that IL6 is an important factor in the crosstalk between NS cHL fibroblasts, bystander cells and HRS cells (Aldinucci et al., 2016).

5.4   TIMP3 and MYOCD are important for cHL fibroblasts

The study identified MYOCD and TIMP3 as generally deregulated genes in cHL CAF. While MYOCD was expressed at similar levels in NS and MC cHL CAF in the gene expression arrays, TIMP3 was more strongly expressed in NS cHL CAF. This is in line with the specific accumulation of ECM in the NS cHL type. MYOCD is an important transcription factor for the differentiation to myofibroblasts and smooth muscle cells, enhancing transcription of myosin heavy chain MYH11, Actin alpha 2, Actin beta and Actin gamma 1 (ACTA2, ACTB, ACTG1), thus promoting contractility of the cells (Miano, 2015; Raphel et al., 2012). CNN1, which is another MYOCD downstream target (Miano, 2015), was also strongly expressed in NS cHL fibroblasts. MYOCD overexpression alone was sufficient to induce a mature smooth muscle cell-like phenotype in human embryonic stem cells (Raphel et al., 2012). Furthermore, MYOCD can lead to increased type I collagen expression (Shi & Rockey, 2017) which is again confirmed by the upregulation of Collagen

Type I Alpha 1 Chain (*COL1A1*). Enhanced expression of MYOCD together with TIMP3, which inhibits the degradation of ECM are thus likely the factors that are most responsible for the accumulation of fibrotic tissue in the NS cHL subtype. Surprisingly, TIMP3 protein was not only expressed by fibroblasts, but also by the HRS cells of most cHL cases, suggesting that HRS cells themselves also inhibit degradation of ECM and thereby contribute to the accumulation of ECM. This is surprising, since TIMP3 expression is frequently lost in several types of advanced cancers (Catasus et al., 2013; Guan et al., 2013; C. H. Hsu et al., 2012). Moreover, deletion of the four TIMPs in dermal fibroblasts resulted in a CAF-like phenotype (Shimoda et al., 2014). However, we found in contrast an overexpression of TIMP3 in NS cHL CAF suggesting that this cell type apparently differs from CAFs derived from solid cancers.

5.5 Luteolin reverses the NS cHL CAF phenotype and suggests an additional senescence-like CAF phenotype

The NS cHL CAF phenotype which is acquired by these specialised fibroblasts can be inhibited by luteolin treatment, which also inhibits proliferation and TIMP3 secretion of these cells. It is a naturally-occuring flavonoid with potential antioxidant functions, negative impact on inflammation and the ability to regulate apoptosis. Their antitumour activities were discussed by Kanadaswami *et al.* (Kanadaswami et al., 2005) luteolin being one of the most active flavones targeting ATP binding site of catalytic subunits of kinases that drive the proliferation of neoplastic cells. It was further described to impact myofibroblast phenotype through RhoA which made it an interesting agent within this study since RhoA is common feature of activated fibroblasts of the analysed lymphadenopathies (Gray et al., 2014).

Surprisingly, NS cHL CAF did not undergo complete apoptosis but exhibited a condition that is likely related to cell cycle arrest. Moreover, their morphology changed from fusiform to large, flat-shaped cells. The senescence-associated secretory phenotype (SASP) is described as a condition accommodated by high expression of IL6 and IL8 leading to fibrosis and interruption of normal tissues (Coppé et al., 2008) as well as morphological changes with the consequence of paracrine promotion of tumourigenesis (Gonzalez-Meljem et al., 2018). At the same time β-Galactosidase expression was only observed in

a small fraction of CAF (data not shown). Luteolin treatment did not increase β-Galactosidase expression (data not shown). Following literature SASP cells secrete distinct proteins like annexins, collagen 6, TGFβ among others that can be all found as commonly expressed among CAF of all groups. Nonetheless, secretion might not be as high as compared to the selected common transcripts. Considering CAF´s ability to proliferate we could not conclusively confirm a SASP phenotype even though CAFs express characteristic SASP transcripts. However, luteolin treatment drove the CAF into a resting but viable phenotype. The finding suggests that active NS cHL CAF might be either a heterogenous group of CAF underlying SASP driving fibrosis and immunomodulatory functions or a far more interchangeable condition within NS cHL CAF as discussed by Prata *et al.* (Prata et al., 2018). Furthermore, the SASP Atlas describes the alteration of the fibroblastic secretome ruling biological processes associated with the tissue structure and organisation through collagen formation, ECM organisation and degradation or its maintenance, actin cytoskeleton and integrin interactions (Basisty et al., 2020). Further than this the secretion of extracellular vesicles (eSASP) is affected which mainly contributes to biological pathways associated with inflammation and membrane organisation as cell-cell adhesion (Basisty et al., 2020). It depicts the importance of the CCL5 signaling pathway which is prominent in cHL (Aldinucci et al., 2020). In line with these assumptions, Gopas *et al.* confirmed the presence of SASP markers in large Reed Sternberg cells of cHL reflecting the increase of lysosomal mass and being connected with a poorer clinical outcome (Gopas et al., 2016; Myrianthopoulos et al., 2019). Taken together, this suggests a strong paracrine dependency among NS cHL CAF and HRS cells which was supported within this study.

5.6   HRS cells stimulate and restore CAFs proliferation by paracrine stimulation

It has been described that IL7 secreted from HRS cells strongly induced proliferation of fibroblasts (Cattaruzza et al., 2009a), however, this observation could not be confirmed when adding purified IL7 to the NS cHL CAF culture. Therefore, interfering with IL6 and IL7 signaling does not seem to be a promising approach with respect to our study data. An explanation might be that the NS cHL CAF are saturated by their very own IL6

production and IL7 is not regulating any proliferation with respect to a suggested type of interchangeable SASP.

In contrast, conditioned media from cHL cell lines contained the required factors to reverse the effect of luteolin and could even enhance the proliferation of these specialised fibroblasts. As a result, it can be concluded that other factors, possibly microvesicles as previously described (Hansen et al., 2014), could be responsible for the induction of proliferation even circumventing luteolin´s impact. For the proliferation of NS cHL CAF, the presence of soluble factors derived from HRS cells in the medium was fully sufficient. Strikingly, the pro-proliferative effect of HRS cells conditioned media sheds doubts on the SASP phenotype and reinforces the idea of a given interchangeable SASP that allows proliferation in acute stimulation as mimicked by the short-term *in vitro* studies. Another option for stimulating fibroblasts other than IL6 and IL7 could have been CCL5 and IL13 which are known to be secreted by HRS cells in order to attract and trigger them as well as IL13´s function as an autocrine growth loop (Aldinucci et al., 2020; Ohshima et al., 2001; Oshima & Puri, 2001). However, CCL5 is described to drive collagen degradation being not fully in line with the accumulation of fibrotic accumulation in NS cHL. In contrast, the addition of NS cHL CAF conditioned media to cHL cell lines did not alter their proliferation which is in line with the observed HRS cell amount of cHL transformed lymph nodes. It further suggests that the direct CAF-HRS cells interplay needs to be discussed with respect to the study´s data.

5.7 Adhesion-mediated interaction of CAF and HRS cells drives pro-Hodgkin´s disease secretion of IL6, IL1B as well as VCAM-1

A close contact of HRS cells to surrounding fibroblasts may not only be a side effect of increased TIMP3 secretion, but may effectively result in the creation of a niche that is protective for the HRS cells. Additionally, HRS cell lines were proven to rapidly attach to the NS cHL CAF whereas non-neoplastic immortalised lymphoblastoid cells and Burkitt lymphoma cells did not show a comparable behavior. The addition of luteolin partially disrupted the direct interaction of the cells to the knowledge that their paracrine stimulation is still functional. In parallel a suited mock interaction was set up consisting of separated NS cHL CAF and HRS cells which have been combined after cell harvest right upfront of

cell lysis for subsequent transcriptome analysis. Transcripts showing upregulation in line with the cellular proliferation and expansion were excluded allowing for secondary data normalisation within the functional analysis. Besides the prominent involvement of IL6 upregulation during active interaction which might be due to the fact that both, HRS cells and NS cHL CAF, express elevated levels by themselves, CCL26 (Eotaxin3) was upregulated. It chemoattracts CCR3 expressing cells such as eosinophils and T-cells. Jundt *et al.* suggested TNFα to be the driving HRS cells secreted factor inducing CAF´s CCL26 expression (Jundt et al., 1999). IL1B was previously described to be expressed at increased levels by stromal cells of NS cHL cases morphologically consistent with fibroblasts (Oelmann et al., 2015) reflecting the study´s findings and assorting its expression to the NS cHL CAF. It is further reported that CXCL8 (IL8) was stimulated by guided HRS cells secreted extracellular vesicles (Aldinucci et al., 2019; Dörsam et al., 2018; Hansen et al., 2014). This might imply CXCL8 upregulation is regulated by NS cHL CAF as well in comparison to CXCL8 upregulation enhanced in eosinophils as reported by Hansen *et al.* (Hansen et al., 2014). JunB Proto-Oncogene (JUNB) was elevated in all fibroblasts among all groups and being reported to be constitutive active in HRS cells (Mathas et al., 2002). Matrix Metallopeptidase 3 (MMP3) is neither reported in cHL cases nor within the fibroblasts expression data of this study even though its decrease might be associated within ECM processes. Annexin 1 (ANXA1) is proven to be commonly upregulated by all fibroblasts among all groups. It is downregulated upon direct interaction assuming its role as potentially non-promoting the HRS cells microenvironment niche.

The induction of VCAM-1 after coculture of fibroblasts and HRS cells as well as the importance of its receptor CD29 in the adhesion between HRS cells and fibroblasts underscores the close interplay relying on cellular adhesion between HRS cells and fibroblasts. Similar observations have been made for bone marrow derived stroma cells which have a proactive role as signaling enhancers for chronic lymphocytic leukemia tumour cells (Sivina et al., 2012). It was further reported among several lymphomas (Shah et al., 2012) and in cHL as an independent prognostic marker for overall survival and disease-free survival being expressed by stromal cells (Christiansen et al., 1998).

5.8 CD29 facilitates adhesion-mediated interaction

CD29 is expressed by NS cHL CAF and HRS cell lines and is suggested to be a major target responsible for the observed adhesion-mediated interaction. Besides CD29, further proteins will be included as previously described to by Fromm *et al.* (Fromm et al., 2006; Fromm & Wood, 2012) studying purification strategies for cHL and defining suited surface marker expression molecules of which CD54 (Intercellular Adhesion Molecule 1, ICAM1) was chosen. Further molecules chosen to block in the adhesion studies have been CD47 (integrin associated protein) and CD18 (integrin beta chain 2; *ITGB2*) binding to CD11 proteins expressed by HRS cells (Fromm et al., 2006; Fromm & Wood, 2012) and reacting with CD54. CD49b (integrin alpha 2, *ITGA2*) was chosen as it constitutes a complex together with CD29. In a preliminary pilot trial CD29 indicated the major impact on disruption of the NS cHL CAF – HRS cells interaction when blocked *in vitro*. None of the other factors exhibited a similar impact. It belongs to a large integrin subfamily constituting multiple different heterodimers and being present on all nucleated cells thus facilitating numerous receptors of leukocytes, collagen, laminin and tripeptide Arg-Gly-Asp (RGD sequences) involved in adhesion processes (Barczyk et al., 2010; Zeltz et al., 2020). Late stage clinical trials studied integrin-targeting therapies such as anti-β1 agents Volociximab and P5, anti-α5 integrin agent Cilengitide or anti-α4 integrin agents Natalizumab and Vedolizumab in order to influence cancer, fibrosis, thrombosis and inflammation (Kim et al., 2016; Raab-Westphal et al., 2017).

5.9 NS cHL CAF decrease HRS cells susceptibility to Brentuximab-Vedotin treatment

Besides the stimulation of proliferation and immune modulatory impact, it was of interest if NS cHL CAF influence HRS cells susceptibility to Brentuximab-Vedotin treatment which is considered for therapy against relapsed and refractory CD30-positive hematologic malignancies (Rothe et al., 2012). Since the coculture model allowed separation of HRS cells adhering to CAF and floating, non-interacting HRS cells, apoptosis and survival was determined in both fractions after treatment of the whole coculture set up. After incubation fractions have been separated and analysed separately (Figure 24). It turned out that HRS cells interacting with CAF being located at the attached cellular monolayer are less

susceptible to Brentuximab-Vedotin than floating HRS cells of the non-interacting fraction. HRS cells cocultured with fibroblasts were protected from Brentuximab-Vedotin induced cell death only when they were adherent to fibroblasts and thus had direct contact to the stromal cell component. The amount of viable untreated floating cells was displayed in order to prove that this fraction mostly consists of viable cells suggesting that apoptotic cells detected died due to the treatment. Cell counts among all fractions have been monitored (data not shown) to assure that there was no shift towards the floating fractions caused by dying and detaching HRS cells from the monolayer fraction. Similar effects have been reported in other lymphoma entities associated with the presence of CAF. CAFs were able to protect lymphoma cells from apoptosis induced by chemotherapeutic treatments with Rituximab, Bortezumib and ABT-737 in cHL and non-Hodgkin lymphomas *in vitro* (Celegato et al., 2014; Mraz et al., 2011; Staiger et al., 2017a)

6 Outlook

The study was aiming at characterising fibroblasts in NS cHL on a molecular level in comparison to those from lymphadenitis. Techniques involved primary culture of fibroblasts. Primary cHL nodes are difficult to work with, hence there is minimal data in this field. The limited number of clinical samples tested should be seen in this light. Moreover, the studied groups consist of activated CAF leading to a few differentially regulated transcripts being heterogeneous among groups. However, despite the given heterogeneity of the gene expression profiles a few deregulated transcripts were confirmed by means of validation using an independent study cohort emphasising the results, eventually. Methylation clearly is a suited tool to distinguish groups as seen in other clinical applications (Capper et al., 2018). Soluble factors derived from HRS cells restore the proliferation of CAF and further interact through proper cell-cell adhesion mediated by CD29 – VCAM1. The altered expression after proper functional interaction of CAF and HRS cells fully reflects what was previously published and suggested among literature and can be seen as a powerful result to confirm the feasibility of the study design. A new way to explore the spatial expression within complex tissue composition, methods such as the MACSIMA platform (Miltenyi Biotec, Bergisch Gladbach, Germany) or Digital spatial profiling platform (NanoString Technologies, Seattle, WA, US) could compute segmented regions of interest dependent on their expression allocating signalling to distant CAF not interacting with HRS cells and CAF directly interacting with HRS cells (Helmink et al., 2020; Koldej & Ritchie, 2020). Finally, fibroblasts appear to provide HRS cells with a selective advantage against Brentuximab-Vedotin.

The study could have been extended in a number of ways. By blocking CD29 in the active coculture, it can be assumed that HRS cells are fully susceptible to Brentuximab-Vedotin upon accumulation of HRS cells within the floating fraction. Moreover, other agents such as anthracyclines could have been applied in order to determine the CAF´s impact. This set up was not performed due to the clear interest in facilitating a proper functional CAF – HRS cell niche in comparison to HRS cells standalone cellular fraction. *In vitro* liposarcoma and prostate cancer studies proved CAF´s ability to antagonize cancer cell´s susceptibility to doxorubicin (Cheteh et al., 2017; Harati et al., 2016). However, it was also shown that Doxorubicin can drive inflammation in cardiac myofibroblasts (Narikawa et al., 2019) depicting its effect in dependence of cellular origin and tumour entity or stage. A

more advanced study design could specifically target the CAF first in order to inhibit the protective niche and subsequently treat HRS cells with Brentuximab-Vedotin. Additionally, genetic engineering of CAF and HRS cells could allow for disabling TIMP3 expression in order to deepen the perspective of the contradictory presence of it in cHL compared to solid cancers. By targeting TIMP3 it would be possible to address fibrosis and HRS cells as both express TIMP3. Another approach could be to target IL6 receptors by Tocilizumab. This agent was already proved to improve remission of rheumatoid arthritis in phase III clinical trials (NCT00109408, NCT00106522, NCT00106574) and juvenile idiopathic arthritis (NCT00642460) (Emery et al., 2008; Genovese et al., 2008; Jones et al., 2010; Yokota et al., 2012). With respect to the found link of IL6 expression and SASP phenotype in cHL HRS cells and fibroblasts, novel methods could help to understand this mechanism. A new assay called SenTraGor (SenTraGor, Athens, Greece) is based on biotinylated Sudan Black B chemical reagent providing a method with no restrictions to any material thus well suited for archival tissues (Myrianthopoulos et al., 2019).

In the era of targeted therapies, which selectively inhibit the growth of tumour cells, the supportive and proactive role of the tumour surrounding fibroblasts should not be underestimated (Sivina et al., 2012). A few studies intensely emphasise the importance of FAP proteins expressed by CAF assuming FAP being a therapeutically suited target (Dienus et al., 2010; Kelly, 2005; Koczorowska et al., 2016; Teichgräber et al., 2015). Rabenhold *et al.* cloned a single-chain diabody fragment targeting FAP and endoglin (CD105, partially expressed among minor populations of fibroblasts) treating fibrosarcoma cell lines and resulted in specific and higher cytotoxicity towards target cells when compared to other treatments (Rabenhold et al., 2015). There are first approaches using genetically modified autologous mesenchymal stroma cells delivering tumour killing factors in patients (von Einem et al., 2019), however, this has to be further developed before it can be applied in cHL since patients already have a very high rate of cure using standard regimens. Since conventional combined modality treatment also acts on accompanying fibroblasts it has some effects that are not delivered by targeted therapies and might thus might be a matter of choice in selected patients. These therapies may accomplish treating non-responders. The urge is therefore for therapies that have highest specificity with the fewest adverse effects.

7 Summary (Deutsche Zusammenfassung)

Das klassische Hodgkin Lymphom (cHL) ist eines der häufigsten malignen Lymphome der westlichen Welt, global betrachtet jedoch eine seltene Erkrankung. Der nodulär sklerosierende Typ (NS cHL) tritt mit einer Häufigkeit von 50-60% neben drei weiteren Erscheinungsformen des cHL als häufigster Subtyp auf. Das wesentliche Merkmal, das diesen Subtyp von den anderen unterscheidet, sind expandierende Fibroblasten im Tumormilieu, die das Lymphominfiltrat in sklerosierenden Bändern mittels akkumulierter extrazellulärer Matrix (ECM) umgeben. Einige Studien haben die Interaktion zwischen den malignen Zellen des cHL, den Hodgkin-Reed-Sternberg (HRS) Zellen, und dem Tumormilieu beschrieben. Darin werden neben Tumor-assoziierten Fibroblasten (CAF; engl. *Cancer-associated fibroblasts*) vor allem die Bedeutung von T-Lymphozyten und anderen inflammatorischen Zelltypen sowie *Bystander* Zellen im cHL diskutiert. Jedoch fehlt bislang ein tiefgründiges Verständnis der Rolle der CAF selbst und deren Zusammenspiel mit den neoplastischen HRS Zellen des cHL.

Die HRS Zellen sind nur zu ca. 1% im transformierten Lymphknoten vertreten und sind an ihrer Form und Größe, sowie einem distinkten Biomarkerprofil erkennbar. Sie sind im Vergleich zum typischen Rundzellinfiltrat sehr groß und haben unförmige und pleomorphe Kerne, d.h. eine HRS Zelle kann einen Kern oder aufgrund unvollständiger Zytokinese auch mehrere Kerne aufweisen. Sie zeichnen sich weiterhin durch den Verlust des klassischen B-Zell-Phänotyps aus und exprimieren CD30 an Ihrer Zelloberfläche sowie partiell auch CD15. Der Nachweis von somatischer Hypermutation lässt auf die Passage der B-Zell Reifung im Keimzentrum schließen. CD30 ist im Rahmen der Therapie mit Brentuximab-Vedotin die Zielstruktur der HRS Zellen. Nach Bindung des monoklonalen Antikörpers wird der konjugierte Wirkstoff Monomethylauristatin E internalisiert und wirkt zytostatisch.

Im gesunden Lymphknoten kleidet das Fibroblasten-Retikular-Netzwerk (FRC Netzwerk) die Kapsel und Sinus aus und bildet mittels seinem Konduit-System das Areal des Kortex aus. Das FRC Netzwerk stützt die Struktur und wahrt die Architektur des Lymphknotens, worin sich vor allem T-Lymphozyten bewegen. Im gesunden Zustand initiiert das Protein Podoplanin (exprimiert durch FRC) die Kontraktion der FRC durch Stimulierung der Myosin-Expression. In inflammatorischen Prozessen unterbinden aktivierte dendritische Zellen den Podoplanin-Signalweg, indem sie es durch das Protein

Clec2 binden. Infolgedessen relaxieren und elongieren die FRC, was eine Ursache für die Schwellung von Lymphknoten darstellt. Diese Reaktion ist mit überstandener Infektion selbst-limitierend. Bei akuter Infektion respektive Entzündung ziehen die FRC durch die Ausschüttung von Interleukin-7 weiterhin Subpopulation von T-Lymphozyten an, die den korrespondierenden Rezeptor exprimieren. Die Rekrutierung dieser T-Lymphozyten stellt eine weitere Funktion der FRC dar: Die Regulation von Inflammation und damit einhergehende Heilung. Eine anhaltende Inflammation wird unterbunden, indem regulatorische T-Lymphozyten *transforming-growth-factor-beta* (TGFβ) exprimieren, welches von FRC über den korrespondierenden Rezeptor aufgenommen wird und die Expression von Kollagenen anregt. Die Produktion von Kollagen macht die FRC weniger zugänglich für T-Lymphozyten und der Signalweg im Rahmen der akuten Inflammation wird supprimiert. Während der malignen Transformationen von Zellen innerhalb eines Lymphknotens wird dieser Effekt insofern gesteuert, als dass die TGFβ Expression stark ansteigen kann und die FRC Kollagene akkumulieren. Der Kontakt zum Immunsystem geht dadurch verloren und damit auch die Funktionalität tumorsupprimierender immunonkologischer Prozesse. Zu sehen ist dies beispielsweise durch die Akkumulation von Fibrose im Gewebe. In soliden Tumoren werden FRC zu CAF, was auch in wenigen hämatologischen Neoplasien beschrieben ist. Beispiele hierfür sind das follikuläre Lymphom oder das NS cHL. Neben den malignen onkogenen Eigenschaften neoplastischer Zellen, schafft das Tumormikromilieu ebenso onkogene Bedingungen und kann unter anderem die Angiogenese sowie Invasion und Metastasierung von Tumoren beeinflussen und fördern. Ebenso können die FRC durch die Akkumulation von Fibrose Nischen für neoplastische Zellen bilden und erhalten, die zu ihrer Versorgung beitragen oder vor tumorsupprimierenden Einflüssen wie dem Immunsystem oder auch Wirkstoffen schützen respektive abschirmen.

Im Rahmen dieser Arbeit soll insbesondere die Rolle der CAF im NS cHL untersucht werden. Dieser cHL Subtyp unterscheidet sich durch eine prominente Fibrose von den anderen cHL Subtypen und es ist unklar, warum es Fibrose-abhängige und Fibrose-unabhängige Formen des cHL gibt, da sich die neoplastischen Zellen zwischen den genannten Subtypen morphologisch nicht unterscheiden. Das Ziel und Alleinstellungsmerkmal dieser Studie ist neben der Charakterisierung cHL-assoziierter CAF der Aufbau eines *in vitro* Modells, mit welchem die Interaktion zwischen CAF und HRS Zellen studiert werden kann. Ausgangslage stellen primäre native Restmaterialien

der Diagnostik nach Sicherung des Befundes dar. Aus den primären Geweben wurden die CAF isoliert, *in vitro* kultiviert und expandiert. Qualitätskontrollen sicherten die Beschaffenheit und Eignung der Zellen und stellten die Grundlage für den Einschluss der CAF in die anschließenden Analysen dar. Qualitätskriterien sind hierbei die Morphologie der Zellen, die Fähigkeit zu adhärieren und die Expression von Oberflächen-Molekülen, die die Spezifität der Zellen bestätigen aber auch Verunreinigungen durch andere Zellen ausschließen (Lymphozyten und dendritische Zellen).

Zur Charakterisierung des Transkriptoms wurde RNA aus den CAF isoliert, um Unterschiede zwischen den Gruppen zu identifizieren. Die zu untersuchenden Gruppen setzten sich aus Fibroblasten aus Fällen der unspezifischen Lymphadenitis (LA Fib) als nicht-maligne Kontrollgruppe, Fibrose-unabhängigen cHL (Mischtyp cHL, MC cHL CAF) und Fibrose-abhängigen cHL (noduläre Sklerose cHL, NS cHL CAF) zusammen. Allem voran ging aus den Daten hervor, dass die Gemeinsamkeiten aller Transkripte biologische Prozesse der Inflammation und Wundheilung betrifft. Dies suggeriert und bestätigt, dass die Inflammation und Wundheilung ein initialer Faktor ist, der sich darüber hinaus im cHL zu einem Seneszenz-assoziierten Phänotypen entwickeln könnte. NS cHL CAF sind in ihrem Transkriptom heterogen aber unterscheiden sich stärker von den Fibroblasten, die aus LA und MC cHL generiert wurden. Beide letztgenannten Gruppen sind ihrem Expressionsprofil ähnlicher als Fibroblasten aus NS cHL. Signifikant deregulierte Transkripte, die in dieser Arbeit näher untersucht wurden und die in NS cHL CAF stärker als in den anderen beiden Gruppen exprimiert werden sind *Myocardin* (MYOCD), *Calponin1* (CNN1), *tissue-inhibitor-of-metalloproteinase-3* (TIMP3) und *Interleukin-6*. NS cHL CAF zeigen als Population einen myofibroblastischen und inflammatorischen Phänotypen durch die verstärkte Expression von MYOCD, CNN1 und IL-6. Die Expression von *TIMP3* kann mit der starken Sklerosierung korreliert werden, da es den Abbau der ECM durch die Matrix-Metalloproteasen (MMP) inhibiert. Die Methylierung von Promoterregionen der NS cHL CAF unterscheidet sich von denen der LA CAF, jedoch konnte eine direkte Korrelation zu deregulierten Transkripten nicht nachgewiesen werden. Die Validierung auf Transkript- und Proteinebene an einer unabhängigen Kohorte mittels immunhistochemischer Färbung bestätigte das Ergebnis. TIMP3 ist hierbei das Protein, welches auch auf Proteinebene signifikant stärker von NS cHL CAF exprimiert wird und stellt somit den ersten Hinweis auf die grundlegende

Differenzierung zwischen den CAFs der cHL Subtypen dar. Beiden Subtypen gemein ist, dass die neoplastischen HRS Zellen auch TIMP3 exprimieren. Ein möglicher Übertragungsweg von TIMP3 von einer Zelle zur anderen kann der Transport über extrazelluläre Vesikel sein, was in dieser Arbeit nicht nachgewiesen wurde.

In dieser Arbeit wurden weiterhin die parakrine und direkt-gesteuerte Interaktion beider Zellfraktionen (HRS Zellen und NS cHL CAF), der Einfluss der Zellen aufeinander und daraus folgende Konsequenzen experimentell untersucht. NS cHL CAF werden parakrin durch sekretierte Faktoren (konditioniertes HRS Zell-Medium) von HRS Zellen zur Proliferation angeregt. NS cHL CAF wiederum steigern die Proliferation der HRS Zellen nicht. Interleukin-6 und Interleukin-7 allein können die Proliferation der NS cHL CAF nicht steigern. Auf Grundlage veröffentlichter Daten wurde das Flavinoid Luteolin als möglicher Inhibitor für CAF herangezogen. Luteolin inhibiert die Proliferation der NS cHL CAF und normalisiert die Überexpression der genannten Biomarker *CNN1*, *TIMP3*, *IL6* und *MYOCD*. Bei gleichzeitiger Behandlung der NS cHL CAF mit Luteolin und HRS Zellen sezernierten Faktoren kann die inhibierende Wirkung von Luteolin wieder aufgehoben werden. Somit ist die zweite Erkenntnis dieser Arbeit, dass die HRS Zellen die NS cHL CAF parakrin mitogen beeinflussen. Die Folgeversuche richten sich gezielt auf die direkte Zell-Zell-Interaktion, was in einem Kokulturmodell aus NS cHL CAF und HRS Zellen untersucht wurde. Hierfür wurden verschiedene HRS Zelllinien (L-428, L-1236, KM-H2) herangezogen. Eine nicht-maligne lymphoblastoide Zelllinie (CB5B8) und eine Burkitt Lymphom Zelllinie wurden als Referenz verwendet. Im Vergleich zu den Referenzgruppen konnte quantitativ bestätigt werden, dass die HRS Zellen spezifisch an die NS cHL CAF adhärieren. L-1236 und KM-H2 HRS Zellen interagieren stärker mit den NS cHL CAF als die L-428 HRS Zellen. Mehr L-428 HRS Zellen befanden sich in Suspension als im adhärenten *Monolayer*. Nach Behandlung mit Luteolin wurde dieser Vorgang nicht vollständig inhibiert aber beeinträchtigt. Die Interaktion zwischen CAF und HRS Zellen ist spezifisch und initiiert weiterhin eine Kaskade inflammatorischer Ereignisse durch die Expression diverser Zytokine. Dabei spielt die Sekretion von Interleukin-6 und Interleukin-1B eine zentrale Rolle, da sie unmittelbar weitere Transkripte wie VCAM-1, CCL26, CXCL8 und JunB positiv regulieren. Aus diesem Versuch kann gefolgert werden, dass die direkte Interaktion zwischen NS cHL CAF und HRS Zellen spezifisch ist und das pathogene Tumormikromilieu begünstigt.

Neben einer Auswahl bekannter Adhäsionsmoleküle führte das Blockieren von CD29 (Integrin beta 1) zu einer nahezu vollständigen Aufhebung der direkten Adhäsions-vermittelten Zell-Zell-Interaktion. CD29 war zu Beginn dieser Arbeit eines der Kriterien für den Einschluss von kultivierten primären Fibroblasten. CD29 wird ebenfalls von den HRS Zelllinien auf der Zelloberfläche exprimiert und konnte zusammenfassend als ein entscheidender Faktor für die vorher beschriebene Interaktion und deren tumorförderndes Wachstum identifiziert werden. Um die Bedeutung der Adhäsions-vermittelten Zell-Zell-Interaktion zu verstehen, wurde die HRS Zelllinie L-428 herangezogen. Die Kokultur aus HRS Zellen und NS cHL CAF bildet zwei Fraktionen aus: Der adhärente *Monolayer* als echte Kokultur und eine nicht-adhärente Fraktion, die aus HRS Zellen besteht. In einem Reaktionsansatz wurden die Fraktionen gleichermaßen mit Brentuximab-Vedotin behandelt. In beiden Zellfraktionen wurde die Vitalität und die Apoptose anschließend getrennt voneinander quantifiziert. Die HRS Zellen, die keine Interaktion zu den NS cHL CAF herstellen, sind signifikant vermehrt anfällig für die zytostatische Wirkung von Brentuximab-Vedotin, wohingegen die HRS Zellen, die mit den NS cHL CAF interagieren, eine signifikant höhere Vitalität zeigen.

Zusammenfassend beweist diese Arbeit die Stabilität des durch HRS Zellen reprogrammierten CAF Phänotyps mit inflammatorischen und myofibroblastischen Merkmalen im NS cHL. Gemeinsame Merkmale zum MC cHL und der LA sind biologische Prozesse der Wundheilung wohingegen die NS cHL CAF spezifisch TIMP3 überexprimieren. Ein geeignetes *in vitro* Modell für die Analyse parakriner und direkter Interaktion über Adhärenz zwischen CAF und HRS Zellen wurde etabliert. Die Fibroblasten sind parakrin von den HRS Zellen abhängig und werden durch sie vor der Wirkung von Luteolin geschützt. Dieses Modell unterstützt die Bedeutung der CAF für die Entstehung einer tumorfördernden Nische im infiltrierten Lymphknoten. Die Interaktion wird nachweislich über das Integrin CD29 vermittelt und reguliert weiterhin die Chemotaxis, Migration und Interleukin-13 und Interleukin-4 vermittelte biologische Prozesse, die stark durch Interleukin-6 und Interleukin-1B gesteuert werden. Letztlich bietet diese Nische einen Überlebensvorteil vor der gerichteten Therapie mit Brentuximab-Vedotin. TIMP3 ist ein möglicher Hauptfaktor für die typische starke Sklerosierung, die im NS cHL zu sehen ist und das Überleben der HRS Zellen begünstigt.

References

Acton, S. E., Farrugia, A. J., Astarita, J. L., Mourao-Sa, D., Jenkins, R. P., Nye, E., Hooper, S., van Blijswijk, J., Rogers, N. C., Snelgrove, K. J., Rosewell, I., Moita, L. F., Stamp, G., Turley, S. J., Sahai, E., & Reis e Sousa, C. (2014). Dendritic cells control fibroblastic reticular network tension and lymph node expansion. *Nature*, *514*(7523), 498-502. https://doi.org/10.1038/nature13814

Aldinucci, D., Borghese, C., & Casagrande, N. (2019). Formation of the Immunosuppressive Microenvironment of Classic Hodgkin Lymphoma and Therapeutic Approaches to Counter It. *Int J Mol Sci*, *20*(10). https://doi.org/10.3390/ijms20102416

Aldinucci, D., Borghese, C., & Casagrande, N. (2020). The CCL5/CCR5 Axis in Cancer Progression. *Cancers (Basel)*, *12*(7). https://doi.org/10.3390/cancers12071765

Aldinucci, D., Celegato, M., Borghese, C., Colombatti, A., & Carbone, A. (2011). IRF4 silencing inhibits Hodgkin lymphoma cell proliferation, survival and CCL5 secretion. *Br J Haematol*, *152*(2), 182-190. https://doi.org/10.1111/j.1365-2141.2010.08497.x

Aldinucci, D., Celegato, M., & Casagrande, N. (2016). Microenvironmental interactions in classical Hodgkin lymphoma and their role in promoting tumor growth, immune escape and drug resistance. *Cancer Lett*, *380*(1), 243-252. https://doi.org/10.1016/j.canlet.2015.10.007

Aldinucci, D., & Colombatti, A. (2014). The inflammatory chemokine CCL5 and cancer progression. *Mediators Inflamm*, *2014*, 292376. https://doi.org/10.1155/2014/292376

Aldinucci, D., Gloghini, A., Pinto, A., Colombatti, A., & Carbone, A. (2012). The role of CD40/CD40L and interferon regulatory factor 4 in Hodgkin lymphoma microenvironment. *Leuk Lymphoma*, *53*(2), 195-201. https://doi.org/10.3109/10428194.2011.605190

Aldinucci, D., Gloghini, A., Pinto, A., De Filippi, R., & Carbone, A. (2010). The classical Hodgkin's lymphoma microenvironment and its role in promoting tumour growth and immune escape. *J Pathol*, *221*(3), 248-263. https://doi.org/10.1002/path.2711

Aldinucci, D., Lorenzon, D., Olivo, K., Rapana, B., & Gattei, V. (2004). Interactions between tissue fibroblasts in lymph nodes and Hodgkin/Reed-Sternberg cells. *Leuk Lymphoma*, *45*(9), 1731-1739. https://doi.org/10.1080/10428190410001683633

Aldinucci, D., Lorenzon, D., Olivo, K., Rapana, B., & Gattei, V. (2004). Interactions between tissue fibroblasts in lymph nodes and Hodgkin/Reed-Sternberg cells. *Leuk Lymphoma*, *45*(9), 1731-1739. https://doi.org/10.1080/10428190410001683633

Allen, M., & Louise Jones, J. (2011). Jekyll and Hyde: the role of the microenvironment on the progression of cancer. *J Pathol*, *223*(2), 162-176. https://doi.org/10.1002/path.2803

Anderson, A. O., & Shaw, S. (1993). T cell adhesion to endothelium: the FRC conduit system and other anatomic and molecular features which facilitate the adhesion cascade in lymph node. *Semin Immunol*, *5*(4), 271-282. https://doi.org/10.1006/smim.1993.1031

Astarita, J. L., Cremasco, V., Fu, J., Darnell, M. C., Peck, J. R., Nieves-Bonilla, J. M., Song, K., Kondo, Y., Woodruff, M. C., Gogineni, A., Onder, L., Ludewig, B., Weimer, R. M., Carroll, M. C., Mooney, D. J., Xia, L., & Turley, S. J. (2015). The CLEC-2-podoplanin axis controls the contractility of fibroblastic reticular cells and lymph node microarchitecture. *Nat*

Immunol, 16(1), 75-84. https://doi.org/10.1038/ni.3035

Bailey, M. H., Tokheim, C., Porta-Pardo, E., Sengupta, S., Bertrand, D., Weerasinghe, A., Colaprico, A., Wendl, M. C., Kim, J., Reardon, B., Kwok-Shing Ng, P., Jeong, K. J., Cao, S., Wang, Z., Gao, J., Gao, Q., Wang, F., Liu, E. M., Mularoni, L., Rubio-Perez, C., Nagarajan, N., Cortes-Ciriano, I., Zhou, D. C., Liang, W. W., Hess, J. M., Yellapantula, V. D., Tamborero, D., Gonzalez-Perez, A., Suphavilai, C., Ko, J. Y., Khurana, E., Park, P. J., Van Allen, E. M., Liang, H., Group, M. C. W., Cancer Genome Atlas Research, N., Lawrence, M. S., Godzik, A., Lopez-Bigas, N., Stuart, J., Wheeler, D., Getz, G., Chen, K., Lazar, A. J., Mills, G. B., Karchin, R., & Ding, L. (2018). Comprehensive Characterization of Cancer Driver Genes and Mutations. *Cell, 174*(4), 1034-1035. https://doi.org/10.1016/j.cell.2018.07.034

Bailey, M. H., Tokheim, C., Porta-Pardo, E., Sengupta, S., Bertrand, D., Weerasinghe, A., Colaprico, A., Wendl, M. C., Kim, J., Reardon, B., Ng, P. K., Jeong, K. J., Cao, S., Wang, Z., Gao, J., Gao, Q., Wang, F., Liu, E. M., Mularoni, L., Rubio-Perez, C., Nagarajan, N., Cortes-Ciriano, I., Zhou, D. C., Liang, W. W., Hess, J. M., Yellapantula, V. D., Tamborero, D., Gonzalez-Perez, A., Suphavilai, C., Ko, J. Y., Khurana, E., Park, P. J., Van Allen, E. M., Liang, H., Group, M. C. W., Cancer Genome Atlas Research, N., Lawrence, M. S., Godzik, A., Lopez-Bigas, N., Stuart, J., Wheeler, D., Getz, G., Chen, K., Lazar, A. J., Mills, G. B., Karchin, R., & Ding, L. (2018). Comprehensive Characterization of Cancer Driver Genes and Mutations. *Cell, 173*(2), 371-385 e318. https://doi.org/10.1016/j.cell.2018.02.060

Bankov, K., Doring, C., Ustaszewski, A., Giefing, M., Herling, M., Cencioni, C., Spallotta, F., Gaetano, C., Kuppers, R., Hansmann, M. L., & Hartmann, S. (2019). Fibroblasts in Nodular Sclerosing Classical Hodgkin Lymphoma Are Defined by a Specific Phenotype and Protect Tumor Cells from Brentuximab-Vedotin Induced Injury. *Cancers (Basel), 11*(11). https://doi.org/10.3390/cancers11111687

Barczyk, M., Carracedo, S., & Gullberg, D. (2010). Integrins. *Cell Tissue Res, 339*(1), 269-280. https://doi.org/10.1007/s00441-009-0834-6

Basisty, N., Kale, A., Jeon, O. H., Kuehnemann, C., Payne, T., Rao, C., Holtz, A., Shah, S., Sharma, V., Ferrucci, L., Campisi, J., & Schilling, B. (2020). A proteomic atlas of senescence-associated secretomes for aging biomarker development. *PLoS Biol, 18*(1), e3000599. https://doi.org/10.1371/journal.pbio.3000599

Becker, L. M., & LeBleu, V. S. (2018). Endoglin Targeting in Colorectal Tumor Microenvironment. *Clin Cancer Res, 24*(24), 6110-6111. https://doi.org/10.1158/1078-0432.CCR-18-2023

Benjamini, Y., & Hochberg, Y. (1995). Controlling the False Discovery Rate - a Practical and Powerful Approach to Multiple Testing. *Journal of the Royal Statistical Society Series B-Statistical Methodology, 57*(1), 289-300. https://doi.org/DOI 10.1111/j.2517-6161.1995.tb02031.x

Berriz, G. F., King, O. D., Bryant, B., Sander, C., & Roth, F. P. (2003). Characterizing gene sets with FuncAssociate. *Bioinformatics, 19*(18), 2502-2504. https://doi.org/10.1093/bioinformatics/btg363

Bindea, G., Mlecnik, B., Hackl, H., Charoentong, P., Tosolini, M., Kirilovsky, A., Fridman, W. H., Pages, F., Trajanoski, Z., & Galon, J. (2009). ClueGO: a Cytoscape plug-in to decipher

functionally grouped gene ontology and pathway annotation networks. *Bioinformatics*, *25*(8), 1091-1093. https://doi.org/10.1093/bioinformatics/btp101

Brendolan, A., & Caamano, J. H. (2012). Mesenchymal cell differentiation during lymph node organogenesis. *Front Immunol*, *3*, 381. https://doi.org/10.3389/fimmu.2012.00381

Brown, F. D., & Turley, S. J. (2015). Fibroblastic reticular cells: organization and regulation of the T lymphocyte life cycle. *J Immunol*, *194*(4), 1389-1394. https://doi.org/10.4049/jimmunol.1402520

Brune, V., Tiacci, E., Pfeil, I., Doring, C., Eckerle, S., van Noesel, C. J., Klapper, W., Falini, B., von Heydebreck, A., Metzler, D., Brauninger, A., Hansmann, M. L., & Kuppers, R. (2008). Origin and pathogenesis of nodular lymphocyte-predominant Hodgkin lymphoma as revealed by global gene expression analysis. *J Exp Med*, *205*(10), 2251-2268. https://doi.org/10.1084/jem.20080809

Capper, D., Jones, D. T. W., Sill, M., Hovestadt, V., Schrimpf, D., Sturm, D., Koelsche, C., Sahm, F., Chavez, L., Reuss, D. E., Kratz, A., Wefers, A. K., Huang, K., Pajtler, K. W., Schweizer, L., Stichel, D., Olar, A., Engel, N. W., Lindenberg, K., Harter, P. N., Braczynski, A. K., Plate, K. H., Dohmen, H., Garvalov, B. K., Coras, R., Holsken, A., Hewer, E., Bewerunge-Hudler, M., Schick, M., Fischer, R., Beschorner, R., Schittenhelm, J., Staszewski, O., Wani, K., Varlet, P., Pages, M., Temming, P., Lohmann, D., Selt, F., Witt, H., Milde, T., Witt, O., Aronica, E., Giangaspero, F., Rushing, E., Scheurlen, W., Geisenberger, C., Rodriguez, F. J., Becker, A., Preusser, M., Haberler, C., Bjerkvig, R., Cryan, J., Farrell, M., Deckert, M., Hench, J., Frank, S., Serrano, J., Kannan, K., Tsirigos, A., Bruck, W., Hofer, S., Brehmer, S., Seiz-Rosenhagen, M., Hanggi, D., Hans, V., Rozsnoki, S., Hansford, J. R., Kohlhof, P., Kristensen, B. W., Lechner, M., Lopes, B., Mawrin, C., Ketter, R., Kulozik, A., Khatib, Z., Heppner, F., Koch, A., Jouvet, A., Keohane, C., Muhleisen, H., Mueller, W., Pohl, U., Prinz, M., Benner, A., Zapatka, M., Gottardo, N. G., Driever, P. H., Kramm, C. M., Muller, H. L., Rutkowski, S., von Hoff, K., Fruhwald, M. C., Gnekow, A., Fleischhack, G., Tippelt, S., Calaminus, G., Monoranu, C. M., Perry, A., Jones, C., Jacques, T. S., Radlwimmer, B., Gessi, M., Pietsch, T., Schramm, J., Schackert, G., Westphal, M., Reifenberger, G., Wesseling, P., Weller, M., Collins, V. P., Blumcke, I., Bendszus, M., Debus, J., Huang, A., Jabado, N., Northcott, P. A., Paulus, W., Gajjar, A., Robinson, G. W., Taylor, M. D., Jaunmuktane, Z., Ryzhova, M., Platten, M., Unterberg, A., Wick, W., Karajannis, M. A., Mittelbronn, M., Acker, T., Hartmann, C., Aldape, K., Schuller, U., Buslei, R., Lichter, P., Kool, M., Herold-Mende, C., Ellison, D. W., Hasselblatt, M., Snuderl, M., Brandner, S., Korshunov, A., von Deimling, A., & Pfister, S. M. (2018). DNA methylation-based classification of central nervous system tumours. *Nature*, *555*(7697), 469-474. https://doi.org/10.1038/nature26000

Catasus, L., Pons, C., Munoz, J., Espinosa, I., & Prat, J. (2013). Promoter hypermethylation contributes to TIMP3 down-regulation in high stage endometrioid endometrial carcinomas. *Histopathology*, *62*(4), 632-641. https://doi.org/10.1111/his.12047

Cattaruzza, L., Gloghini, A., Olivo, K., Di Francia, R., Lorenzon, D., De Filippi, R., Carbone, A., Colombatti, A., Pinto, A., & Aldinucci, D. (2009). Functional coexpression of Interleukin (IL)-7 and its receptor (IL-7R) on Hodgkin and Reed-Sternberg cells: Involvement of IL-7 in tumor cell growth and microenvironmental interactions of Hodgkin's lymphoma. *Int J Cancer*, *125*(5), 1092-1101. https://doi.org/10.1002/ijc.24389

Celegato, M., Borghese, C., Casagrande, N., Carbone, A., Colombatti, A., & Aldinucci, D. (2014). Bortezomib down-modulates the survival factor interferon regulatory factor 4 in Hodgkin lymphoma cell lines and decreases the protective activity of Hodgkin lymphoma-associated fibroblasts. *Leuk Lymphoma*, *55*(1), 149-159. https://doi.org/10.3109/10428194.2013.800196

Cheteh, E. H., Augsten, M., Rundqvist, H., Bianchi, J., Sarne, V., Egevad, L., Bykov, V. J., Ostman, A., & Wiman, K. G. (2017). Human cancer-associated fibroblasts enhance glutathione levels and antagonize drug-induced prostate cancer cell death. *Cell Death Dis*, *8*(6), e2848. https://doi.org/10.1038/cddis.2017.225

Christiansen, I., Sundstrom, C., Enblad, G., & Totterman, T. H. (1998). Soluble vascular cell adhesion molecule-1 (sVCAM-1) is an independent prognostic marker in Hodgkin's disease. *Br J Haematol*, *102*(3), 701-709. https://doi.org/10.1046/j.1365-2141.1998.00840.x

Chyou, S., Ekland, E. H., Carpenter, A. C., Tzeng, T. C., Tian, S., Michaud, M., Madri, J. A., & Lu, T. T. (2008). Fibroblast-type reticular stromal cells regulate the lymph node vasculature. *J Immunol*, *181*(6), 3887-3896. https://doi.org/10.4049/jimmunol.181.6.3887

Cohen, J. N., Guidi, C. J., Tewalt, E. F., Qiao, H., Rouhani, S. J., Ruddell, A., Farr, A. G., Tung, K. S., & Engelhard, V. H. (2010). Lymph node-resident lymphatic endothelial cells mediate peripheral tolerance via Aire-independent direct antigen presentation. *J Exp Med*, *207*(4), 681-688. https://doi.org/10.1084/jem.20092465

Coppe, J. P., Patil, C. K., Rodier, F., Sun, Y., Munoz, D. P., Goldstein, J., Nelson, P. S., Desprez, P. Y., & Campisi, J. (2008). Senescence-associated secretory phenotypes reveal cell-nonautonomous functions of oncogenic RAS and the p53 tumor suppressor. *PLoS Biol*, *6*(12), 2853-2868. https://doi.org/10.1371/journal.pbio.0060301

Cortez, E., Roswall, P., & Pietras, K. (2014). Functional subsets of mesenchymal cell types in the tumor microenvironment. *Semin Cancer Biol*, *25*, 3-9. https://doi.org/10.1016/j.semcancer.2013.12.010

Costa, A., Kieffer, Y., Scholer-Dahirel, A., Pelon, F., Bourachot, B., Cardon, M., Sirven, P., Magagna, I., Fuhrmann, L., Bernard, C., Bonneau, C., Kondratova, M., Kuperstein, I., Zinovyev, A., Givel, A. M., Parrini, M. C., Soumelis, V., Vincent-Salomon, A., & Mechta-Grigoriou, F. (2018). Fibroblast Heterogeneity and Immunosuppressive Environment in Human Breast Cancer. *Cancer Cell*, *33*(3), 463-479 e410. https://doi.org/10.1016/j.ccell.2018.01.011

Cremasco, V., Woodruff, M. C., Onder, L., Cupovic, J., Nieves-Bonilla, J. M., Schildberg, F. A., Chang, J., Cremasco, F., Harvey, C. J., Wucherpfennig, K., Ludewig, B., Carroll, M. C., & Turley, S. J. (2014). B cell homeostasis and follicle confines are governed by fibroblastic reticular cells. *Nat Immunol*, *15*(10), 973-981. https://doi.org/10.1038/ni.2965

Diehl, V. (2010). Hematology. Are macrophages the bad guys in Hodgkin lymphoma? *Nat Rev Clin Oncol*, *7*(6), 301-302. https://doi.org/10.1038/nrclinonc.2010.71

Diehl, V., Thomas, R. K., & Re, D. (2004). Part II: Hodgkin's lymphoma--diagnosis and treatment. *Lancet Oncol*, *5*(1), 19-26. https://doi.org/10.1016/s1470-2045(03)01320-2

Dienus, K., Bayat, A., Gilmore, B. F., & Seifert, O. (2010). Increased expression of fibroblast activation protein-alpha in keloid fibroblasts: implications for development of a novel treatment option. *Arch Dermatol Res, 302*(10), 725-731. https://doi.org/10.1007/s00403-010-1084-x

Dominici, M., Le Blanc, K., Mueller, I., Slaper-Cortenbach, I., Marini, F., Krause, D., Deans, R., Keating, A., Prockop, D., & Horwitz, E. (2006). Minimal criteria for defining multipotent mesenchymal stromal cells. The International Society for Cellular Therapy position statement. *Cytotherapy, 8*(4), 315-317. https://doi.org/10.1080/14653240600855905

Dorsam, B., Bosl, T., Reiners, K. S., Barnert, S., Schubert, R., Shatnyeva, O., Zigrino, P., Engert, A., Hansen, H. P., & von Strandmann, E. P. (2018). Hodgkin Lymphoma-Derived Extracellular Vesicles Change the Secretome of Fibroblasts Toward a CAF Phenotype. *Front Immunol, 9*, 1358. https://doi.org/10.3389/fimmu.2018.01358

Dubrot, J., Duraes, F. V., Potin, L., Capotosti, F., Brighouse, D., Suter, T., LeibundGut-Landmann, S., Garbi, N., Reith, W., Swartz, M. A., & Hugues, S. (2014). Lymph node stromal cells acquire peptide-MHCII complexes from dendritic cells and induce antigen-specific CD4(+) T cell tolerance. *J Exp Med, 211*(6), 1153-1166. https://doi.org/10.1084/jem.20132000

Dvorak, H. F. (1986). Tumors: wounds that do not heal. Similarities between tumor stroma generation and wound healing. *N Engl J Med, 315*(26), 1650-1659. https://doi.org/10.1056/NEJM198612253152606

Eikelenboom, P., Nassy, J. J., Post, J., Versteeg, J. C., & Langevoort, H. L. (1978). The histogenesis of lymph nodes in rat and rabbit. *Anat Rec, 190*(2), 201-215. https://doi.org/10.1002/ar.1091900204

Emery, P., Keystone, E., Tony, H. P., Cantagrel, A., van Vollenhoven, R., Sanchez, A., Alecock, E., Lee, J., & Kremer, J. (2008). IL-6 receptor inhibition with tocilizumab improves treatment outcomes in patients with rheumatoid arthritis refractory to anti-tumour necrosis factor biologicals: results from a 24-week multicentre randomised placebo-controlled trial. *Ann Rheum Dis, 67*(11), 1516-1523. https://doi.org/10.1136/ard.2008.092932

Filer, A. (2013). The fibroblast as a therapeutic target in rheumatoid arthritis. *Curr Opin Pharmacol, 13*(3), 413-419. https://doi.org/10.1016/j.coph.2013.02.006

Fischer, M., Juremalm, M., Olsson, N., Backlin, C., Sundstrom, C., Nilsson, K., Enblad, G., & Nilsson, G. (2003). Expression of CCL5/RANTES by Hodgkin and Reed-Sternberg cells and its possible role in the recruitment of mast cells into lymphomatous tissue. *Int J Cancer, 107*(2), 197-201. https://doi.org/10.1002/ijc.11370

Fletcher, A. L., Acton, S. E., & Knoblich, K. (2015). Lymph node fibroblastic reticular cells in health and disease. *Nat Rev Immunol, 15*(6), 350-361. https://doi.org/10.1038/nri3846

Fletcher, A. L., Lukacs-Kornek, V., Reynoso, E. D., Pinner, S. E., Bellemare-Pelletier, A., Curry, M. S., Collier, A. R., Boyd, R. L., & Turley, S. J. (2010). Lymph node fibroblastic reticular cells directly present peripheral tissue antigen under steady-state and inflammatory conditions. *J Exp Med, 207*(4), 689-697. https://doi.org/10.1084/jem.20092642

Fletcher, A. L., Malhotra, D., Acton, S. E., Lukacs-Kornek, V., Bellemare-Pelletier, A., Curry, M.,

Armant, M., & Turley, S. J. (2011). Reproducible isolation of lymph node stromal cells reveals site-dependent differences in fibroblastic reticular cells. *Front Immunol*, *2*, 35. https://doi.org/10.3389/fimmu.2011.00035

Fletcher, A. L., Malhotra, D., & Turley, S. J. (2011). Lymph node stroma broaden the peripheral tolerance paradigm. *Trends Immunol*, *32*(1), 12-18. https://doi.org/10.1016/j.it.2010.11.002

Fortin, J. P., Triche, T. J., Jr., & Hansen, K. D. (2017). Preprocessing, normalization and integration of the Illumina HumanMethylationEPIC array with minfi. *Bioinformatics*, *33*(4), 558-560. https://doi.org/10.1093/bioinformatics/btw691

Freeman, A. M., & Matto, P. (2020). Adenopathy. In *StatPearls*. https://www.ncbi.nlm.nih.gov/pubmed/30020622

Fromm, J. R., Kussick, S. J., & Wood, B. L. (2006). Identification and purification of classical Hodgkin cells from lymph nodes by flow cytometry and flow cytometric cell sorting. *Am J Clin Pathol*, *126*(5), 764-780. https://doi.org/10.1309/7371-XK6F-6P74-74XX

Fromm, J. R., & Wood, B. L. (2012). Strategies for immunophenotyping and purifying classical Hodgkin lymphoma cells from lymph nodes by flow cytometry and flow cytometric cell sorting. *Methods*, *57*(3), 368-375. https://doi.org/10.1016/j.ymeth.2012.03.028

Genovese, M. C., McKay, J. D., Nasonov, E. L., Mysler, E. F., da Silva, N. A., Alecock, E., Woodworth, T., & Gomez-Reino, J. J. (2008). Interleukin-6 receptor inhibition with tocilizumab reduces disease activity in rheumatoid arthritis with inadequate response to disease-modifying antirheumatic drugs: the tocilizumab in combination with traditional disease-modifying antirheumatic drug therapy study. *Arthritis Rheum*, *58*(10), 2968-2980. https://doi.org/10.1002/art.23940

Gentleman, R. C., Carey, V. J., Bates, D. M., Bolstad, B., Dettling, M., Dudoit, S., Ellis, B., Gautier, L., Ge, Y., Gentry, J., Hornik, K., Hothorn, T., Huber, W., Iacus, S., Irizarry, R., Leisch, F., Li, C., Maechler, M., Rossini, A. J., Sawitzki, G., Smith, C., Smyth, G., Tierney, L., Yang, J. Y., & Zhang, J. (2004). Bioconductor: open software development for computational biology and bioinformatics. *Genome Biol*, *5*(10), R80. https://doi.org/10.1186/gb-2004-5-10-r80

Gonzalez-Meljem, J. M., Apps, J. R., Fraser, H. C., & Martinez-Barbera, J. P. (2018). Paracrine roles of cellular senescence in promoting tumourigenesis. *Br J Cancer*, *118*(10), 1283-1288. https://doi.org/10.1038/s41416-018-0066-1

Gopas, J., Stern, E., Zurgil, U., Ozer, J., Ben-Ari, A., Shubinsky, G., Braiman, A., Sinay, R., Ezratty, J., Dronov, V., Balachandran, S., Benharroch, D., & Livneh, E. (2016). Reed-Sternberg cells in Hodgkin's lymphoma present features of cellular senescence. *Cell Death Dis*, *7*(11), e2457. https://doi.org/10.1038/cddis.2016.185

Graw, F., & Regoes, R. R. (2012). Influence of the fibroblastic reticular network on cell-cell interactions in lymphoid organs. *PLoS Comput Biol*, *8*(3), e1002436. https://doi.org/10.1371/journal.pcbi.1002436

Gray, A. L., Stephens, C. A., Bigelow, R. L., Coleman, D. T., & Cardelli, J. A. (2014). The polyphenols (-)-epigallocatechin-3-gallate and luteolin synergistically inhibit TGF-beta-induced myofibroblast phenotypes through RhoA and ERK inhibition. *PLoS One*, *9*(10),

e109208. https://doi.org/10.1371/journal.pone.0109208

Gretz, J. E., Anderson, A. O., & Shaw, S. (1997). Cords, channels, corridors and conduits: critical architectural elements facilitating cell interactions in the lymph node cortex. *Immunol Rev*, *156*, 11-24. https://doi.org/10.1111/j.1600-065x.1997.tb00955.x

Gretz, J. E., Kaldjian, E. P., Anderson, A. O., & Shaw, S. (1996). Sophisticated strategies for information encounter in the lymph node: the reticular network as a conduit of soluble information and a highway for cell traffic. *J Immunol*, *157*(2), 495-499. https://www.ncbi.nlm.nih.gov/pubmed/8752893

Gretz, J. E., Norbury, C. C., Anderson, A. O., Proudfoot, A. E., & Shaw, S. (2000). Lymph-borne chemokines and other low molecular weight molecules reach high endothelial venules via specialized conduits while a functional barrier limits access to the lymphocyte microenvironments in lymph node cortex. *J Exp Med*, *192*(10), 1425-1440. https://doi.org/10.1084/jem.192.10.1425

Guan, Z., Zhang, J., Song, S., & Dai, D. (2013). Promoter methylation and expression of TIMP3 gene in gastric cancer. *Diagn Pathol*, *8*, 110. https://doi.org/10.1186/1746-1596-8-110

Haley, P., Perry, R., Ennulat, D., Frame, S., Johnson, C., Lapointe, J. M., Nyska, A., Snyder, P., Walker, D., Walter, G., & Group, S. T. P. I. W. (2005). STP position paper: best practice guideline for the routine pathology evaluation of the immune system. *Toxicol Pathol*, *33*(3), 404-407; discussion 408. https://doi.org/10.1080/01926230590934304

Hanahan, D., & Weinberg, R. A. (2000). The hallmarks of cancer. *Cell, 100*(1), 57-70. https://doi.org/10.1016/s0092-8674(00)81683-9

Hanahan, D., & Weinberg, R. A. (2011). Hallmarks of cancer: the next generation. *Cell*, *144*(5), 646-674. https://doi.org/10.1016/j.cell.2011.02.013

Hansen, H. P., Engels, H. M., Dams, M., Paes Leme, A. F., Pauletti, B. A., Simhadri, V. L., Durkop, H., Reiners, K. S., Barnert, S., Engert, A., Schubert, R., Quondamatteo, F., Hallek, M., & Pogge von Strandmann, E. (2014). Protrusion-guided extracellular vesicles mediate CD30 trans-signalling in the microenvironment of Hodgkin's lymphoma. *J Pathol*, *232*(4), 405-414. https://doi.org/10.1002/path.4306

Harati, K., Daigeler, A., Hirsch, T., Jacobsen, F., Behr, B., Wallner, C., Lehnhardt, M., & Becerikli, M. (2016). Tumor-associated fibroblasts promote the proliferation and decrease the doxorubicin sensitivity of liposarcoma cells. *Int J Mol Med*, *37*(6), 1535-1541. https://doi.org/10.3892/ijmm.2016.2556

Hayakawa, M., Kobayashi, M., & Hoshino, T. (1988). Direct contact between reticular fibers and migratory cells in the paracortex of mouse lymph nodes: a morphological and quantitative study. *Arch Histol Cytol*, *51*(3), 233-240. https://doi.org/10.1679/aohc.51.233

Helmink, B. A., Reddy, S. M., Gao, J., Zhang, S., Basar, R., Thakur, R., Yizhak, K., Sade-Feldman, M., Blando, J., Han, G., Gopalakrishnan, V., Xi, Y., Zhao, H., Amaria, R. N., Tawbi, H. A., Cogdill, A. P., Liu, W., LeBleu, V. S., Kugeratski, F. G., Patel, S., Davies, M. A., Hwu, P., Lee, J. E., Gershenwald, J. E., Lucci, A., Arora, R., Woodman, S., Keung, E. Z., Gaudreau, P. O., Reuben, A., Spencer, C. N., Burton, E. M., Haydu, L. E., Lazar, A. J., Zapassodi, R., Hudgens, C. W., Ledesma, D. A., Ong, S., Bailey, M., Warren, S., Rao, D., Krijgsman, O., Rozeman, E. A., Peeper, D., Blank, C. U., Schumacher, T. N.,

Butterfield, L. H., Zelazowska, M. A., McBride, K. M., Kalluri, R., Allison, J., Petitprez, F., Fridman, W. H., Sautes-Fridman, C., Hacohen, N., Rezvani, K., Sharma, P., Tetzlaff, M. T., Wang, L., & Wargo, J. A. (2020). B cells and tertiary lymphoid structures promote immunotherapy response. *Nature*, *577*(7791), 549-555. https://doi.org/10.1038/s41586-019-1922-8

Hirosue, S., & Dubrot, J. (2015). Modes of Antigen Presentation by Lymph Node Stromal Cells and Their Immunological Implications. *Front Immunol*, *6*, 446. https://doi.org/10.3389/fimmu.2015.00446

Hsu, C. H., Peng, K. L., Kang, M. L., Chen, Y. R., Yang, Y. C., Tsai, C. H., Chu, C. S., Jeng, Y. M., Chen, Y. T., Lin, F. M., Huang, H. D., Lu, Y. Y., Teng, Y. C., Lin, S. T., Lin, R. K., Tang, F. M., Lee, S. B., Hsu, H. M., Yu, J. C., Hsiao, P. W., & Juan, L. J. (2012). TET1 suppresses cancer invasion by activating the tissue inhibitors of metalloproteinases. *Cell Rep*, *2*(3), 568-579. https://doi.org/10.1016/j.celrep.2012.08.030

Hsu, S. M., Waldron, J., Xie, S. S., & Hsu, P. L. (1995). Hodgkin's Disease and Anaplastic Large Cell Lymphoma Revisited. 1. unique cytokine and cytokine receptor profile distinguished from that of non-hodgkin's lymphomas. *J Biomed Sci*, *2*(4), 302-313. https://doi.org/10.1007/BF02255217

Huber, W., von Heydebreck, A., Sultmann, H., Poustka, A., & Vingron, M. (2002). Variance stabilization applied to microarray data calibration and to the quantification of differential expression. *Bioinformatics*, *18 Suppl 1*, S96-104. https://doi.org/10.1093/bioinformatics/18.suppl_1.s96

Irizarry, R. A., Bolstad, B. M., Collin, F., Cope, L. M., Hobbs, B., & Speed, T. P. (2003). Summaries of Affymetrix GeneChip probe level data. *Nucleic Acids Res*, *31*(4), e15. https://doi.org/10.1093/nar/gng015

Jang, S., Kelley, K. W., & Johnson, R. W. (2008). Luteolin reduces IL-6 production in microglia by inhibiting JNK phosphorylation and activation of AP-1. *Proc Natl Acad Sci U S A*, *105*(21), 7534-7539. https://doi.org/10.1073/pnas.0802865105

Jeon, E. S., Heo, S. C., Lee, I. H., Choi, Y. J., Park, J. H., Choi, K. U., Park, D. Y., Suh, D. S., Yoon, M. S., & Kim, J. H. (2010). Ovarian cancer-derived lysophosphatidic acid stimulates secretion of VEGF and stromal cell-derived factor-1 alpha from human mesenchymal stem cells. *Exp Mol Med*, *42*(4), 280-293. https://doi.org/10.3858/emm.2010.42.4.027

Jones, G., Sebba, A., Gu, J., Lowenstein, M. B., Calvo, A., Gomez-Reino, J. J., Siri, D. A., Tomsic, M., Alecock, E., Woodworth, T., & Genovese, M. C. (2010). Comparison of tocilizumab monotherapy versus methotrexate monotherapy in patients with moderate to severe rheumatoid arthritis: the AMBITION study. *Ann Rheum Dis*, *69*(1), 88-96. https://doi.org/10.1136/ard.2008.105197

Jundt, F., Anagnostopoulos, I., Bommert, K., Emmerich, F., Muller, G., Foss, H. D., Royer, H. D., Stein, H., & Dorken, B. (1999). Hodgkin/Reed-Sternberg cells induce fibroblasts to secrete eotaxin, a potent chemoattractant for T cells and eosinophils. *Blood*, *94*(6), 2065-2071. https://www.ncbi.nlm.nih.gov/pubmed/10477736

Justiz Vaillant, A. A., & Stang, C. M. (2020). Lymphoproliferative Disorders. In *StatPearls*. https://www.ncbi.nlm.nih.gov/pubmed/30725847

Kadin, M., Butmarc, J., Elovic, A., & Wong, D. (1993). Eosinophils are the major source of transforming growth factor-beta 1 in nodular sclerosing Hodgkin's disease. *Am J Pathol*, *142*(1), 11-16. https://www.ncbi.nlm.nih.gov/pubmed/8424449

Kaldjian, E. P., Gretz, J. E., Anderson, A. O., Shi, Y., & Shaw, S. (2001). Spatial and molecular organization of lymph node T cell cortex: a labyrinthine cavity bounded by an epithelium-like monolayer of fibroblastic reticular cells anchored to basement membrane-like extracellular matrix. *Int Immunol*, *13*(10), 1243-1253. https://doi.org/10.1093/intimm/13.10.1243

Kandaswami, C., Lee, L. T., Lee, P. P., Hwang, J. J., Ke, F. C., Huang, Y. T., & Lee, M. T. (2005). The antitumor activities of flavonoids. *In Vivo*, *19*(5), 895-909. https://www.ncbi.nlm.nih.gov/pubmed/16097445

Karai, L. J., Kadin, M. E., Hsi, E. D., Sluzevich, J. C., Ketterling, R. P., Knudson, R. A., & Feldman, A. L. (2013). Chromosomal rearrangements of 6p25.3 define a new subtype of lymphomatoid papulosis. *Am J Surg Pathol*, *37*(8), 1173-1181. https://doi.org/10.1097/PAS.0b013e318282d01e

Kelly, T. (2005). Fibroblast activation protein-alpha and dipeptidyl peptidase IV (CD26): cell-surface proteases that activate cell signaling and are potential targets for cancer therapy. *Drug Resist Updat*, *8*(1-2), 51-58. https://doi.org/10.1016/j.drup.2005.03.002

Kim, M. Y., Cho, W. D., Hong, K. P., Choi da, B., Hong, J. W., Kim, S., Moon, Y. R., Son, S. M., Lee, O. J., Lee, H. C., & Song, H. G. (2016). Novel monoclonal antibody against beta 1 integrin enhances cisplatin efficacy in human lung adenocarcinoma cells. *J Biomed Res*, *30*(3), 217-224. https://doi.org/10.7555/JBR.30.2016K0005

Koczorowska, M. M., Tholen, S., Bucher, F., Lutz, L., Kizhakkedathu, J. N., De Wever, O., Wellner, U. F., Biniossek, M. L., Stahl, A., Lassmann, S., & Schilling, O. (2016). Fibroblast activation protein-alpha, a stromal cell surface protease, shapes key features of cancer associated fibroblasts through proteome and degradome alterations. *Mol Oncol*, *10*(1), 40-58. https://doi.org/10.1016/j.molonc.2015.08.001

Koldej, R. M., Ritchie, D.S. (2020). High multiplex analysis of the immune microenvironment in bone marrow trephine samples using GeoMX™ digital spatial profiling. *Immuno-Oncology Technology*, *5*, 1-9. https://doi.org/10.1016/j.iotech.2020.02.001

Koliaraki, V., Pasparakis, M., & Kollias, G. (2015). IKKbeta in intestinal mesenchymal cells promotes initiation of colitis-associated cancer. *J Exp Med*, *212*(13), 2235-2251. https://doi.org/10.1084/jem.20150542

Kuppers, R., Engert, A., & Hansmann, M. L. (2012). Hodgkin lymphoma. *J Clin Invest*, *122*(10), 3439-3447. https://doi.org/10.1172/JCI61245

Kuppers, R., & Rajewsky, K. (1998). The origin of Hodgkin and Reed/Sternberg cells in Hodgkin's disease. *Annu Rev Immunol*, *16*, 471-493. https://doi.org/10.1146/annurev.immunol.16.1.471

Kuppers, R., Rajewsky, K., Zhao, M., Simons, G., Laumann, R., Fischer, R., & Hansmann, M. L. (1994). Hodgkin disease: Hodgkin and Reed-Sternberg cells picked from histological sections show clonal immunoglobulin gene rearrangements and appear to be derived from B cells at various stages of development. *Proc Natl Acad Sci U S A*, *91*(23), 10962-

10966. https://doi.org/10.1073/pnas.91.23.10962

Leavy, O. (2010). Immune tolerance: New peacekeepers identified. *Nat Rev Immunol*, *10*(5), 290. https://doi.org/10.1038/nri2766

Lee, J. I., & Campbell, J. S. (2014). Role of desmoplasia in cholangiocarcinoma and hepatocellular carcinoma. *J Hepatol*, *61*(2), 432-434. https://doi.org/10.1016/j.jhep.2014.04.014

Lee, J. I., & Campbell, J. S. (2014). Role of desmoplasia in cholangiocarcinoma and hepatocellular carcinoma. *J Hepatol*, *61*(2), 432-434. https://doi.org/10.1016/j.jhep.2014.04.014

Lee, J. W., Epardaud, M., Sun, J., Becker, J. E., Cheng, A. C., Yonekura, A. R., Heath, J. K., & Turley, S. J. (2007). Peripheral antigen display by lymph node stroma promotes T cell tolerance to intestinal self. *Nat Immunol*, *8*(2), 181-190. https://doi.org/10.1038/ni1427

Lupu, R., & Menendez, J. A. (2006). Pharmacological inhibitors of Fatty Acid Synthase (FASN)--catalyzed endogenous fatty acid biogenesis: a new family of anti-cancer agents? *Curr Pharm Biotechnol*, *7*(6), 483-493. https://doi.org/10.2174/138920106779116928

Ma, Y., Visser, L., Roelofsen, H., de Vries, M., Diepstra, A., van Imhoff, G., van der Wal, T., Luinge, M., Alvarez-Llamas, G., Vos, H., Poppema, S., Vonk, R., & van den Berg, A. (2008). Proteomics analysis of Hodgkin lymphoma: identification of new players involved in the cross-talk between HRS cells and infiltrating lymphocytes. *Blood*, *111*(4), 2339-2346. https://doi.org/10.1182/blood-2007-09-112128

Magnusson, F. C., Liblau, R. S., von Boehmer, H., Pittet, M. J., Lee, J. W., Turley, S. J., & Khazaie, K. (2008). Direct presentation of antigen by lymph node stromal cells protects against CD8 T-cell-mediated intestinal autoimmunity. *Gastroenterology*, *134*(4), 1028-1037. https://doi.org/10.1053/j.gastro.2008.01.070

Mak, T. W., Saunders, M. E., & Jett, B. D. (2014). *Primer to the Immune Response* (2nd ed.). https://doi.org/10.1016/C2009-0-62217-0

Malhotra, D., Fletcher, A. L., Astarita, J., Lukacs-Kornek, V., Tayalia, P., Gonzalez, S. F., Elpek, K. G., Chang, S. K., Knoblich, K., Hemler, M. E., Brenner, M. B., Carroll, M. C., Mooney, D. J., Turley, S. J., & Immunological Genome Project, C. (2012). Transcriptional profiling of stroma from inflamed and resting lymph nodes defines immunological hallmarks. *Nat Immunol*, *13*(5), 499-510. https://doi.org/10.1038/ni.2262

Malhotra, D., Fletcher, A. L., & Turley, S. J. (2013). Stromal and hematopoietic cells in secondary lymphoid organs: partners in immunity. *Immunol Rev*, *251*(1), 160-176. https://doi.org/10.1111/imr.12023

Marafioti, T., Hummel, M., Foss, H. D., Laumen, H., Korbjuhn, P., Anagnostopoulos, I., Lammert, H., Demel, G., Theil, J., Wirth, T., & Stein, H. (2000). Hodgkin and reed-sternberg cells represent an expansion of a single clone originating from a germinal center B-cell with functional immunoglobulin gene rearrangements but defective immunoglobulin transcription. *Blood*, *95*(4), 1443-1450. https://www.ncbi.nlm.nih.gov/pubmed/10666223

Martinez, V. G., Pankova, V., Krasny, L., Singh, T., Makris, S., White, I. J., Benjamin, A. C., Dertschnig, S., Horsnell, H. L., Kriston-Vizi, J., Burden, J. J., Huang, P. H., Tape, C. J., & Acton, S. E. (2019). Fibroblastic Reticular Cells Control Conduit Matrix Deposition

during Lymph Node Expansion. *Cell Rep*, *29*(9), 2810-2822 e2815. https://doi.org/10.1016/j.celrep.2019.10.103

Mathas, S., Hinz, M., Anagnostopoulos, I., Krappmann, D., Lietz, A., Jundt, F., Bommert, K., Mechta-Grigoriou, F., Stein, H., Dorken, B., & Scheidereit, C. (2002). Aberrantly expressed c-Jun and JunB are a hallmark of Hodgkin lymphoma cells, stimulate proliferation and synergize with NF-kappa B. *EMBO J*, *21*(15), 4104-4113. https://doi.org/10.1093/emboj/cdf389

Mebius, R. E. (2003). Organogenesis of lymphoid tissues. *Nat Rev Immunol*, *3*(4), 292-303. https://doi.org/10.1038/nri1054

Meraviglia, V., Azzimato, V., Piacentini, L., Chiesa, M., Kesharwani, R. K., Frati, C., Capogrossi, M. C., Gaetano, C., Pompilio, G., Colombo, G. I., & Rossini, A. (2014). Syngeneic cardiac and bone marrow stromal cells display tissue-specific microRNA signatures and microRNA subsets restricted to diverse differentiation processes. *PLoS One*, *9*(9), e107269. https://doi.org/10.1371/journal.pone.0107269

Miano, J. M. (2015). Myocardin in biology and disease. *J Biomed Res*, *29*(1), 3-19. https://doi.org/10.7555/JBR.29.20140151

Mills, S. E. (2012). *Histology for Pathologists* (4th edition ed.). Lippincott Williams and Wilkins.

Miyasaka, M., & Tanaka, T. (2004). Lymphocyte trafficking across high endothelial venules: dogmas and enigmas. *Nat Rev Immunol*, *4*(5), 360-370. https://doi.org/10.1038/nri1354

Mottok, A. (2020). [Microenvironment in classical Hodgkin lymphoma]. *Pathologe*, *41*(3), 254-260. https://doi.org/10.1007/s00292-020-00774-z (Tumormikromilieu im klassischen Hodgkin-Lymphom.)

Mraz, M., Zent, C. S., Church, A. K., Jelinek, D. F., Wu, X., Pospisilova, S., Ansell, S. M., Novak, A. J., Kay, N. E., Witzig, T. E., & Nowakowski, G. S. (2011). Bone marrow stromal cells protect lymphoma B-cells from rituximab-induced apoptosis and targeting integrin alpha-4-beta-1 (VLA-4) with natalizumab can overcome this resistance. *Br J Haematol*, *155*(1), 53-64. https://doi.org/10.1111/j.1365-2141.2011.08794.x

Myrianthopoulos, V., Evangelou, K., Vasileiou, P. V. S., Cooks, T., Vassilakopoulos, T. P., Pangalis, G. A., Kouloukoussa, M., Kittas, C., Georgakilas, A. G., & Gorgoulis, V. G. (2019). Senescence and senotherapeutics: a new field in cancer therapy. *Pharmacol Ther*, *193*, 31-49. https://doi.org/10.1016/j.pharmthera.2018.08.006

Narikawa, M., Umemura, M., Tanaka, R., Hikichi, M., Nagasako, A., Fujita, T., Yokoyama, U., Ishigami, T., Kimura, K., Tamura, K., & Ishikawa, Y. (2019). Doxorubicin induces trans-differentiation and MMP1 expression in cardiac fibroblasts via cell death-independent pathways. *PLoS One*, *14*(9), e0221940. https://doi.org/10.1371/journal.pone.0221940

Oelmann, E., Stein, H., Berdel, W. E., & Herbst, H. (2015). Expression of Interleukin-1 and Interleukin-1 Receptors Type 1 and Type 2 in Hodgkin Lymphoma. *PLoS One*, *10*(9), e0138747. https://doi.org/10.1371/journal.pone.0138747

Ohlund, D., Elyada, E., & Tuveson, D. (2014). Fibroblast heterogeneity in the cancer wound. *J Exp Med*, *211*(8), 1503-1523. https://doi.org/10.1084/jem.20140692

Ohlund, D., Handly-Santana, A., Biffi, G., Elyada, E., Almeida, A. S., Ponz-Sarvise, M., Corbo, V., Oni, T. E., Hearn, S. A., Lee, E. J., Chio, II, Hwang, C. I., Tiriac, H., Baker, L. A.,

Engle, D. D., Feig, C., Kultti, A., Egeblad, M., Fearon, D. T., Crawford, J. M., Clevers, H., Park, Y., & Tuveson, D. A. (2017). Distinct populations of inflammatory fibroblasts and myofibroblasts in pancreatic cancer. *J Exp Med*, *214*(3), 579-596. https://doi.org/10.1084/jem.20162024

Ohshima, K., Akaiwa, M., Umeshita, R., Suzumiya, J., Izuhara, K., & Kikuchi, M. (2001). Interleukin-13 and interleukin-13 receptor in Hodgkin's disease: possible autocrine mechanism and involvement in fibrosis. *Histopathology*, *38*(4), 368-375. https://doi.org/10.1046/j.1365-2559.2001.01083.x

Onder, L., Narang, P., Scandella, E., Chai, Q., Iolyeva, M., Hoorweg, K., Halin, C., Richie, E., Kaye, P., Westermann, J., Cupedo, T., Coles, M., & Ludewig, B. (2012). IL-7-producing stromal cells are critical for lymph node remodeling. *Blood*, *120*(24), 4675-4683. https://doi.org/10.1182/blood-2012-03-416859

Oshima, Y., & Puri, R. K. (2001). Suppression of an IL-13 autocrine growth loop in a human Hodgkin/Reed-Sternberg tumor cell line by a novel IL-13 antagonist. *Cell Immunol*, *211*(1), 37-42. https://doi.org/10.1006/cimm.2001.1828

Ozdowski, L., & Gupta, V. (2020). Physiology, Lymphatic System. In *StatPearls*. https://www.ncbi.nlm.nih.gov/pubmed/32491765

Pallangyo, C. K., Ziegler, P. K., & Greten, F. R. (2015). IKKbeta acts as a tumor suppressor in cancer-associated fibroblasts during intestinal tumorigenesis. *J Exp Med*, *212*(13), 2253-2266. https://doi.org/10.1084/jem.20150576

Paulsson, J., & Micke, P. (2014). Prognostic relevance of cancer-associated fibroblasts in human cancer. *Semin Cancer Biol*, *25*, 61-68. https://doi.org/10.1016/j.semcancer.2014.02.006

Pradervand, S., Paillusson, A., Thomas, J., Weber, J., Wirapati, P., Hagenbuchle, O., & Harshman, K. (2008). Affymetrix Whole-Transcript Human Gene 1.0 ST array is highly concordant with standard 3' expression arrays. *Biotechniques*, *44*(6), 759-762. https://doi.org/10.2144/000112751

Prata, L., Ovsyannikova, I. G., Tchkonia, T., & Kirkland, J. L. (2018). Senescent cell clearance by the immune system: Emerging therapeutic opportunities. *Semin Immunol*, *40*, 101275. https://doi.org/10.1016/j.smim.2019.04.003

Raab-Westphal, S., Marshall, J. F., & Goodman, S. L. (2017). Integrins as Therapeutic Targets: Successes and Cancers. *Cancers (Basel)*, *9*(9). https://doi.org/10.3390/cancers9090110

Rabenhold, M., Steiniger, F., Fahr, A., Kontermann, R. E., & Ruger, R. (2015). Bispecific single-chain diabody-immunoliposomes targeting endoglin (CD105) and fibroblast activation protein (FAP) simultaneously. *J Control Release*, *201*, 56-67. https://doi.org/10.1016/j.jconrel.2015.01.022

Raphel, L., Talasila, A., Cheung, C., & Sinha, S. (2012). Myocardin overexpression is sufficient for promoting the development of a mature smooth muscle cell-like phenotype from human embryonic stem cells. *PLoS One*, *7*(8), e44052. https://doi.org/10.1371/journal.pone.0044052

Rengstl, B., Kim, S., Doring, C., Weiser, C., Bein, J., Bankov, K., Herling, M., Newrzela, S., Hansmann, M. L., & Hartmann, S. (2017). Small and big Hodgkin-Reed-Sternberg cells of Hodgkin lymphoma cell lines L-428 and L-1236 lack consistent differences in gene

expression profiles and are capable to reconstitute each other. *PLoS One*, *12*(5), e0177378. https://doi.org/10.1371/journal.pone.0177378

Rengstl, B., Newrzela, S., Heinrich, T., Weiser, C., Thalheimer, F. B., Schmid, F., Warner, K., Hartmann, S., Schroeder, T., Kuppers, R., Rieger, M. A., & Hansmann, M. L. (2013). Incomplete cytokinesis and re-fusion of small mononucleated Hodgkin cells lead to giant multinucleated Reed-Sternberg cells. *Proc Natl Acad Sci U S A*, *110*(51), 20729-20734. https://doi.org/10.1073/pnas.1312509110

Rengstl, B., Rieger, M. A., & Newrzela, S. (2014). On the origin of giant cells in Hodgkin lymphoma. *Commun Integr Biol*, *7*, e28602. https://doi.org/10.4161/cib.28602

Roozendaal, R., Mebius, R. E., & Kraal, G. (2008). The conduit system of the lymph node. *Int Immunol*, *20*(12), 1483-1487. https://doi.org/10.1093/intimm/dxn110

Rossini, A., Frati, C., Lagrasta, C., Graiani, G., Scopece, A., Cavalli, S., Musso, E., Baccarin, M., Di Segni, M., Fagnoni, F., Germani, A., Quaini, E., Mayr, M., Xu, Q., Barbuti, A., DiFrancesco, D., Pompilio, G., Quaini, F., Gaetano, C., & Capogrossi, M. C. (2011). Human cardiac and bone marrow stromal cells exhibit distinctive properties related to their origin. *Cardiovasc Res*, *89*(3), 650-660. https://doi.org/10.1093/cvr/cvq290

Rossini, A., Frati, C., Lagrasta, C., Graiani, G., Scopece, A., Cavalli, S., Musso, E., Baccarin, M., Di Segni, M., Fagnoni, F., Germani, A., Quaini, E., Mayr, M., Xu, Q., Barbuti, A., DiFrancesco, D., Pompilio, G., Quaini, F., Gaetano, C., & Capogrossi, M. C. (2011). Human cardiac and bone marrow stromal cells exhibit distinctive properties related to their origin. *Cardiovasc Res*, *89*(3), 650-660. https://doi.org/10.1093/cvr/cvq290

Rothe, A., Sasse, S., Goergen, H., Eichenauer, D. A., Lohri, A., Jager, U., Bangard, C., Boll, B., von Bergwelt Baildon, M., Theurich, S., Borchmann, P., & Engert, A. (2012). Brentuximab vedotin for relapsed or refractory CD30+ hematologic malignancies: the German Hodgkin Study Group experience. *Blood*, *120*(7), 1470-1472. https://doi.org/10.1182/blood-2012-05-430918

Sasse, S., Momotow, J., & Engert, A. (2020). [Checkpoint inhibitors in Hodgkin lymphoma]. *Internist (Berl)*, *61*(7), 660-668. https://doi.org/10.1007/s00108-020-00811-2 (Checkpoint-Inhibitoren bei Hodgkin-Lymphom.)

Scandella, E., Bolinger, B., Lattmann, E., Miller, S., Favre, S., Littman, D. R., Finke, D., Luther, S. A., Junt, T., & Ludewig, B. (2008). Restoration of lymphoid organ integrity through the interaction of lymphoid tissue-inducer cells with stroma of the T cell zone. *Nat Immunol*, *9*(6), 667-675. https://doi.org/10.1038/ni.1605

Schafer, M., & Werner, S. (2008). Cancer as an overhealing wound: an old hypothesis revisited. *Nat Rev Mol Cell Biol*, *9*(8), 628-638. https://doi.org/10.1038/nrm2455

Schmitz, R., Stanelle, J., Hansmann, M. L., & Kuppers, R. (2009). Pathogenesis of classical and lymphocyte-predominant Hodgkin lymphoma. *Annu Rev Pathol*, *4*, 151-174. https://doi.org/10.1146/annurev.pathol.4.110807.092209

Schneider, C. A., Rasband, W. S., & Eliceiri, K. W. (2012). NIH Image to ImageJ: 25 years of image analysis. *Nat Methods*, *9*(7), 671-675. https://doi.org/10.1038/nmeth.2089

Scott, D. W., & Gascoyne, R. D. (2014). The tumour microenvironment in B cell lymphomas. *Nat Rev Cancer*, *14*(8), 517-534. https://doi.org/10.1038/nrc3774

Shah, N., Cabanillas, F., McIntyre, B., Feng, L., McLaughlin, P., Rodriguez, M. A., Romaguera, J., Younes, A., Hagemeister, F. B., Kwak, L., & Fayad, L. (2012). Prognostic value of serum CD44, intercellular adhesion molecule-1 and vascular cell adhesion molecule-1 levels in patients with indolent non-Hodgkin lymphomas. *Leuk Lymphoma*, *53*(1), 50-56. https://doi.org/10.3109/10428194.2011.616611

Shi, Z., & Rockey, D. C. (2017). Upregulation of the actin cytoskeleton via myocardin leads to increased expression of type 1 collagen. *Lab Invest*, *97*(12), 1412-1426. https://doi.org/10.1038/labinvest.2017.96

Shimoda, M., Principe, S., Jackson, H. W., Luga, V., Fang, H., Molyneux, S. D., Shao, Y. W., Aiken, A., Waterhouse, P. D., Karamboulas, C., Hess, F. M., Ohtsuka, T., Okada, Y., Ailles, L., Ludwig, A., Wrana, J. L., Kislinger, T., & Khokha, R. (2014). Loss of the Timp gene family is sufficient for the acquisition of the CAF-like cell state. *Nat Cell Biol*, *16*(9), 889-901. https://doi.org/10.1038/ncb3021

Siegert, S., Huang, H. Y., Yang, C. Y., Scarpellino, L., Carrie, L., Essex, S., Nelson, P. J., Heikenwalder, M., Acha-Orbea, H., Buckley, C. D., Marsland, B. J., Zehn, D., & Luther, S. A. (2011). Fibroblastic reticular cells from lymph nodes attenuate T cell expansion by producing nitric oxide. *PLoS One*, *6*(11), e27618. https://doi.org/10.1371/journal.pone.0027618

Siegert, S., & Luther, S. A. (2012). Positive and negative regulation of T cell responses by fibroblastic reticular cells within paracortical regions of lymph nodes. *Front Immunol*, *3*, 285. https://doi.org/10.3389/fimmu.2012.00285

Singh, R. R., Kunkalla, K., Qu, C., Schlette, E., Neelapu, S. S., Samaniego, F., & Vega, F. (2011). ABCG2 is a direct transcriptional target of hedgehog signaling and involved in stroma-induced drug tolerance in diffuse large B-cell lymphoma. *Oncogene*, *30*(49), 4874-4886. https://doi.org/10.1038/onc.2011.195

Sivina, M., Hartmann, E., Vasyutina, E., Boucas, J. M., Breuer, A., Keating, M. J., Wierda, W. G., Rosenwald, A., Herling, M., & Burger, J. A. (2012). Stromal cells modulate TCL1 expression, interacting AP-1 components and TCL1-targeting micro-RNAs in chronic lymphocytic leukemia. *Leukemia*, *26*(8), 1812-1820. https://doi.org/10.1038/leu.2012.63

Staege, M. S., Kewitz, S., Bernig, T., Kuhnol, C., & Mauz-Korholz, C. (2015). Prognostic Biomarkers for Hodgkin Lymphoma. *Pediatr Hematol Oncol*, *32*(7), 433-454. https://doi.org/10.3109/08880018.2015.1071903

Staiger, A. M., Duppel, J., Dengler, M. A., van der Kuip, H., Vohringer, M. C., Aulitzky, W. E., Rosenwald, A., Ott, G., & Horn, H. (2017). An analysis of the role of follicular lymphoma-associated fibroblasts to promote tumor cell viability following drug-induced apoptosis. *Leuk Lymphoma*, *58*(8), 1922-1930. https://doi.org/10.1080/10428194.2016.1263841

Staiger, A. M., Duppel, J., Dengler, M. A., van der Kuip, H., Vohringer, M. C., Aulitzky, W. E., Rosenwald, A., Ott, G., & Horn, H. (2017). An analysis of the role of follicular lymphoma-associated fibroblasts to promote tumor cell viability following drug-induced apoptosis. *Leuk Lymphoma*, *58*(8), 1922-1930. https://doi.org/10.1080/10428194.2016.1263841

Stebegg, M., Kumar, S. D., Silva-Cayetano, A., Fonseca, V. R., Linterman, M. A., & Graca, L. (2018). Regulation of the Germinal Center Response. *Front Immunol*, *9*, 2469. https://doi.org/10.3389/fimmu.2018.02469

Steidl, C., Lee, T., Shah, S. P., Farinha, P., Han, G., Nayar, T., Delaney, A., Jones, S. J., Iqbal, J., Weisenburger, D. D., Bast, M. A., Rosenwald, A., Muller-Hermelink, H. K., Rimsza, L. M., Campo, E., Delabie, J., Braziel, R. M., Cook, J. R., Tubbs, R. R., Jaffe, E. S., Lenz, G., Connors, J. M., Staudt, L. M., Chan, W. C., & Gascoyne, R. D. (2010). Tumor-associated macrophages and survival in classic Hodgkin's lymphoma. *N Engl J Med*, *362*(10), 875-885. https://doi.org/10.1056/NEJMoa0905680

Suzuki, R., & Shimodaira, H. (2006). Pvclust: an R package for assessing the uncertainty in hierarchical clustering. *Bioinformatics*, *22*(12), 1540-1542. https://doi.org/10.1093/bioinformatics/btl117

Swerdlow, S. H., Campo, E., Harris, N. L., Jaffe, E. S., Pileri, S. A., & Stein, H. (2017). *WHO Classification: Tumours of the Haematopoietic and Lymphoid Tissues. 4th Ed.* (4th revised Ed. ed.). World Health Organization.

Swerdlow, S. H., & Cook, J. R. (2020). As the world turns, evolving lymphoma classifications-past, present and future. *Hum Pathol*, *95*, 55-77. https://doi.org/10.1016/j.humpath.2019.08.019

Tang, H., Leung, L., Saturno, G., Viros, A., Smith, D., Di Leva, G., Morrison, E., Niculescu-Duvaz, D., Lopes, F., Johnson, L., Dhomen, N., Springer, C., & Marais, R. (2017). Lysyl oxidase drives tumour progression by trapping EGF receptors at the cell surface. *Nat Commun*, *8*, 14909. https://doi.org/10.1038/ncomms14909

Teichgraber, V., Monasterio, C., Chaitanya, K., Boger, R., Gordon, K., Dieterle, T., Jager, D., & Bauer, S. (2015). Specific inhibition of fibroblast activation protein (FAP)-alpha prevents tumor progression in vitro. *Adv Med Sci*, *60*(2), 264-272. https://doi.org/10.1016/j.advms.2015.04.006

Tesch, H., Jucker, M., Klein, S., Abts, H., Gunther, A., Krueger, G. R., & Diehl, V. (1992). Hodgkin and Reed-Sternberg cells express interleukin 6 and interleukin 6 receptors. *Leuk Lymphoma*, *7*(4), 297-303. https://doi.org/10.3109/10428199209049781

Thomas, R. K., Re, D., Wolf, J., & Diehl, V. (2004). Part I: Hodgkin's lymphoma--molecular biology of Hodgkin and Reed-Sternberg cells. *Lancet Oncol*, *5*(1), 11-18. https://doi.org/10.1016/s1470-2045(03)01319-6

Tiacci, E., Doring, C., Brune, V., van Noesel, C. J., Klapper, W., Mechtersheimer, G., Falini, B., Kuppers, R., & Hansmann, M. L. (2012). Analyzing primary Hodgkin and Reed-Sternberg cells to capture the molecular and cellular pathogenesis of classical Hodgkin lymphoma. *Blood*, *120*(23), 4609-4620. https://doi.org/10.1182/blood-2012-05-428896

Tykocinski, M., Schinella, R. A., & Greco, M. A. (1983). Fibroblastic reticulum cells in human lymph nodes. An ultrastructural study. *Arch Pathol Lab Med*, *107*(8), 418-422. https://www.ncbi.nlm.nih.gov/pubmed/6688169

Vaahtomeri, K., & Sixt, M. (2014). Physiology: Relax and come in. *Nature*, *514*(7523), 441-442. https://doi.org/10.1038/514441a

Vega, F., Coombes, K. R., Thomazy, V. A., Patel, K., Lang, W., & Jones, D. (2006). Tissue-specific function of lymph node fibroblastic reticulum cells. *Pathobiology*, *73*(2), 71-81. https://doi.org/10.1159/000094491

Villanova, P., Mauad, V. A. Q., Borducchi, D. M. M., & Giglio, A. D. (2020). Interim interleukin 6

levels correlate with progression-free survival in patients with classic Hodgkin's disease: a pilot study. *Hematol Transfus Cell Ther*, *42*(1), 90-92. https://doi.org/10.1016/j.htct.2018.11.009

von Andrian, U. H., & Mempel, T. R. (2003). Homing and cellular traffic in lymph nodes. *Nat Rev Immunol*, *3*(11), 867-878. https://doi.org/10.1038/nri1222

von Einem, J. C., Guenther, C., Volk, H. D., Grutz, G., Hirsch, D., Salat, C., Stoetzer, O., Nelson, P. J., Michl, M., Modest, D. P., Holch, J. W., Angele, M., Bruns, C., Niess, H., & Heinemann, V. (2019). Treatment of advanced gastrointestinal cancer with genetically modified autologous mesenchymal stem cells: Results from the phase 1/2 TREAT-ME-1 trial. *Int J Cancer*, *145*(6), 1538-1546. https://doi.org/10.1002/ijc.32230

Wagner, E. F. (2016). Cancer: Fibroblasts for all seasons. *Nature*, *530*(7588), 42-43. https://doi.org/10.1038/530042a

Wein, F., & Kuppers, R. (2016). The role of T cells in the microenvironment of Hodgkin lymphoma. *J Leukoc Biol*, *99*(1), 45-50. https://doi.org/10.1189/jlb.3MR0315-136R

Werner, L., Dreyer, J. H., Hartmann, D., Barros, M. H. M., Buttner-Herold, M., Grittner, U., & Niedobitek, G. (2020). Tumor-associated macrophages in classical Hodgkin lymphoma: hormetic relationship to outcome. *Sci Rep*, *10*(1), 9410. https://doi.org/10.1038/s41598-020-66010-z

Wernig, G., Chen, S. Y., Cui, L., Van Neste, C., Tsai, J. M., Kambham, N., Vogel, H., Natkunam, Y., Gilliland, D. G., Nolan, G., & Weissman, I. L. (2017). Unifying mechanism for different fibrotic diseases. *Proc Natl Acad Sci U S A*, *114*(18), 4757-4762. https://doi.org/10.1073/pnas.1621375114

Willard-Mack, C. L. (2006). Normal structure, function, and histology of lymph nodes. *Toxicol Pathol*, *34*(5), 409-424. https://doi.org/10.1080/01926230600867727

Yang, C. Y., Vogt, T. K., Favre, S., Scarpellino, L., Huang, H. Y., Tacchini-Cottier, F., & Luther, S. A. (2014). Trapping of naive lymphocytes triggers rapid growth and remodeling of the fibroblast network in reactive murine lymph nodes. *Proc Natl Acad Sci U S A*, *111*(1), E109-118. https://doi.org/10.1073/pnas.1312585111

Yokota, S., Tanaka, T., & Kishimoto, T. (2012). Efficacy, safety and tolerability of tocilizumab in patients with systemic juvenile idiopathic arthritis. *Ther Adv Musculoskelet Dis*, *4*(6), 387-397. https://doi.org/10.1177/1759720X12455960

Zeltz, C., Primac, I., Erusappan, P., Alam, J., Noel, A., & Gullberg, D. (2020). Cancer-associated fibroblasts in desmoplastic tumors: emerging role of integrins. *Semin Cancer Biol*, *62*, 166-181. https://doi.org/10.1016/j.semcancer.2019.08.004

Appendices

Table 23: Genes differentially expressed between fibroblasts derived from cHL and lymphadenitis
($p < 0.05$; FC $\geq \lfloor 1.5 \rfloor$; FDR ≤ 0.3).

FC CAF cHL vs. CAF LA	p-Value	FDR	Gene Symbol	Gene Description
4.2	0.006	0.281	*TIMP3*	TIMP metallopeptidase inhibitor 3
3.9	0.00006	0.138	*MYOCD*	myocardin
2.0	0.004	0.278	*RGS4*	regulator of G-protein signalling 4
1.9	0.006	0.281	*IER3*	immediate early response 3
1.7	0.001	0.187	*ENO2*	enolase 2 (gamma, neuronal)
1.6	0.005	0.278	*SERPINE1*	serpin peptidase inhibitor, clade E (nexin, plasminogen activator inhibitor type 1), member 1
1.6	0.004	0.278	*PMS2L2*	postmeiotic segregation increased 2-like 2 pseudogene
1.6	0.002	0.215	*GPX7*	glutathione peroxidase 7
1.5	0.005	0.278	*CT47A10*	cancer/testis antigen family 47, member A10
−1.5	0.004	0.278	*TSHZ2*	teashirt zinc finger homeobox 2
−1.5	0.0004	0.152	*KIAA1598*	KIAA1598
−1.6	0.005	0.278	*BMP2K*	BMP2 inducible kinase
−1.6	0.004	0.278	*CD14*	CD14 molecule
−1.6	0.006	0.281	*OSBPL8*	oxysterol binding protein-like 8
−1.6	0.0002	0.138	*PDE4DIP*	phosphodiesterase 4D interacting protein
−1.7	0.004	0.278	*CCNL1*	cyclin L1
−1.7	0.004	0.278	*SMG1*	SMG1 phosphatidylinositol 3-kinase-related kinase
−1.7	0.002	0.215	*MOCOS*	molybdenum cofactor sulfurase
−1.7	0.005	0.281	*SMG1*	SMG1 phosphatidylinositol 3-kinase-related kinase

FC CAF cHL vs. CAF LA	p-Value	FDR	Gene Symbol	Gene Description
−1.7	0.0002	0.138	*RNA5SP187*	RNA, 5S ribosomal pseudogene 187
−1.8	0.005	0.281	*DSEL*	dermatan sulfate epimerase-like
−1.8	0.002	0.230	*SCARNA9*	small Cajal body-specific RNA 9
−1.8	0.004	0.278	*ALPK2*	alpha-kinase 2
−1.9	0.005	0.281	*TFAP2A*	transcription factor AP-2 alpha (activating enhancer binding protein 2 alpha)
−2.0	0.001	0.206	*RNA5SP129*	RNA, 5S ribosomal pseudogene 129
−2.1	0.003	0.247	*PRKG2*	protein kinase, cGMP-dependent, type II
−2.2	0.0002	0.138	*VIT*	vitrin
−2.4	0.0001	0.138	*MT-TA*	mitochondrially encoded tRNA alanine
−2.7	0.0003	0.138	*GPNMB*	glycoprotein (transmembrane) nmb
−2.9	0.002	0.215	*HTR2B*	5-hydroxytryptamine (serotonin) receptor 2B, G protein-coupled
−4.0	0.001	0.161	*DSC3*	desmocollin 3

Table 24: Commonly expressed transcripts among all samples and groups exhibiting absolute expression values > 10 group considering a global standard deviation < 0.2 among all samples

LA CAF expression value		cHL CAF expression value		Gene	
Mean	SD	Mean	SD	Symbol	Description
13.0	0.2	13.2	0.3	***FN1***	fibronectin 1
12.4	0.2	12.5	0.3	***ACTB***	actin, beta
12.1	0.3	12.1	0.9	*THBS1*	thrombospondin 1
12.1	0.1	12.1	0.2	***VIM***	vimentin
12.0	0.3	12.1	0.3	*TPM2*	tropomyosin 2 (beta)
12.0	0.5	12.1	1.2	***ACTA2***	actin, alpha 2, smooth muscle, aorta

LA CAF expression value		cHL CAF expression value		Gene	
Mean	SD	Mean	SD	Symbol	Description
11.8	0.4	11.9	0.6	*ACTG1*	actin, gamma 1
11.8	0.2	11.9	0.6	*MYL9*	myosin, light chain 9, regulatory
11.7	0.3	11.6	0.2	*ANXA5*	annexin A5
11.7	0.1	11.8	0.1	*ANXA2*	annexin A2
11.7	0.2	11.7	0.4	***RHOA***	ras homolog family member A
11.6	0.2	11.9	0.4	*IGFBP3*	insulin-like growth factor binding protein 3
11.6	0.4	11.2	0.5	*LAMC1*	laminin, gamma 1 (formerly LAMB2)
11.5	0.3	11.4	0.3	*CALR*	calreticulin
11.4	0.1	11.5	0.2	*CAPNS1*	calpain, small subunit 1
11.2	0.3	11.6	0.9	***IL6***	interleukin 6
11.1	0.1	11.1	0.2	*TPM1*	tropomyosin 1 (alpha)
11.0	0.1	11.0	0.2	*YWHAQ*	tyrosine 3-monooxygenase/tryptophan 5-monooxygenase activation protein, theta
11.0	0.2	11.1	0.2	*ANXA1*	annexin A1
11.0	0.2	11.1	0.3	***TIMP2***	TIMP metallopeptidase inhibitor 2
10.9	0.3	11.0	0.4	*PFN1*	profilin 1
10.8	0.3	10.7	0.1	*YWHAB*	tyrosine 3-monooxygenase/tryptophan 5-monooxygenase activation protein, beta
10.8	0.2	10.4	0.4	*CAV1*	caveolin 1, caveolae protein, 22kDa
10.8	0.1	10.8	0.3	***S100A6***	S100 calcium binding protein A6
10.8	0.4	10.4	0.7	*IGFBP4*	insulin-like growth factor binding protein 4
10.7	0.3	10.6	0.3	*CAPN2*	calpain 2, (m/II) large subunit

LA CAF expression value		cHL CAF expression value		Gene	
Mean	SD	Mean	SD	Symbol	Description
10.6	0.3	10.7	0.6	*ACTN4*	actinin, alpha 4
10.6	0.3	10.2	0.6	*GNG12*	guanine nucleotide binding protein (G protein), gamma 12
10.5	0.3	10.7	0.3	*GJA1*	gap junction protein, alpha 1, 43kDa
10.4	0.3	10.1	1.0	***COL1A1***	collagen, type I, alpha 1
10.4	0.4	10.3	0.8	*CFL1*	cofilin 1 (non-muscle)
10.4	0.2	10.3	0.2	***ITGB1***	integrin, beta 1 (fibronectin receptor, beta polypeptide, antigen CD29 includes MDF2, MSK12)
10.4	0.4	10.2	0.9	***CNN2***	calponin 2
10.3	0.3	10.4	0.3	*GNG10*	guanine nucleotide binding protein (G protein), gamma 10
10.3	0.4	9.8	0.3	*JAK1*	Janus kinase 1
10.3	0.4	9.8	1.0	*PLCG2*	phospholipase C, gamma 2 (phosphatidylinositol-specific)
10.2	0.4	10.1	0.3	*ATP2A2*	ATPase, Ca++ transporting, cardiac muscle, slow twitch 2
10.2	0.2	9.9	0.4	*IQGAP1*	IQ motif containing GTPase activating protein 1
10.1	0.4	10.3	0.6	***ITGAV***	integrin, alpha V
10.1	0.6	10.1	0.6	***MMP2***	matrix metallopeptidase 2 (gelatinase A, 72kDa gelatinase, 72kDa type IV collagenase)
10.0	0.3	10.0	0.5	***ENG***	endoglin
10.6	0.2	10.7	0.4	***SNAI2***	snail family zinc finger 2
10.7	0.2	10.6	0.6	*ALCAM*	activated leukocyte cell adhesion molecule
9.8	0.2	9.8	0.4	*FGF2*	fibroblast growth factor 2 (basic)
10.5	0.5	11.2	0.6	*VCAN*	versican

Acknowledgements

Eidesstattliche Erklärung und Versicherung

Ich erkläre hiermit, dass ich mich bisher keiner Doktorprüfung im Mathematisch-Naturwissenschaftlichen Bereich unterzogen habe.

_28.09.2020_

Frankfurt am Main, Datum

Katrin Bankov

Ich erkläre hiermit, dass ich die vorgelegte Dissertation über

Molecular characterisation of nodular sclerosing classical Hodgkin lymphoma derived fibroblasts and their beneficial interaction with Hodgkin Reed Sternberg cells

selbständig angefertigt und mich anderer Hilfsmittel als der in ihr angegebenen nicht bedient habe, insbesondere, dass alle Entlehnungen aus anderen Schriften mit Angabe der betreffenden Schrift gekennzeichnet sind. Ich versichere, die Grundsätze der guten wissenschaftlichen Praxis beachtet, und nicht die Hilfe einer kommerziellen Promotionsvermittlung in Anspruch genommen zu haben.

_28.09.2020_

Frankfurt am Main, Datum

Katrin Bankov

Curriculum Vitae

Personal Background:

Name, Title   Bankov, Katrin Dipl. Ing. (FH) Biotechnology, M.Sc. Molecular Biotechnology

Date of birth   September 2, 1986

Place of birth   Magdeburg, Germany

Citizenship   German

Address:

Business   Dr. Senckenberg Institute of Pathology, University Hospital Frankfurt, Theodor-Stern-Kai 7, 60590 Frankfurt am Main, Germany, katrin.bankov@kgu.de

Private   Schwalbacher Strasse 27, 60326 Frankfurt am Main,

Current Position:

Since 9/2018   Laboratory and project management of Senckenberg Biobank, Dr. Senckenberg Institute of Pathology, University Hospital Frankfurt, Theodor-Stern-Kai 7, 60590 Frankfurt am Main

Educational Background:

2006 - 2009   Studies of Biotechnology, Dipl. Ing. (FH), University of Cooperative Education, Riesa, Germany

                     Diploma Thesis was held at IDT Biologica GmbH, Tornau, Germany

2009 - 2012   Studies of Molecular Biotechnology, RWTH Aachen, Aachen, Germany

                     Master Thesis was held at RKI ZKBS1, Berlin, Germany

                     Refer to: Witkowski P, Bourquain D et al., Virology 2016

1/2016	Doctoral Studies at the Faculty of Biochemistry, Chemistry, Pharmacy, Goethe University, Frankfurt am Main, Germany
	Experimental work was held at Dr. Senckenberg Institute of Pathology, University Hospital Frankfurt, Frankfurt am Main, Germany
	Refer to Rengstl B, Kim S et al, Plos One 2017; Bankov K et al., Cancers 2019

Professional Training

04 – 09/2011	Research Attachment at Kaldis Lab, IMCB, A*STAR, Singapore
2015	FELASA B Certificate, Frankfurt am Main, Germany
2018	Expertise certification according to GenTSV § 15, Jena, Germany
2019	Expertise certification GCP, University Hospital Frankfurt, Frankfurt am Main, Germany

Awards

2011	SIPGA full research grant and travel award, SIPGA, Singapore

Original Articles in Peer-Reviewed Journals

Bankov K, Döring C, Ustaszewski A, Giefing M, Herling M, Cencioni C, Spallotta F, Gaetano C, Küppers R, Hansmann ML, Hartmann S. Fibroblasts in Nodular Sclerosing Classical Hodgkin Lymphoma Are Defined by a Specific Phenotype and Protect Tumor Cells from Brentuximab-Vedotin Induced Injury. Cancers (Basel). 2019 Oct 30;11(11):1687. doi: 10.3390/cancers11111687. PMID: 31671543

Peveling-Oberhag J, **Bankov K**, Dultz G, Ballo O, Lohmeyer J, Brunnberg U, Marcu V, Walter D, Zeuzem S, Hansmann ML, Welzel TM, Vermehren J. miRNA-26b downregulation in peripheral blood mononuclear cells of patients with hepatitis C associated lymphomas is restored by successful interferon-free antiviral therapy. Antivir Ther. 2019;24(6):437-442

Ackermann A, Schrecker C, Bon D, Friedrichs N, **Bankov K**, Wild P, Plotz G, Zeuzem S, Herrmann E, Hansmann ML, Brieger A. Downregulation of SPTAN1 is related to MLH1 deficiency and metastasis in colorectal cancer. PLoS One. 2019 Mar 11;14(3):e0213411

Bankov K, Döring C, Schneider M, Hartmann S, Winkelmann R, Albert JG, Bechstein WO, Zeuzem S, Hansmann ML, Peveling-Oberhag J, Walter D. Sequencing of intraductal biopsies is feasible and potentially impacts clinical management of patients with indeterminate biliary stricture and cholangiocarcinoma. Clin Transl Gastroenterol. 2018 Apr 30;9(4):151

Rengstl B, Kim S, Döring C, Weiser C, Bein J, **Bankov K**, Herling M, Newrzela S, Hansmann ML, Hartmann S. Small and big Hodgkin-Reed-Sternberg cells of Hodgkin lymphoma cell lines L-428 and L-1236 lack consistent differences in gene expression profiles and are capable to reconstitute each other. PLoS One. 2017 May 15;12(5):e0177378

Peveling-Oberhag J, Arcaini L, **Bankov K**, Zeuzem S, Herrmann E. The anti-lymphoma activity of antiviral therapy in HCV-associated B-cell non-Hodgkin lymphomas: a meta-analysis. J Viral Hepat. 2016 Jul;23(7):536-44

Witkowski PT, Bourquain D, **Bankov K**, Auste B, Dabrowski PW, Nitsche A, Krüger DH, Schaade L. Infection of human airway epithelial cells by different subtypes of Dobrava-Belgrade virus reveals gene expression patterns corresponding to their virulence potential. Virology. 2016 Jun; 493:189-201

Walter D, Döring C, Feldhahn M, Battke F, Hartmann S, Winkelmann R, Schneider M, **Bankov K**, Schnitzbauer A, Zeuzem S, Hansmann ML, Peveling-Oberhag J. Intratumoral heterogeneity of intrahepatic cholangiocarcinoma. Oncotarget. 2017 Feb 28;8(9):14957-14968